The lateral distribution of the electromagnetic component in extensive air showers of size 10(^4) to 10(^6) particles

Shaat, E. A. M.

THE LATERAL DISTRIBUTION OF THE ELECTROMAGNETIC COMPONENT IN EXTENSIVE AIR SHOWERS OF SIZE 10^4 TO 10^6 PARTICLES

BY

E.A.M. SHAAT, B.Sc., M.Sc.

A Thesis submitted to
The University of Durham
for the Degree of
Doctor of Philosophy

July, 1979

ABSTRACT

A small air shower array of diameter 120 m is described. This array is used to study extensive air showers of sizes ranging from 10^4 to 10^6 and also to supply information required for the hadron studies carried out using a flash-tube chamber placed in the Cosmic Ray laboratory of the University of Durham. The array was also used to trigger the Magnetic Automated Research Spectrograph which had its location in that laboratory.

Eight liquid scintillation counters have been added to the initial fourteen plastic detectors. The array detecting elements are located in a triangular geometry around the Physics Department.

In the data handling procedures, the initial array data were assembled, digitised and then transferred to an on-line I.B.M. 1130 computer disc where the data were primarily stored before being transferred to the larger I.B.M. 370/168 computer in order to be analysed. The array could be triggered in different ways depending upon the mode chosen and upon other experiments present.

Results are presented showing the effect of the inclusion of the liquid counters on the accuracy with which the analysis programme determines the location of the shower core and on the shower size value resulting from the data analysis.

The depth of the liquid in the liquid counters was 20 cm which means that these liquid detectors responded to the photons and nuclear active particles of the extensive air showers. The lateral distributions of the electron-photon component of EAS as measured by one of the liquid counters and one of the plastic detectors (5 cm thick) are deduced and compared with the results of other experiments. The present results show good agreement with those of other workers when the effect of the thickness of the used detectors is taken into account, except for the results of Hasagawa (1962).

A comparison is made between the distributions of the number of flash-tubes discharged in the red-side top measuring tray of the Spectrograph and the theoretically predicted distributions.

PREFACE

The work done in this thesis was carried out during the period 1974 to 1979 while the author was working under the supervision of Dr. M.G. Thompson in the Cosmic Ray Group of the Physics Department of the University of Durham.

When the author joined the group, the Air Shower Array was under construction. The author was responsible for the construction of eight liquid scintillation counters with their necessary electronics, the calibration of these counters and, together with her colleagues, the running of the experiment.

The analysis of the data reported here was carried out by the author using the analysis programme of Smith (1976) with some modifications. The interpretation of the results from the liquid counters was the responsibility of the author.

The design and operation of the array has been described by Rada, et al. (1977).

ACKNOWLEDGEMENTS

I would like to thank Professors B.H. Bransden and A.W. Wolfendale for the privilege of working in the Physics Department's Laboratories. I am grateful for the special attention and encouragement of Professor Wolfendale.

I am deeply grateful to my supervisor, Dr. M.G. Thompson, for his help, advice and guidance through all stages of this work.

I wish to express my thanks to Dr. A.C. Smith, Mr. T. Stewart, Mr. M. Treasure, Mr. J. Baxendale and all members of the M.A.R.S. group for their friendly co-operation and assistance.

I also wish to thank Mrs. S.E. Davidson for her help in transferring and accessing the experimental data through the computing system. I am most grateful to Mr. K. Tindale for his skilled assistance in the experiment's construction. Mr. C. Mullaney and the Electronics Workshop staff are thanked for their assistance with the experimental electronics.

Grateful thanks go to Mrs. P. Russell for her excellent drawing of the diagrams, and to Mrs. M. Chipchase for her precise and rapid typing of this thesis.

I am indebted to my husband, Mr. N. AboElnaga, for his help, support and encouragement all the time.

Finally, I wish to extend special thanks to the Egyptian Government for the provision of a Scholarship and to the staff of the Egyptian Education Office for their support.

C O N T E N T S

CHAPTER ONE

INTRODUCTION

1.1 Historical Background

At the end of the last century, it was believed that gases were perfect insulators provided that the applied electric field was not extremely high. However, Elster and Geitel (1899), Geitel (1900) and Wilson (1900) discovered the existence of significant residual conductivity in samples of air in their ionisation chambers although no known radiations were allowed to reach this air. The conductivity was explained as being due to external radiation since it was found that it could be reduced by shielding the ionisation chamber by lead.

At first it was thought that radioactive materials on the earth were the cause of such conductivity. To test this assumption, Hess (1912) and soon afterwards Kolhörster (1913, 1914) flew ionisation chambers in balloons. As a consequence of their studies they found that as the balloon altitude increased, the ionisation in the chambers decreased up to an altitude of 700 metres and then started to increase. The initial decrease could be explained as the result of the ionisation chamber being increasingly separated from the earth's radioactivity but the eventual increase of conductivity had to be due to another reason. Hess (1912) made a hypothesis to account for the observed ionisation increase in which he said that it was caused by radiation characterised by high penetration power arriving from outer space. Owing to the observation that the ionisation was nearly the same day and night, Hess concluded that the source of the radiation could not be mainly the sun. This penetrating radiation became known as cosmic radiation.

1.2 Observation of Cosmic Radiation Under Water

Millikan and Cameron (1926) succeeded in giving further proof that the radiation was extraterrestrial. These workers lowered sealed electroscopes to different depths below the surface of two lakes in California one at an altitude of 1554 m and the other 3600 m above sea level. They found that as the depth increased, the ionisation decreased rapidly but this happened just within the first metre or so of the water surface after which there was only a slow decrease of ionisation with increasing depth.

These workers compared the rate of ionisation in the electroscopes at the different altitudes when they reached the same depth below water and found that it was not the same. However, when they looked at the equivalent depths taking into account the additional 2046 m of air above the first lake, the rates of ionisation were very near to each other. Therefore, knowing that there was an equality of the cosmic ray intensity at the two places, they came to the conclusion that the intervening air between the two lakes was just an absorber and that it did not contain any sources of radiation.

1.3 The Discovery of the Existence of Charged Particles Among the Cosmic Radiation.

At the beginning of the twentieth century, gamma rays radiating from radioactive materials were the most penetrating radiations known. So the first interpretation was that the cosmic radiation ought to be high energy gamma rays. Some years later, Bothe and Kolhörster (1929) used arrangements of Geiger Müller counters which enabled them to conclude that amongst the cosmic rays observed in the lower levels of the earth's atmosphere, there were some charged particles. A year earlier, Clay (1927) discovered a relationship between cosmic ray intensity and geomagnetic latitude, and this relationship subsequently

became known as the latitude effect. This discovery was used by Bothe and Kolhörster as evidence confirming the existence of charged particles above the earth's atmosphere. A few years later, Compton (1933) measured the intensity of cosmic rays at various places over the earth. Johnson and Street (1933) discovered the east-west effect, and this demonstrated that the cosmic ray particles were not just charged but also that most of the particles were carriers of a positive charge.

1.4 The Discovery of some Cosmic Ray Particles

1.4.1 The Positive Electron.

Anderson (1932), while taking photographs of cosmic ray tracks in a vertical Wilson chamber, discovered that amongst 1300 track photographs, 15 tracks were due to positive particles penetrating a lead plate with masses much less than that of the proton. These particles were characterised as carrying a unit charge and having a mass less than twenty times the electron mass. These new particles became known as positrons and owed their origin to a photon entering the lead plate from above, colliding with a lead atom and as a result knocking out from its nucleus an electron-positron pair.

1.4.2 The Pions and Muons

Lattes, Occhialini and Powell (1947) were examining some photographic emulsions taken in the Bolivian Andes at a height of 5,500 m, when they found that some of the charged mesons which came to rest were able to produce secondary mesons and they showed that mesons could exist with different masses. As for the secondary mesons, it was concluded that they had the same mass and that they were ejected with constant kinetic energy. Lattes et al. (1947) gave the symbol π to the primary mesons and the symbol μ to the secondary ones. Concerning their charge, it was found that both π and μ mesons carry a charge equal to that of

the electron.

1.4.3 The kaons and Hyperons

At about the same time, Rochester and Butler (1947) discovered the existence of heavier mesons. It was found that the new particles could be classified into two types. The first class contained the k-mesons and the mesons mass was calculated to be about 970 electron masses. The second class of particles were known as hyperons and were found to have masses between 2180 and 2600 electron masses. Both classes of particles can decay in many different ways.

1.5 The Origin of Cosmic Rays

Since 1948, work has been done in attempts to determine the origin of cosmic rays. At first, it was thought that the sun was the main source of the cosmic rays. The isotropy of the radiation was attributed to the capturing of the particles in the solar system by an external magnetic field. Since solar flares are always accompanied by an increase of cosmic ray intensity, it was concluded that there is an acceleration mechanism available on the sun which is responsible for generating particles of energy up to 10 GeV. However, whilst the sun can be considered as a source of some of the low energy primaries it can not be a source of particles of the highest energy. The existence of very high energy primary cosmic ray particles must be due to a much more powerful mechanism. It was assumed that the stars in the galaxy could emit cosmic rays and that the cosmic ray particles travel in curved paths, due to their interaction with galactic electric and magnetic fields, such that they stay in the galaxy for a long time.

Fermi (1949, 1954) proposed that a cosmic ray particle starts with an appreciable energy when it is emitted from the stellar body. The particle then moves in spiral within the local magnetic field. When

such a particle meets another magnetic field moving rapidly towards it, it interacts with this magnetic field and owing to this interaction the particle will be reflected gaining more energy. If two fields of this kind capture the particle between them, the particles energy will continually increase such that eventually it becomes capable of leaking out.

Colgate (1966) suggested the ability of supernovae to provide an acceleration mechanism which could yield an abundance of elements the same as that found in cosmic radiation. Afterwards, came the suggestion of Ostriker and Gunn, (1969) that pulsars which rotate rapidly offer a possible acceleration mechanism responsible for cosmic rays of very high energy. Kempa et al. (1974) surveyed the integral primary energy spectrum and found that such a spectrum is characterised by a bump in the energy range between 10^{13} eV and 10^{16}. Karakula et al. (1974) explained the occurrance of such a bump as being due to cosmic rays coming from galactic pulsars and superimposed on the normal cosmic ray background.

1.6 Methods of Measuring the Primary Cosmic Ray Energy Spectrum

The method of measurement defines the way in which the spectrum of primary cosmic rays is expressed for the following reasons:

(a) When the earth's field is used as a magnetic analyser, which corresponds to intensity measurements at various latitudes, the integral particle flux is found above a certain threshold rigidity.

(b) Using experiments on board satellites or balloons, individual low energy nuclei can be recorded. The spectrum is then defined according to the number of nuclei existing in a given range of energy per nucleon.

(c) Indirect studies of single muons at the lower levels of the atmosphere give the number of primary nucleons with energy per nucleon in a given range.

(d) At the highest energies, measurements of extensive air showers yield the primary spectrum in terms of primary energy per nucleus.

In the region below 10^9 ev/nucleon, direct measurements are useful such as those obtained using satellites. Between 10^9 and 5×10^{11} ev/nucleon balloon-borne detectors are used but the statistical accuracy is low when Z becomes greater than two. For energies above 5×10^{11} eV/nucleon there is no direct information about particles having Z greater than one. Knowledge concerning the energy spectrum is deduced from observations carried out at ground level of the fluxes of protons and muons and the application of an assumed model for the nucleon-nucleus interactions in the atmosphere. Such calculated spectra are found to be in a good agreement with both the direct observations at the lower end of the energy range and with the extensive air shower measurements at the high energy end of the region.

At the energies above 10^{14} ev, studies of extensive air showers are used to measure the spectrum. The EAS technique gives information about the energy of the incoming particles and hence the spectrum is usually given in terms of energy per nucleus.

1.7 The Intensity and Spectrum of Primary Cosmic Rays

The intensity of primary cosmic ray arriving at the earth's atmosphere decreases as the energy of the primaries increases such that for an energy of $\simeq 10^7$ ev per nucleon the intensity is nearly equal to $10^{-6} m^{-2} s^{-1} sr^{-1} ev^{-1}$ while it falls to $10^{-36} m^{-2} s^{-1} sr^{-1} ev^{-1}$ at an energy $\simeq 10^{20}$ ev per nucleus.

Greisen (1966) suggested that there was a possibility that the primary energy spectrum cut off at about 10^{20} ev. Such a cut off was explained by Roll and Wilkinson (1966) as being a consequence of photonuclear reactions of the high energy primary protons with the 2.7^{o}K Black Body radiation. In these reactions, the primary protons lose energy in photopion production. Hillas (1975) suggested that at energies above 10^{17} ev, it was possible for nuclei to suffer photo-disintegration on star-light. From measurements made on air showers, Hillas concluded that no such interactions occur up to about 2×10^{20} ev.

In the same year, Hillas carried out a world survey of the integral primary energy spectrum, see figure 1.1. Grigorov et al. (1970) have made direct measurements of the spectrum using satellites up to energies of $\approx 10^{14}$ ev but their measurements are at variance with the results of other less direct methods at the highest energies. In particular around 10^{15} ev per nucleus, the flux which is obtained from air shower measurements is higher than the flux reported by Grigorov and also the air shower measurements lead to fluxes which are above those obtained from indirect muon calculations.

The Utah group (Elbert et al. 1975) has studied multiple muons underground which are due to primary nuclei having energies up to 10^{14} ev per nucleon. Hillas (1975) suggests that the primary parents are mostly nuclei ($Z>1$) and that at an energy of 10^{14} ev per nucleon, there is a reduction in the proton flux while the helium and heavier nuclei increase relative to a line obtained by extrapolating the spectrum to higher energies from the region of 10^{11} ev per nucleon. Hillas (1975) points out that according to the survey carried out by Ng et al (1973) of muon spectrum experiments, the primary spectrum up to 4×10^{13} ev is characterised by a slope $\gamma_D = -2.7$, the line marked U in figure 1.1. Above this energy and up to 10^{16} ev, a bump appears in the primary

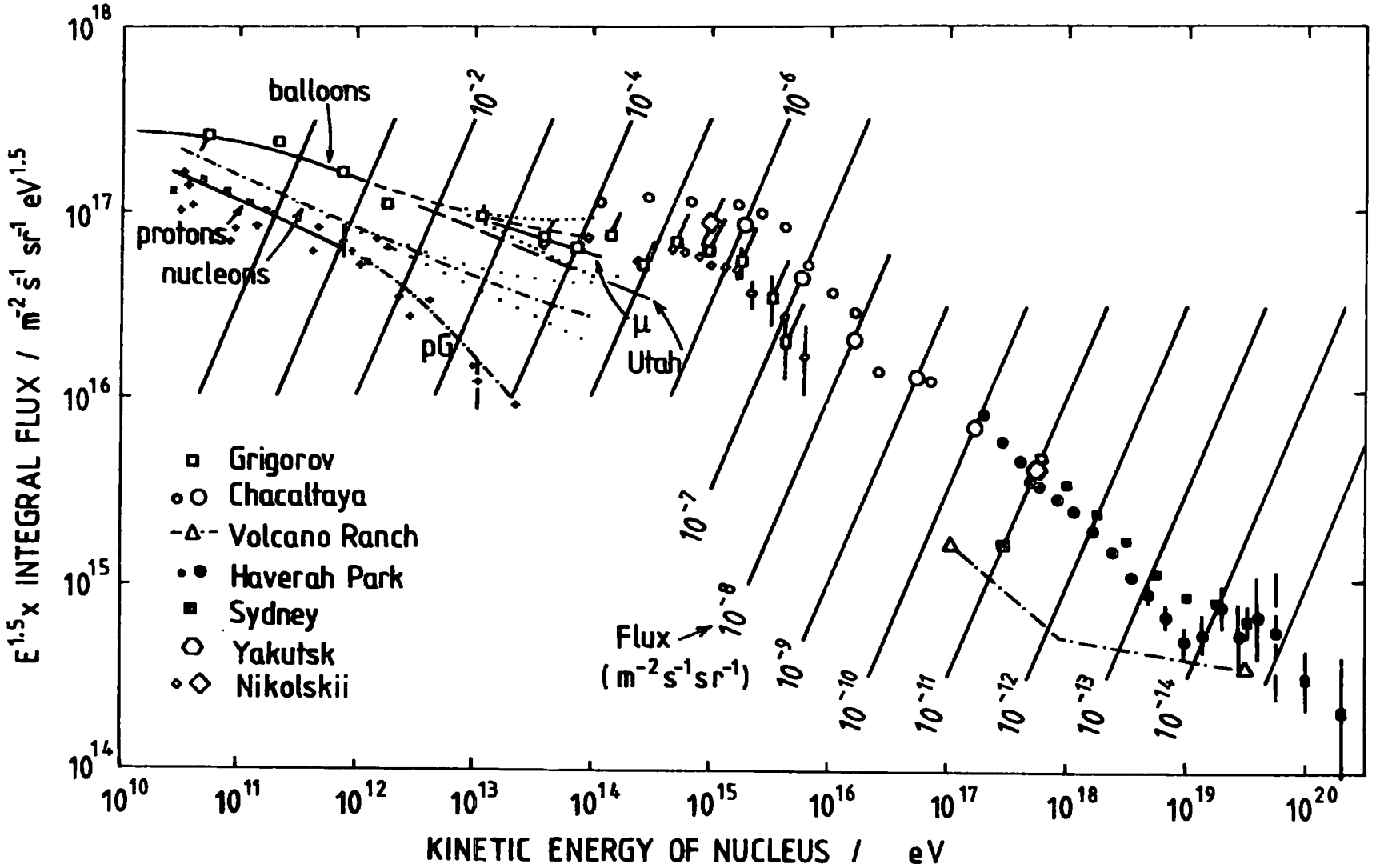

Figure 1.1 The Integral Energy Spectrum Of Primary Particles. (After Hillas, 1975)

spectrum, the origin of which has been explained in section 1.5. At even higher energies there is near agreement between the Sydney, Haverah Park and Chacaltaya EAS groups that the spectrum becomes steeper and that it has a differential slope of -3.35 ± 0.15 to about 10^{18} ev per nucleus.

CHAPTER TWO

EXTENSIVE AIR SHOWERS

2.1 Introduction

Since the discovery of extensive air showers in 1938, a lot of work has been done in order to understand the features of this phenomenon. At first, the studies were concerned with the properties of the phenomenon, but subsequently they began to concentrate on the properties of the primary particles initiating the extensive air showers.

2.2 General Picture of the Air Shower Development

When the primary cosmic ray particles enter the atmosphere, they interact with air nuclei initiating extensive air showers and producing secondary particles. It has been found that most of the secondaries of these interactions are charged and uncharged pions. The neutral pions decay in a very short time $\sim 10^{-16}$ second into two photons which by pair production produce electron-positron pairs. These electrons in turn produce gamma rays by the bremsstrahlung process. The resulting gamma rays initiate more electrons and so electron-photon cascades are generated and these constitute the electromagnetic component of the showers. Due to coulomb scattering in the atmosphere, the particles in the electron-photon cascades spread over large areas and arrive at ground level some distance from the shower axis. As the number of particles in the showers increases, the mean energy per particle decreases until the rate of loss of energy by the bremsstrahlung process becomes less than that by ionisation. This occurs when the electron energy reaches the so called critical value of 84 Mev. After this point is reached there is a decrease in the number of the shower particles.

In addition to the electron-photon cascade, the charged pions, nucleons and other secondary particles produced in the interactions of the primary cosmic rays and in subsequent interactions of these hadrons,

form a nuclear cascade in extensive air showers.

Typically, in the vertical direction charged pions with energies $\lesssim$ 10 Gev are more likely to decay into muons and neutrinos than to interact, and conversly those having energies $\gtrsim$ 10 Gev are more likely to interact with air nuclei before decaying. The muons are characterised by a life time of $\sim$ 2.2 us and there is a high probability that they reach sea level before decaying into electrons. The muons possess high penetrating power and can therefore be observed at quite large distances from the shower axis.

2.3 The Standard Model

The procesess involved in air shower can be understood through the models describing high energy interactions. One model which is used in many calculations is based on the formula obtained by Cocconi, Koester and Perkins (1961) (the CKP formula). De Beer et al. (1966) put the following points as a summary for such a model.

1. High energy nucleons have a mean free path of 80 g/cm^2 and lose in each collision an average of 50% of their energy. The mean free path as well as the energy loss is energy independent.
2. Most of the produced secondary particles are pions being either neutral, positively charged or negatively charged and they are generated in equal numbers.
3. If the pions are allowed to be emitted in the backward direction, their energy distribution in the laboratory system can be given by the emprical CKP relation which is

$$s(E,E_o) = \tfrac{1}{2}\left[\frac{n(E_o)}{\Gamma}\exp\left(-\frac{E}{\Gamma}\right) + \frac{n(E_o)}{G}\exp\left(-\frac{E}{G}\right)\right]$$

where $n(E_o)$ is the multiplicity of the produced pions and E_o is the transferred energy. Γ and G refer to the average energy

carried by those pions in the forward and backward cones respectively such that

$\Gamma = 2\ (E_o k - \frac{1}{2} n\ (E_o)\ G)/n(E_o)$ where K is the inelasticity coefficient.

4. The fraction of the energy lost by a nucleon which does not appear as pions is assumed to be small that it can be neglected.

5. If the inelasticity coefficient K is equal to 0.5, then the multiplicity of the secondary pions will be given by

$n_s = 2.7\ E_p^{\frac{1}{4}}$

where E_p is projectile nucleon energy in Gev.

6. Cocconi, Koester and Perkins suggest that the transverse momentum, P_t, of the created pions is distributed according to the following expression

$$f(P_t) = \frac{P_t}{P_o^2} \exp\ (-\frac{P_t}{P_o})$$

Where $2p_o$, which is the mean transverse momentum, is assumed to be energy independent and to be equal to 400 Mev/c.

7. The pion interactions are catastrophic with an interaction length of 120 g/cm^2. The pions produced as the result of pion interactions have a multiplicity which is the same as that for those produced by protons when k = 1, i.e. $n_s = 3.2\ E_\pi^{\frac{1}{4}}$.

8. In some treatments, the effect of fluctuations in the inelasticity coefficient has been taken into consideration for nucleon - nucleon interactions. The pion interactions however, are unaffected.

2.4 Survey of the Properties of the EAS components

It has been found that the components of air showers can be classified into three main groups. These groups are the electromagnetic, the muonic and the hadronic components.

2.4.1 The Electromagnetic Component

This component is the largest component of an air shower in number, but it does not contain the greatest amount of energy. The following sections describe some of the main parameters of this component.

2.4.1.1 The Electron Lateral Distribution

The relationship between the electron density and the distance of the point of observation from the shower axis is known as the electron lateral distribution. The structure function describing this distribution, has been measured by many groups at sea level as well as at high altitudes. Greisen (1960) surveyed the results of previous experiments and deduced the structure function,

$$\rho(N,r) = \frac{0.4N}{r_1^2} \left(\frac{r_1}{r}\right)^{0.75} \left(\frac{r_1}{r+r_1}\right)^{3.25} \left(1 + \frac{r}{11.4r_1}\right) \qquad 2.1$$

where ρ is the density of particles per square metre, N is the shower size, r is the radial distance and r_1 is the Moliere unit and represents the scattering length of an electron in air. At sea level, r_1 equals 79 m while it becomes equal to about 120 m at mountain altitudes. At distances less than 100 m from the shower axis, there is a good agreement between Greisen's equation and a theoretical one given by Nishimura and Kamata (1952, 1958) which is for a pure electromagnetic cascade having an age parameter equal to 1.25. Greisen (1956) approximated the Nishimura - Kamata function as

$$f\left(\frac{r}{r_1}\right) = c(s) \left(\frac{r}{r_1}\right)^{s-2} \left(\frac{r}{r_1} + 1\right)^{s - 4.5} \qquad 2.2$$

where s is the shower age parameter and c(s) is a normalisation factor. This factor is found to increase with the age parameter, s, until the latter reaches a value of 1.25 and then it decreases. It is also found that the value of the age parameter s remains in the region 1.2 - 1.25 as the shower size decreases from 10^9 to 10^3.

The electron density in the EAS can be measured using Geiger Müller counters and scintillation counters. By using Geiger counters, the lateral distribution of ionising charged particles can be measured. With the scintillation counters because their response depends upon the energy spectrum of the electromagnetic component, their use gives a somewhat steeper lateral distribution. This fact is shown in figure 2.1 where the structure function of Greisen for s = 1.25 is plotted together with that of Hasegawa et al (1962) using scintillation counters. The Hasegawa function is given by

$$\rho(N,r) = \frac{N}{2\pi(120\pi)^{\frac{1}{2}}} \frac{\exp(^{-r}/_{120})}{r^{1.5}} \qquad 2.3$$

In addition using scintillation counters it is considered that the measured shower sizes are most probably greater than the true ones.

The structure function obtained at sea level by the Sydney group and reported by Hillas (1970) is much flatter than that given by Greisen. This is due to the occurrance of many multi-core events in their observations of showers initiated by primaries having energies slightly greater than 10^{15} ev. Their function is

$$\rho(N,r) = 2.12\times10^{-3}\, N \frac{\exp(^{-r}/_{75})}{(r+1)} \qquad 2.4$$

The Keil group (Hillas, 1970) used a neon hodoscope and their data are represented by the lateral function

$$\rho(N,r) = 1.08\times10^{-2}\, N \frac{\exp(^{-r}/_{120})}{(r+1.1)^{1.5}} \qquad 2.5$$

The last two functions are also shown in figure 2.1. It is considered that for radial distances greater than 10 m, there is satisfactory agreement between all the represented functions and that the experimental uncertainties in locating the core are the main reason for the observed differences.

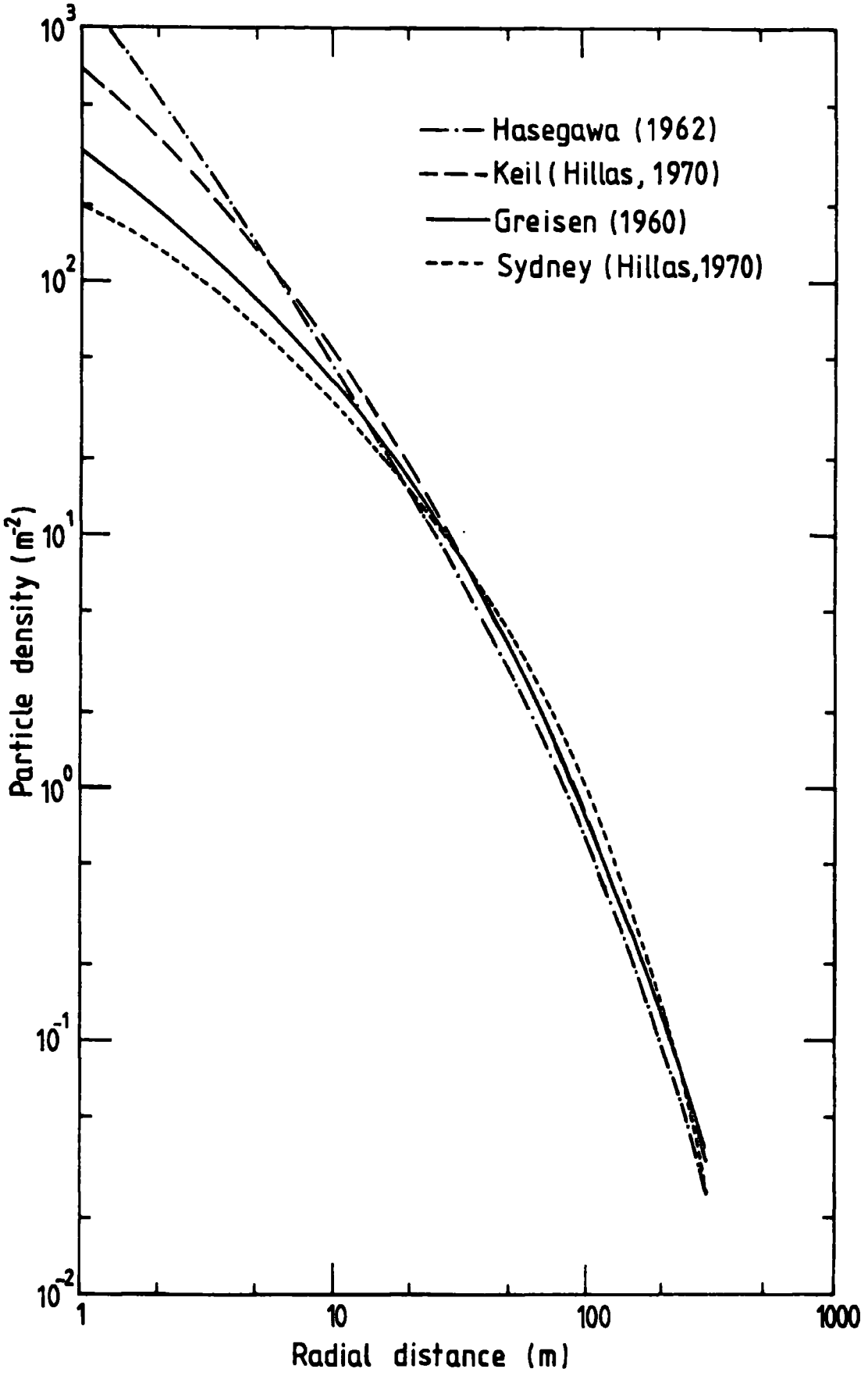

Figure 2.1 The lateral structure function obtained by several authors, normalised to $N = 2 \times 10^5$.

2.4.1.2 The Shower Age Parameter

The shower age parameter, s, indicates the stage of development of the shower. A value of s less than unity, means that the shower is still 'young' and that there will be more development. A value of unity corresponds to shower development reaching a maximum. Further, when s is greater than unity, the number of particles in the shower is decreasing and the shower is considered as an 'old'one. When s reaches two, the number of particles in the shower has fallen to one.

Karakula (1968) predicted theoretically the relation between the age parameter and the shower size using the standard model mentioned earlier. According to his predictions, the shower age parameter varies only slightly with shower size. However, it is found that the theoretical variation is greater than those of the experimental results. Figure 2.2 shows a comparison between Karakula's predictions for two values of the zenith angle, θ, and the experimental observations obtained by Vernov et al. (1970). Vernov's measurements show a slight increase in the age parameter with shower size. However, Dixon and Turver (1974) simulated showers and suggested that the age parameter decreases as the shower size increases. The increase found by Vernov can be explained as being a consequence of using a structure function which is flatter than that given by equations 2.1 and 2.2. Theoretical considerations indicate that the lateral structure of EAS depends upon the distance from the shower axis at which the shower is recorded. This dependance is such that at large distances the function is flatter and at small distances steeper. Accordingly, the age parameter measured at large distances from the shower axis is expected to be larger than average and at small distances lesser. Experimentally, it is found that this is true since the resultant average for the age parameter is $\sim$ 1.15 at radial distances less than 20 metres. The continuous regeneration by the nuclear active

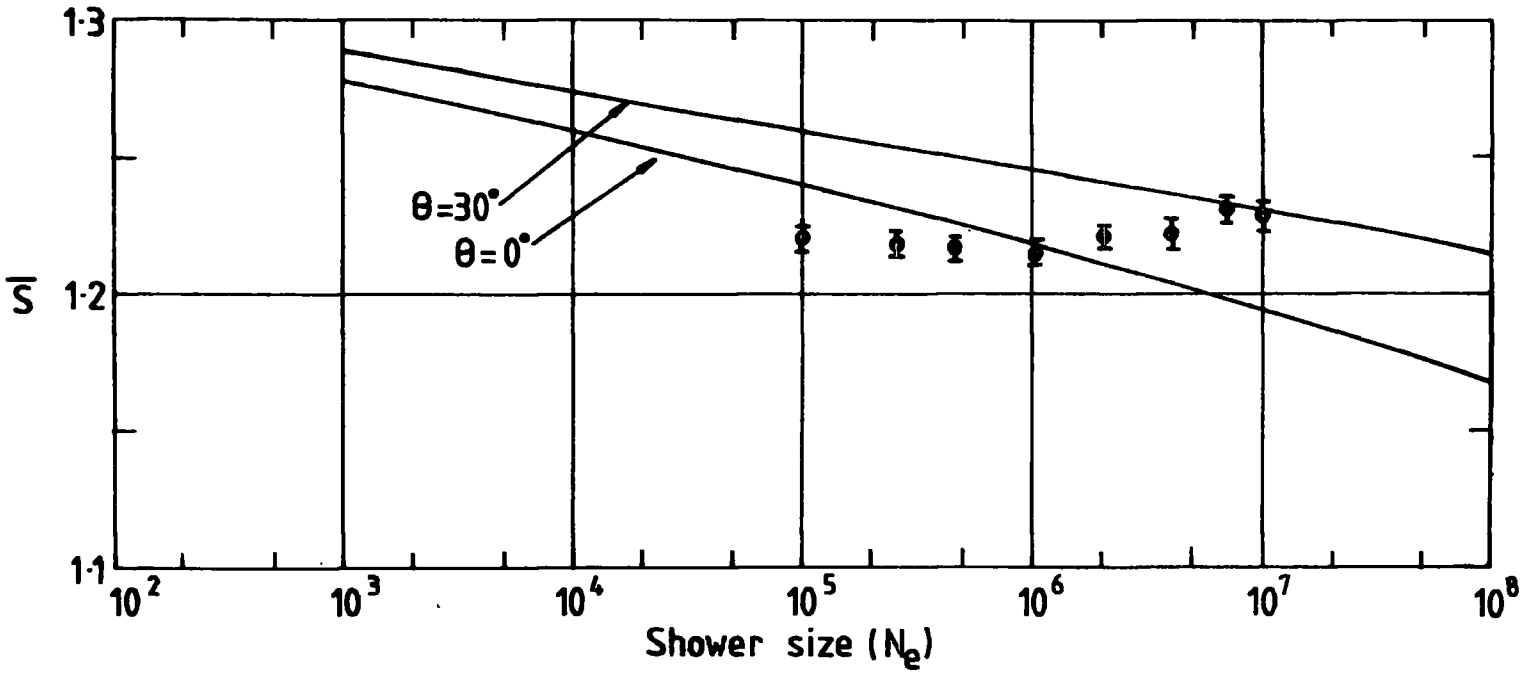

Figure 2.2 The age parameter as a function of electron shower size. The experimental points are from Vernov et al. (1970). (After Smith, 1976)

component of the electromagnetic cascade, is considered to be the reason for the approximate constancy of the shower age parameter with shower size.

2.4.1.3 Fluctuations in the Air Shower Parameters

The fluctuations obtained in shower parameters are considered to be strongly dependent upon the mass composition of the primary cosmic rays. In showers created by protons, fluctuations would be due to several reasons, for example the variation in the depth in the atmosphere at which the first interaction of the primaries takes place and the variation in the coefficient of inelasticity in each interaction. Changes in the multiplicity and energies of the secondary particles could also be responsible for some of the fluctuations. If the primary cosmic rays are mainly protons, then the expected fluctuations of the age parameter will be in the range from 4% to 8% depending upon which model is used for the high energy interactions. The values observed experimentally are about 10% which support the assumption that the majority of the primary particles are protons. As for heavier nuclei, since the showers initiated by them are considered to be several small showers superimposed upon each other, then the fluctuation in s will be the average of the variations which occur in the small showers. Therefore, the fluctuations expected for heavy nuclei initiated showers should be very much less than 1% and probably negligable.

Dixon and Turver (1974) carried out simulation studies to determine the relationship between the depth of the interaction of the initiating primary particle of the shower and the shower size measured at sea level, and the relationship between the interaction depth and the depth at which the shower reaches its maximum development. These studies were carried out for an E_p of 10^{15} ev proton initiated showers. Figure 2.3 shows their results and it can be seen that the number of electrons

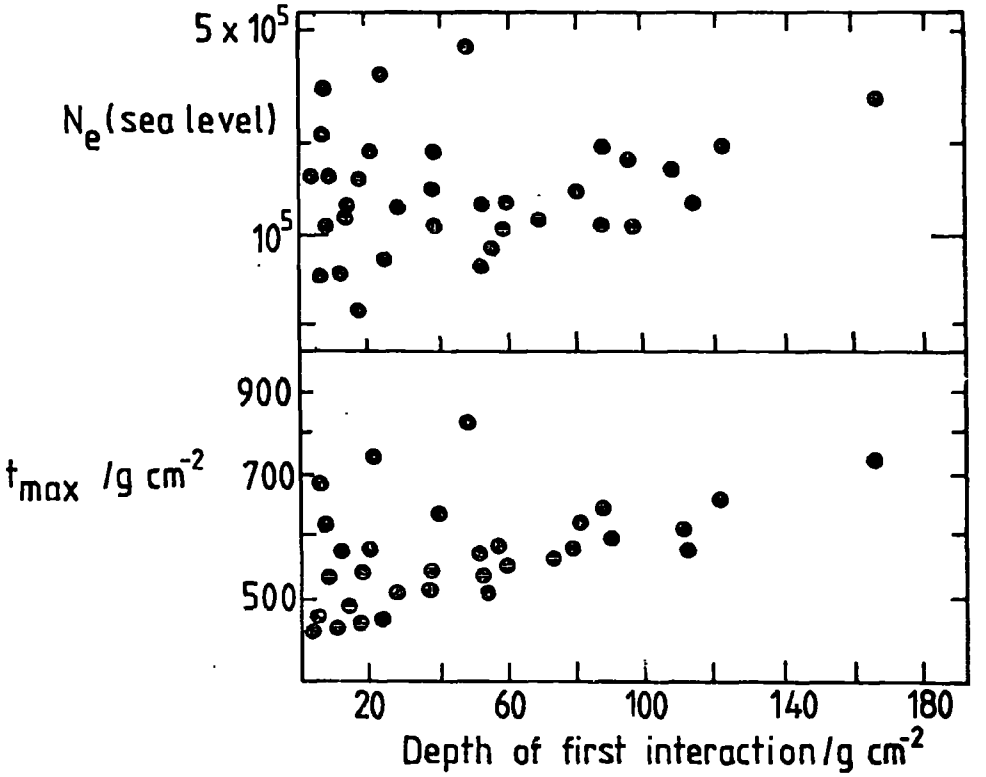

Figure 2.3 The relationship between electron size and depth of cascade maximum with the depth of initial interaction for vertical showers initiated by primary protons of energy 10^{15} eV. (After Dixon & Turver. 1974)

contained in showers produced by a primary of a fixed energy fluctuates greatly but is not strongly dependent on the depth of the initial nucleon-nucleon interaction.

2.4.1.4 Central Electron Density

The ratio between the central electron density and the total number of particles in the air showers is a further parameter which depends upon the mass composition of the primary particles. Such a dependence arises from the fact that the central density is approximately proportional to the energy per nucleon of the primary particles whilst the total number of particles in the shower is considered to be representative of the energy per nucleus of the primaries. The results of Samorski et al (1971) are consistent with the primaries being mostly protons.

2.4.1.5 The longitudinal Development of Extensive Air Showers

Studies of the electron component of showers are persued so that the longitudinal shower development can be investigated. Linsley et al. (1962) and La Pointe et al. (1968) found that the shower size at different atmospheric depths can be deduced by making equi-intensity cuts on the size spectra observed at various zenith angles. Figure 2.4 represents the experimental results of Bradt et al. (1965) obtained at Chacaltaya together with the aerial data of Antonov et al (1971) taken at a height of 10 km. From the data it is apparent that the electromagnetic cascades created by nuclear active particles as a result of their individual interactions, are typically very short and have large fluctuations. The first of these characteristics is explained as being a consequence of the rapid degradation of the energy of the nuclear active particles, or in other words, attributable to the high multiplicity of the secondaries.

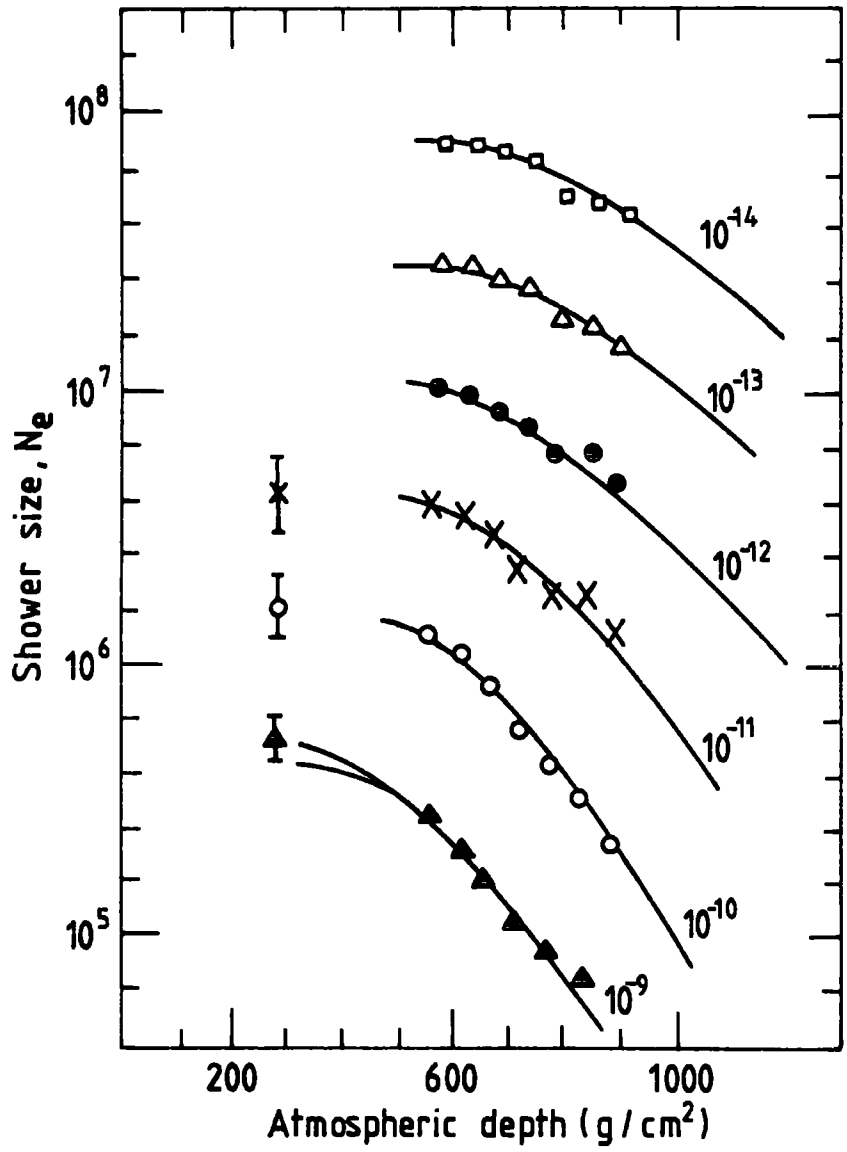

Figure 2.4 Longitudinal development curves obtained from equi-intensity cuts of air showers observed at different atmospheric depths. (After Wdowczyk, 1973)

Dixon and Turver (1974) investigated the dependence of the fluctuations of both the electron shower size at sea level and the depth of maximum development on the energy of the primary protons. Figure 2.5 shows their results together with the results of other workers and some theoretical predictions. There are only small differences between the data and theoretical predictions which are attributed to the use of various different models.

Turver, (1973) investigated the possibility that the rate of development of air showers depends upon the nature of the primaries and could affect the average depth in the atmosphere at which the showers reach their maximum development and the degree of fluctuations occurring in this parameter. It has been found that the level of maximum development of showers generated by protons or light nuclei is deeper in the atmosphere than that of showers due to heavier primaries. Also the fluctuations in the longitudinal development of the first class of shower are expected to be greater than those of the second class.

2.4.2 The Muon Component

It has been established that in order to obtain information about the primary particles and their interaction mechanism, it is better to study the muon component rather than the electron component of showers. This is due to the fact that the interactions between the muons and matter are relatively weak, consequently the muon component at sea level holds much of the information pertaining to the development of the EAS in their early stages and reflects more truly the energy of the primaries of individual showers. In addition to that, since the direction of travel of the muons represents rather well that of their parents, information about the transverse momentum of the parents as well as the longitudinal development of the EAS can be obtained by studying the lateral distribution of muons of different energies. However, it is easier to detect the

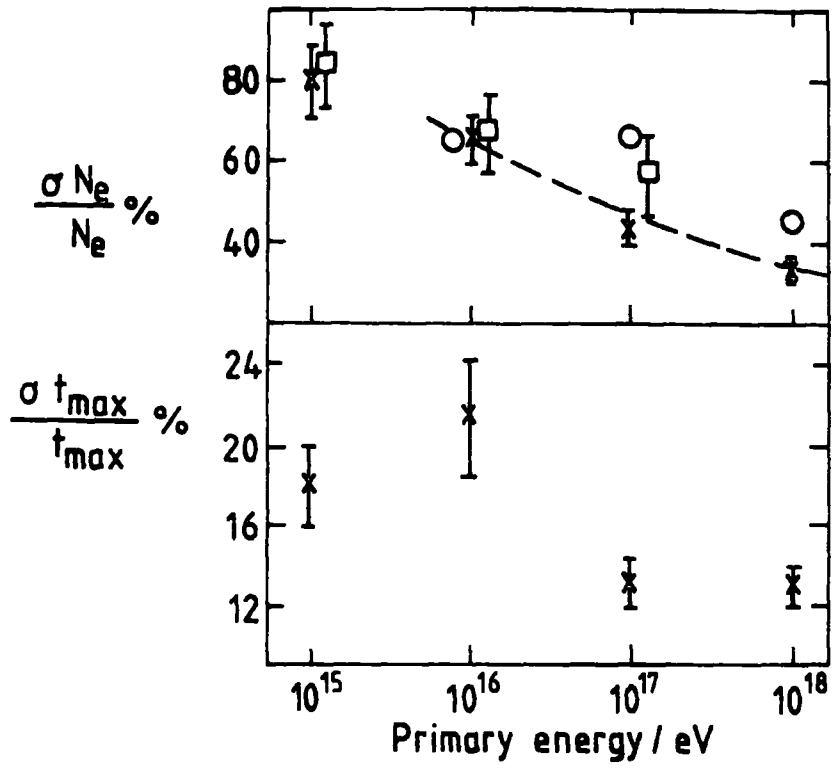

Figure 2.5 The relative standard deviation of electron size and depth of maximum development for showers generated by protons.

- ✱ Dixon and Turver (1974b)
- O Marsden (1971)
- ⊡ Khristiansen et al. (1965)

The curve is that of de Beer et al.(1968)
(After Dixon & Turver, 1974)

electrons than the muons since the muons have a much lower density and large and expensive well shielded detectors are needed in order to get accurate density measurements and to achieve the required discrimination of the muons from the electrons. Such shielding can be obtained either by putting the detectors underground or by covering them by a dense absorbing material, for example, lead. The threshold energy of the recorded muons is defined by the thickness of the shielding material. EAS muons can also be studied using magnetic spectrographs with very large acceptances, the muons being deflected in magnetic fields and hence their momentum calculated.

2.4.2.1 Lateral Distribution of Muons

Clark et al. (1958) studied muons of energies greater than 1.2 Gev in showers of sizes ranging between 2×10^5 and 2×10^8. Greisen (1960) used Clark et al's results in obtaining the following formula for the muon lateral distribution,

$$\rho_\mu(N,r) = 18\left(\frac{N}{10^6}\right)^{0.75} r^{-0.75} \left(1 + \frac{r}{320}\right)^{-2.5} \qquad 2.6$$

where $\rho_\mu(N,r)$ is the density of muons per square metre, r is the distance in metres from the shower axis at which these muons fall and N is the shower size.

The Cornell group (Bennet et al. 1962) investigated the dependence of the lateral distribution structure function of the muons on their threshold energy in the range from 1 Gev to 10 Gev. Such investigations led them to the following relationship.

$$\rho_\mu(N,r,>E_\mu) = 14.4\left(\frac{N}{10^6}\right)^{0.75} r^{-0.75} \left(1 + \frac{r}{320}\right)^{-2.5} \left(\frac{51}{E_\mu+50}\right)\left(\frac{3}{E_\mu+2}\right) 0.14r^{0.37} \qquad 2.7$$

where E_μ is in Gev and r is in metres. Figure 2.6 shows the curve obtained using this formula together with some experimental results for $E_\mu \geq 10$ Gev.

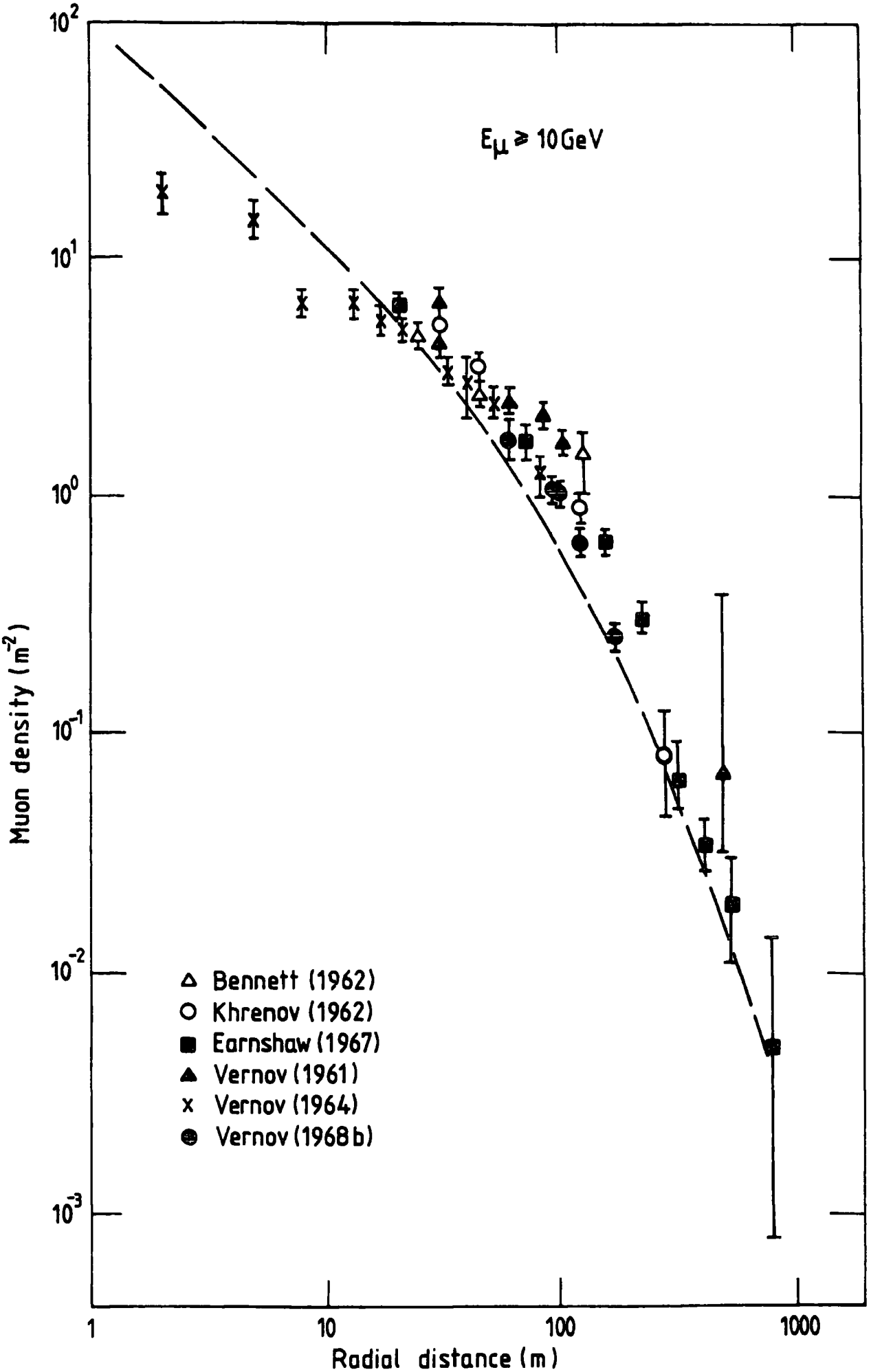

Figure 2.6 The lateral distribution for muons of 10 GeV threshold energy. The data are normalised to 2.10^7. (After Wdowczyk, 1973)

The uncertainties in locating the shower axes are considered by Wdowczyk (1973) to be partly the cause of the relative flattening of the experimental data at small distances from the core.

Comparing the measured lateral distribution of the muons with the theoretical expectation based on the standard model, it is evident that the model predicts narrower distributions than those observed. To get a wider lateral distribution, it has to be concluded that either the pions have a mean transverse momenta greater than 400 Mev/c or the muons are produced higher in the atmosphere than the model assumes.

2.4.2.2 The Relation Between the Number of Muons and the Number of Electrons in Showers

The total number of muons N_μ with energies greater than E_μ in a shower of size N can be obtained by integrating the lateral muon density over the radial distance, r. This number is approximately proportional to the number of electrons $N_e^{0.75}$. The validity of this proportionality is found to exist over a wide range. Also it is found that the muon threshold energy has only a small effect on this index such that the latter decreases only slightly when the energy increases.

2.4.2.3 High Energy Muons

The study of high energy muons, in particular their energy spectrum and charge ratio, enables information about the characteristics of the high energy interactions to be obtained. Such high energy muons are the direct result of the very first interactions of the primaries.

2.4.3 The Nuclear Active Component

The nuclear active component plays a very important role in the development of the EAS since the interactions of the particles in this component lead to the muon and the electromagnetic components of the shower. The number of hadrons in an air shower is much less than that of the other particles and only because of their large energies, it is

possible to separate them from the electrons.

Greider (1973) found that the total number and energy spectrum of the hadrons in a shower of fixed primary energy, was a sensitive parameter reflecting the model assumed for the high energy nuclear interactions. This parameter can be obtained by studying the lateral distribution of the hadrons. Kameda et al. (1965) investigated showers of electron size ranging between 4×10^4 and 4×10^6 particles at sea level and got the following equation for the differential lateral distribution,

$$\rho(E,r,N)dEdr = 0.35N^{0.35} E^{-1.2} e^{-r/r_o} dE\, dr \qquad 2.8$$

where $r_o = 2.4N^{0.32} E^{-0.25}$, r is the radial distance and N and E are measured in units of 10^5 particles and 100 Gev respectively. Figure 2.7 shows the results obtained by other groups for shower sizes in the range from $\sim 10^5$ up to $\sim 3 \times 10^6$ particles. It is found that if the mean transverse momentum is increased from 0.4 Gev/c to a 0.6 Gev/c, there is a good agreement between the experimental results and the calculated energy spectrum based upon the standard model of de Beer (1966). Thus studying hadrons contained in air showers, it is possible to deduce the transverse momenta involved in nuclear interactions.

2.5 Some of the Previous Studies of the Electromagnetic Component

2.5.1 The Tokyo Group

The Hasegawa formula (1962) for the lateral structure function of the electromagnetic component (2.3) was deduced from the measurements obtained in the experiment carried out by the Tokyo group. The experimental arrangements are briefly illustrated in figure 2.8. The detectors used in that project were as follows:

1. Eleven plastic scintillation counters each of an area of $1m^2$.
2. Five fast scintillation detectors, four of which were located on the ground and one was placed about 6 metres above ground

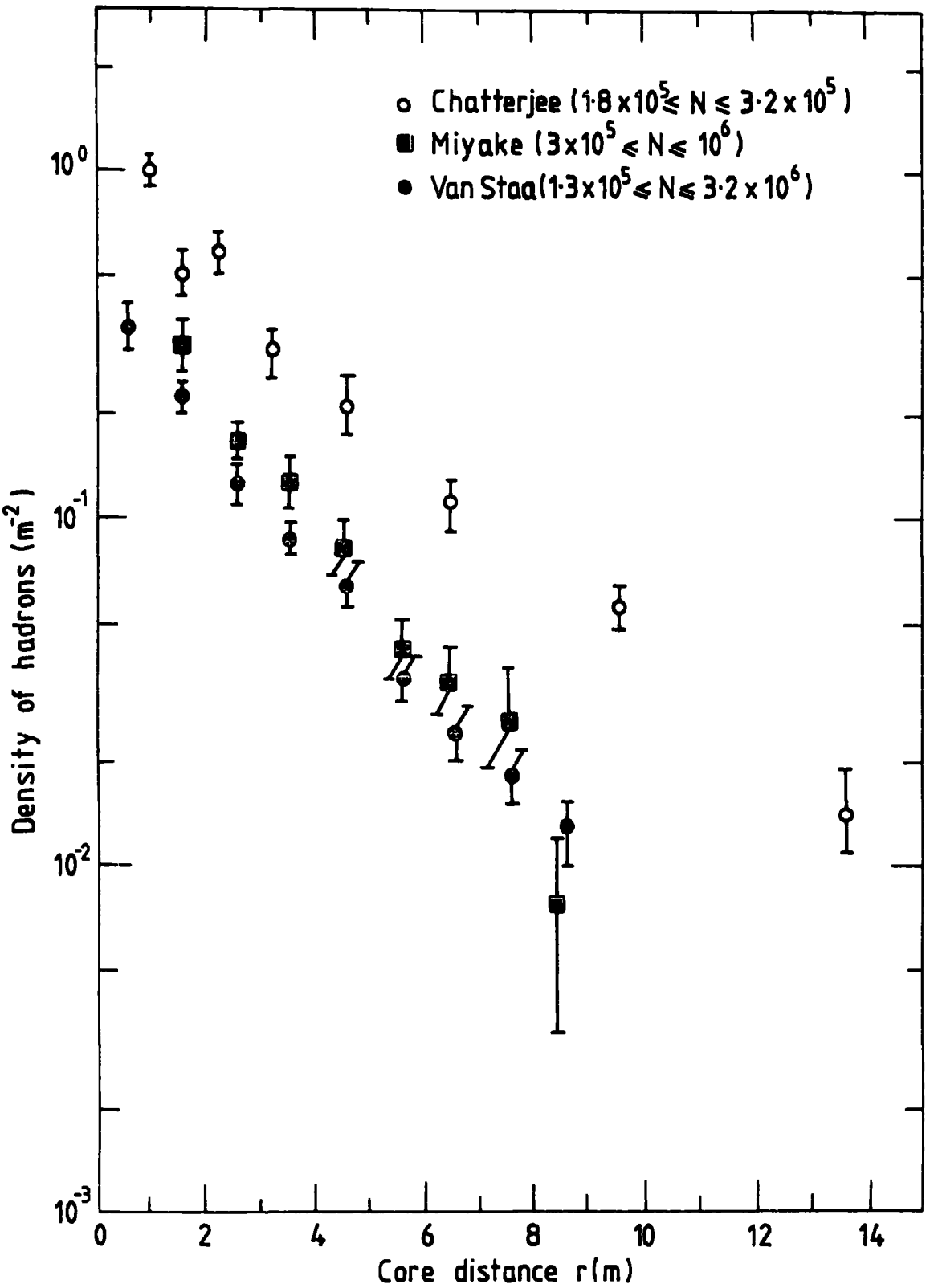

Figure 2.7 The hadron lateral distribution obtained by Chatterjee et al (1968), Miyake et al. (1970) and Van Staa et al. (1973) for a threshold energy of 200GeV and three different shower sizes. (After Smith, 1976)

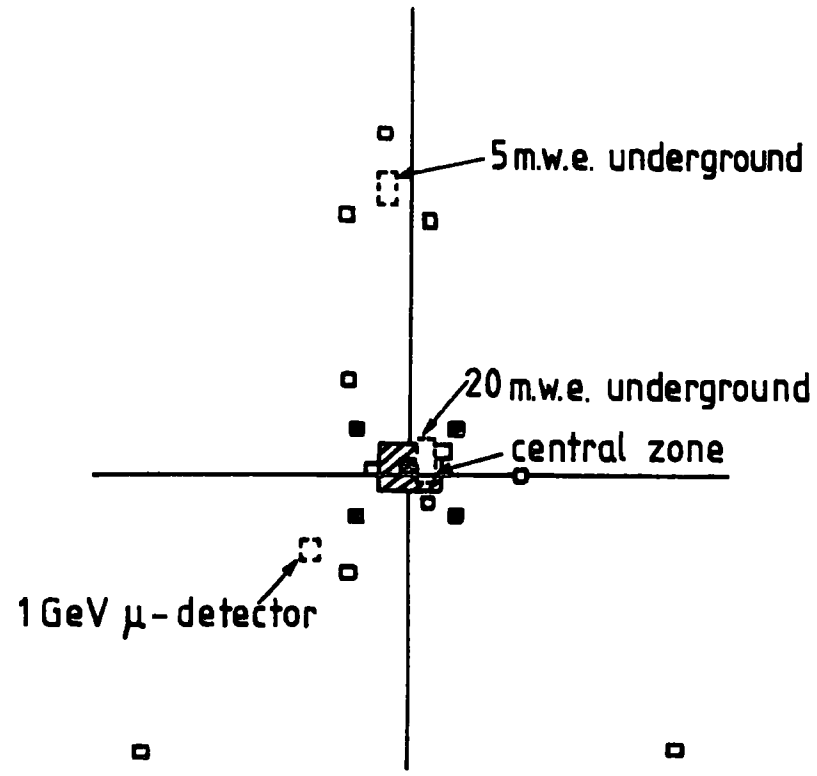

Figure 2.8 The E.A.S. Array Of Tokyo.

□ : charged particle detector.

■ : fast detector.

⬚ : muon detector.

(After Hasegawa et al. [1962])

level. These detectors were used to determine the arrival direction of each recorded shower.

3. A Neon hodoscope which consisted of about 1500 neon tubes, 2 cm in diameter, spread to cover an area of 4 m^2 known as the central zone. This hodoscope was used to study the nature of the core of the detected EAS if that core hit within the hodoscope's area.
4. Four scintillation detectors each of 2 m^2 area located at a depth of 20 m.w.e. used to detect muons of energy $\geq$ 5 Gev.
5. Another muon detector having an area of 1 m^2 placed under a block of concrete in order to detect muons of energy $\geq$ 1 Gev.

The basic idea of that arrangement was to determine for each recorded shower, the shower size N, the location of the shower core and the lateral distribution of particles using the scintillation detectors (1).

2.5.2 The Sydney Group

Sydney group, Bray et al (1964), studied the structure of cores of air showers having sizes $> 2.0 \times 10^5$ using an array the arrangement of which is shown in figure 2.9. As seen from this figure, the apparatus consisted of a closely packed array of 64 large plastic scintillation counters, a more thinly spread array of about 500 Geiger counters (some of which were shielded) and 5 Wilson cloud chambers. Each of the scintillation counters was 41 cm x 41 cm x 10 cm and had its own photomultiplier. These counters were mounted in a 4 m x 4 m square grid contained in a hut. Two Wilson cloud chambers, 30 cm in diameter and 20 cm in depth were included in the array where a 'half' size (40 cm x 25 cm x 10 cm) scintillation detector was mounted above one cloud chamber (Bray et al., 1965). A special Geiger tray consisting of 6 tubes each having an area of 115 cm^2 and of 2 tubes of area 16.1 cm^2 each was placed over one of the 64 scintillation detectors.

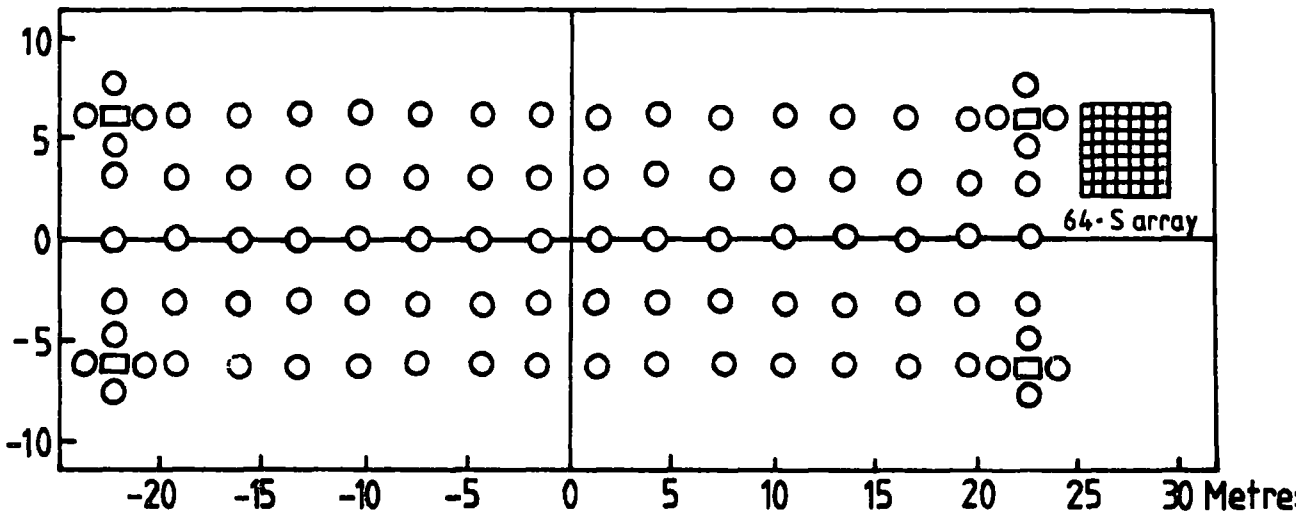

Figure 2.9 A plan of the Sydney air-shower array. Each circle represents a box containing 3 G.M. counters each of area 16·1 cm^2. The four rectangles at the corners represent boxes containing 48 G.M. counters each of area 115 cm^2. The cloud chambers were placed on the top of the 64 scintillator array.
(After Bary et al. [1965])

For each recorded shower, the numbers of particles, C, registered by the cloud chambers were obtained by direct track counting and the Geiger response, G, was determined from the number of counters fired in the array. As for the number of scintillator particles, S, this was calculated by dividing the pulse height, v, measured for these S particles by the pulse height, v_1, corresponding to the passage of single minimum ionizing particles through the detector. This pulse height, v_1, was considered in this experiment to be the mode of the distribution of the pulse heights resulting from the passage of these single ionizing particles. A comparison was then made between the densities of particles (m^{-2}) measured by the cloud chamber and by the 'half' size scintillation detector mounted above it on the one hand and between the densities (m^{-2}) at the special Geiger tray and some of the scintillation counters in its vicinity on the other. They found that the ratio G/C was always near to unity and that both the ratios S/C and S/G were increasing with decreasing core distance.

2.5.3 The Kiel Experiment

The main purpose of the experiment of the Kiel group, Bagge at al. (1965), was to study the electromagnetic structure of shower cores. A plan of the detector arrangement is shown in figure 2.10. This figure shows that the apparatus consisted of 16 scintillation counters each of $1m^2$ area and 5 cm thickness which were used to measure the particle densities at different distances from the shower core. Four of these counters were supplied with fast photomultipliers to be used in the determination of the arrival direction of the recorded showers. At the centre of the array there was a $32m^2$ neon hodoscope with 176,400 flash-tubes placed under about 2.5 g/cm^2 of wood. This hodoscope was used in studying the cores of the EAS. The particle and fast timing data obtained by the scintillation counters were recorded by the use of a digitial system. The Kiel lateral distribution equation for the electromagnetic component (2.5) was deduced from the

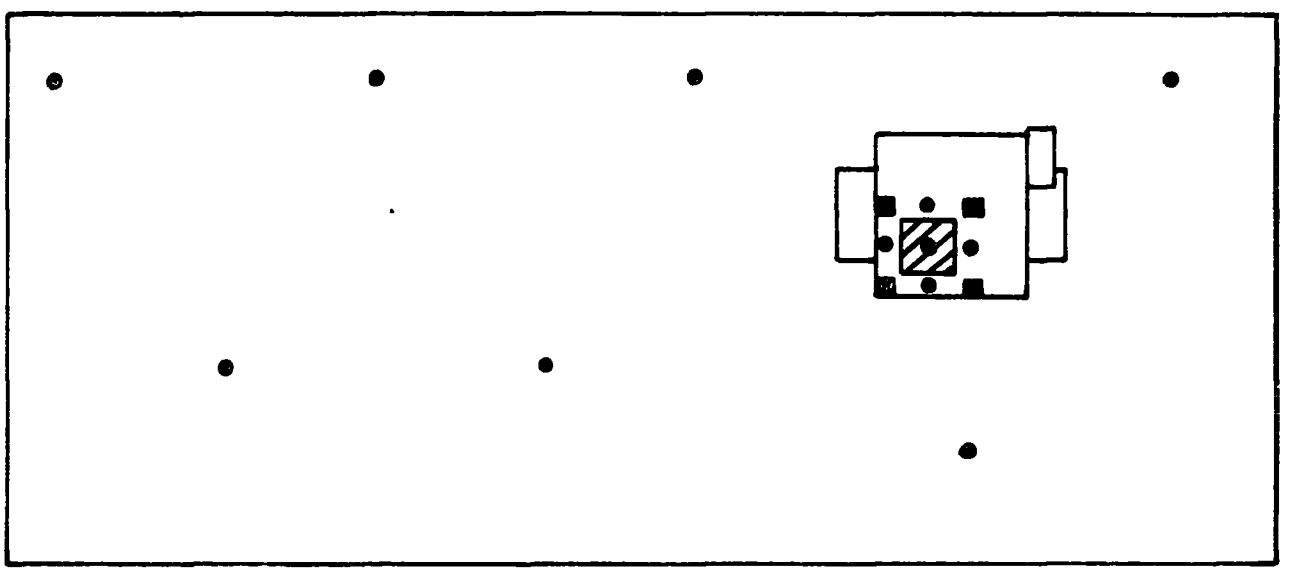

Figure 2.10 Plan of the E.A.S. Array at Kiel.

● = 1m^2 scintillation counters.

■ = 4m^2 scintillation counters with additional fast timing photomultipliers.

▨ = 32m^2 Neon hodoscope.

(After Bagge et al. [1965])

data obtained in this experiment.

This air shower experiment was considerably extended and modified by Bagge et al (1977) in order to obtain more detailed and more accurate information on the region of the core of each recorded shower. The new array contained the following detectors:

1. 27 Unshielded scintillation counters to be used in the determination of the shower size and the core location.
2. 11 Scintillation counters connected with 22 fast timing channels to measure the arrival direction of the detected showers.
3. The 32 m^2 neon hodoscope used in the previous experiment and again used for the same original purpose.
4. 13 Scintillation counters shielded by 2 cm of lead to study the energy flow of the electromagnetic component in the EAS.
5. Another neon hodoscope consisting of 367, 500 flash-tubes covering a total area of $64m^2$ and placed under a layer of 880 g/cm^2 of concrete to detect the shower muons and hadrons.

2.5.4 The France-Poland Experiment

This experiment was carried out by Catz et al (1975) where an equation was assumed to represent the lateral distribution of particle densities as registered by liquid scintillation counters for shower sizes in the range from 1.0×10^5 to 5.0×10^6. The equation (4.3) was similar to that of the Kiel group (2.5) with a slight modification made to give a better agreement with their experimental data. The validity of the Catz equation was found to extend over radial distances from 2 m to at least 70 m. The arrangement used in that experiment is shown in figure 2.11. This figure shows that the array consisted of seven liquid scintillation counters each of an area of 1 m^2 which were placed in a horizontal plane. These counters were used to measure the particle

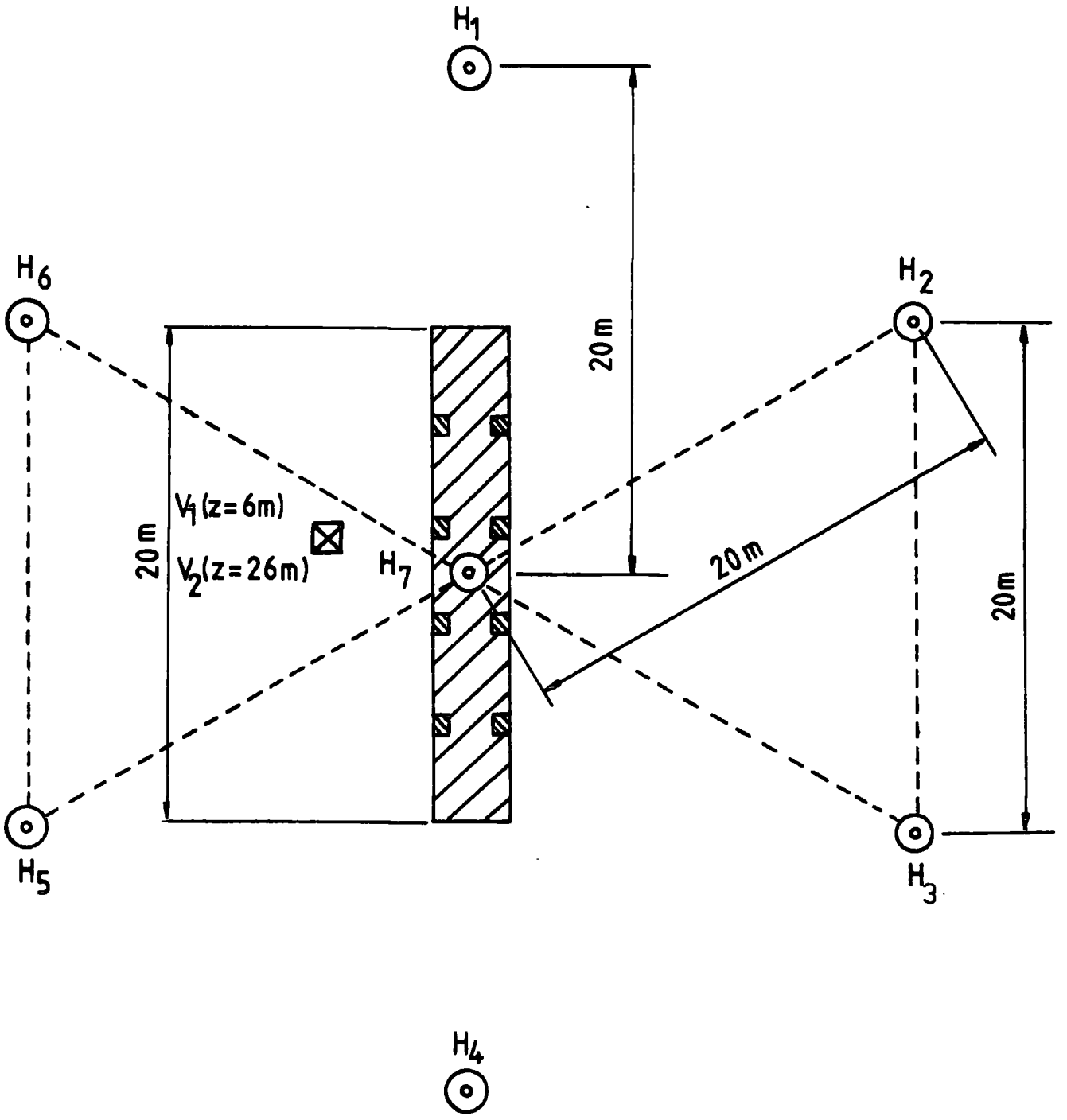

Figure 2.11 The plan of the E.A.S. array used by the France - Poland group.

▨ : Electron detector (Geiger Müllar counters).

▨ : Muon detector (Geiger Müllar counters).

⊙ : Electron detector (liquid scintillation counter + photomultiplier).

⊠ : Electron detector (liquid scintillation counter + fast photomultiplier).

(After Hochart, 1976)

density and four of them were also used to determine the time of arrival of the shower front at each. Figure 2.12 illustrates one of the scintillation counters. In addition to these counters, there were two hodoscopes. The first one consisted of 8 boxes of 9 Geiger counters, each having an area of 130 cm^2, to measure the density of electrons. The second hodoscope consisted of 200 boxes of Geiger counters each of 1500 cm^2 area. This hodoscope which had a total area of 30 m^2 was placed under 40 cm concrete, 30 cm lead and 10 cm iron such that muons of energies greater than 1 Gev only could be recorded.

In this experiment, the equation assumed for the lateral distribution (4.3) was used to find the core positions of about 25,000 showers with an accuracy of 2 to 3 metres. Using these locations, the lateral distribution of the densities at the Geiger counters was deduced. This was done by obtaining the densities at the G.M. counters for every localised shower and comparing these densities with those expected from the previously assumed formula to get the ratio of the G.M. to scintillation counter densities as a function of distance from the shower core. The lateral distribution of G.M. densities was then obtained by combining that ratio with the lateral distribution of the scintillation counter densities. It was found that there was an agreement between the lateral distribution of electrons measured by G.M. counters and the Nishimura-Kamata- Greisen function (2.2) with an age parameter, s, of about 1.25. As for the lateral distribution of densities measured by the liquid scintillation counters, it was found to be clearly steeper than that of the G.M. counters at radial distances below 20 metres from the shower core.

2.5.5 The Moscow Experiment

Alexeyev et al (1977) carried out an experiment to study the lateral distribution of electrons in EAS with $N_e \geq 2.0 \times 10^5$. The detector arrangement

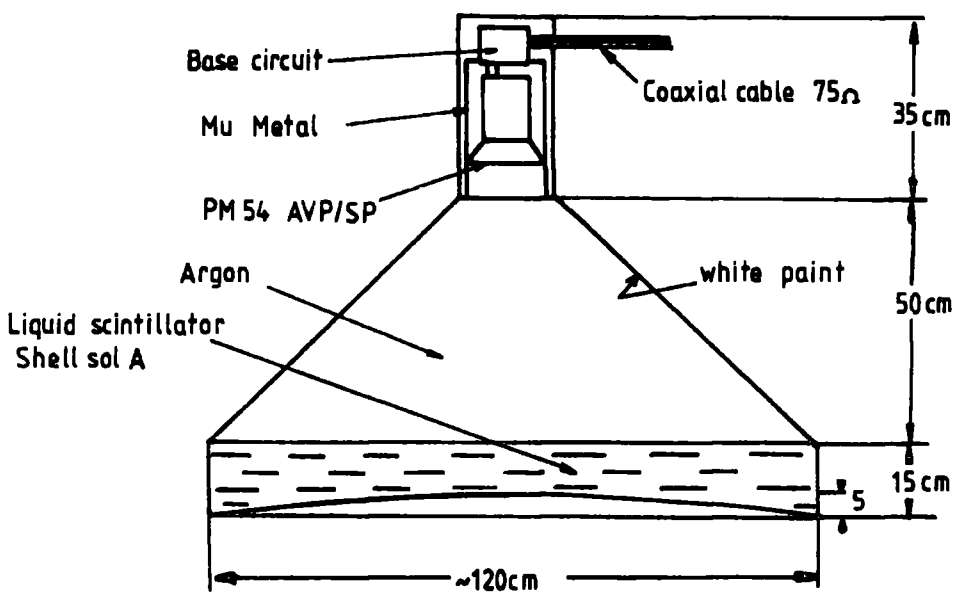

Figure 2.12 The liquid scintillation detector used in the France - Poland experiment. (After Hochart, 1976)

is shown in figure 2.13. The main detecting array which was called the 'Carpet' consisted of 400 liquid scintillation counters arranged in a horizontal square of 14 x 14 m^2. Each of these detectors was 70 x 70 x 30 cm^3 in size and viewed by a single photomultiplier. This main part was placed inside the building. Outside the building there were 6 detectors placed such that four of them were at 30 m and the remaining two were at 40 m from the centre of the array. Each of these outside detectors consisted of 18 scintillation counters of a total area of $9m^2$ as well as three sets of Geiger-Müller counters. The first set consisted of 24 counters each of area 21 cm^2, the second of 24 counters each of area 100 cm^2 and the third of 72 counters each of area 330 cm^2. Two other G.M. trays were placed on the roof of the building near the centre of the array and higher than the Carpet level by 10 metres. These trays contained two sets each of 48 counters. The area of each counter in the first set was 21 cm^2 while that of each in the second set was 100 cm^2.

In order to obtain the required lateral distribution, the angles of the arrival direction of each recorded shower were determined using the delays of outward detectors relative to the central plastic scintillation counter. Only showers with zenith angle $\theta < 30^o$ were included in the data analysis. In the calculation of the core location, the data from the central 400 detectors only were considered and these data were fitted by the Nishimura-Kamata-Greisen function (2.2) using the least squares method. The shower size and the age parameter were also determined. The showers which had their cores inside the central array were the only ones to be finally analysed. The data obtained by the scinillation counters of the outward detectors were used to determine the shower size N_e. All the densities measured by the scintillation detectors and by the G.M. counters were then normalised

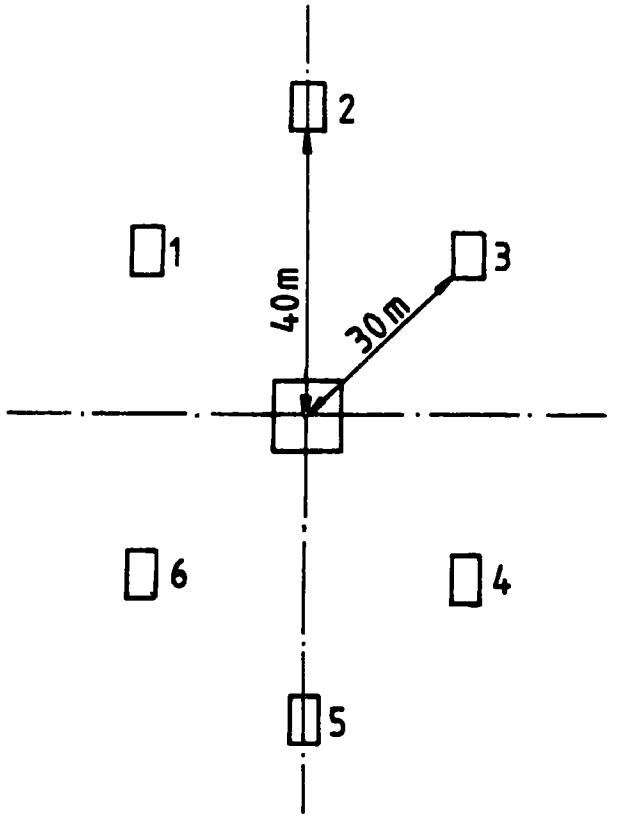

Figure 2.13 A Plan Of The Moscow Air-Shower Array.
(After Alexeyev et al. [1975])

to this N_e to be used in the deduction of the average lateral distribution function. It was found that the lateral distribution of the scintillation detectors was steeper than that of the Geiger counters and that whilst the lateral distribution of the Geiger counters could be fitted well by the N.K.G. function with an age parameter, s, of 1.1, it was not possible for that of the scintillation detectors to be fitted by the function with a single value of s over the complete range of radial distance.

CHAPTER THREE

DURHAM EXTENSIVE AIR SHOWER EXPERIMENT

3.1 Introduction

The air shower produced as the result of the interaction of a primary cosmic ray with an air nuclei has the property of extending over a large area at the level of observation. Consequently, the detectors used in an air shower array may be spread over a similar area. The upper limit of shower size which can be correctly analysed follows the size of the array detecting it.

Two important reasons were behind the idea of building the Durham EAS array. The first of these reasons was the need to have data on particles accompanying the muons traversing the Magnetic Automated Research Sepctrograph (S3.5). The second, was that the hadron studies using the flash-tube chamber (Cooper, 1974) required the knowledge of the size and location of the extensive air showers accompanying the recorded events.

The work for this array started in 1973 and was completed in 1977 when 8 liquid scintillation counters were added, as part of this research, to the initial 14 plastic detectors in order to improve the accuracy with which the parameters of the showers falling within the array could be calculated. Figure 3.1 illustrates the location of each of these detectors together with the MARS spectrogeaph and the flash-tube chamber. This figure shows that the array has an equilateral triangular symmetry which was governed to a great extent by the sites available for the detectors. The data obtained from a symmetrical array can also be used to detect any possible detector biases. Some of the particle detectors of the array are located on the roof of the Physics Department while others are placed on the ground around the Department. The array has a diameter of 120 m. Owing to the location of some of the detectors near walls or buildings, the maximum zenith angle of the showers which

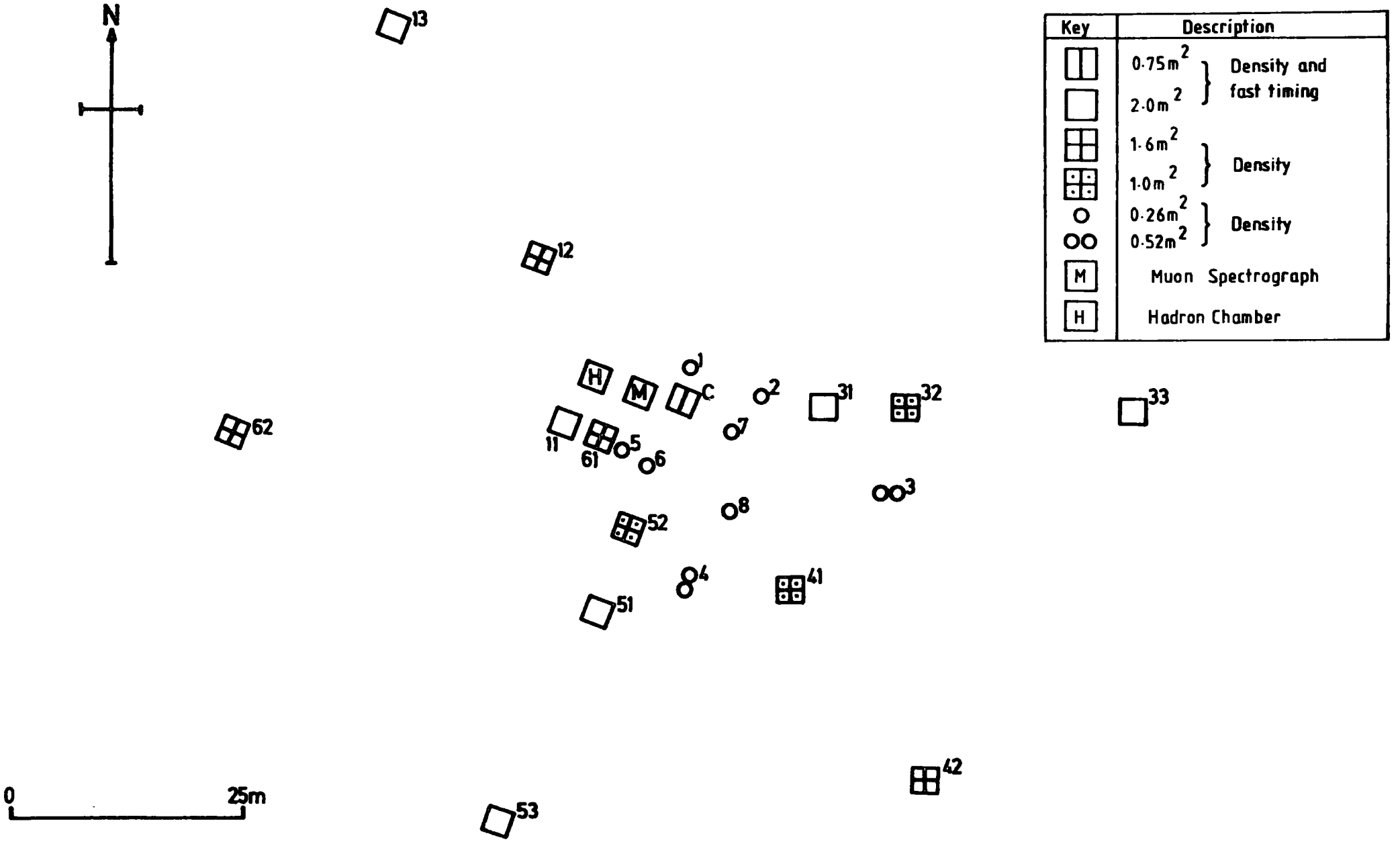

Figure 3.1 The Durham Extensive Air Shower Array

can be accepted for the data analysis is somewhat restricted. In fact, all the detected showers are analysed but for the spectrum measurement and for studying the characteristics of the showers only those with cores falling within the array and with zenith angles less than 30^{o} are utilised.

3.2 The Plastic Scintillation Counters

The plastic counters present in the array can be classified into four main groups according to their areas. Figure 3.2 shows the features of these detectors. The density pulses (3.4.2) from the detectors of the first and the last of these groups are chosen to trigger the array. These detectors also provide timing pulses (3.4.1) according to which the arrival direction of the shower front is calculated.

The first group comprises only one detector which has its position at the centre of the array. It has a geometrical area of 0.75 m^2 and consists of two identical halves of 5cm thick slab of NE102A plastic scintillator. Each of these halves is viewed by three photomultiplier tubes. Two tubes are Philips 53AVP type and these are used for the purpose of measuring the density of the particles passing through the detector. The third tube which is a Philips 56AVP is used to supply the timing pulse that is taken as the reference of the timing pulses from the other detectors.

There are three detectors in the second group each having an area of 1.0 m^2 and consisting of four identical 5 cm thick quarters of unknown scintillator composition. These detectors are different from all others as they have their photomultiplier tubes facing the broad surface of each of the four quarters. This has the advantage of giving each detector a response which is quite uniform over the detector area.

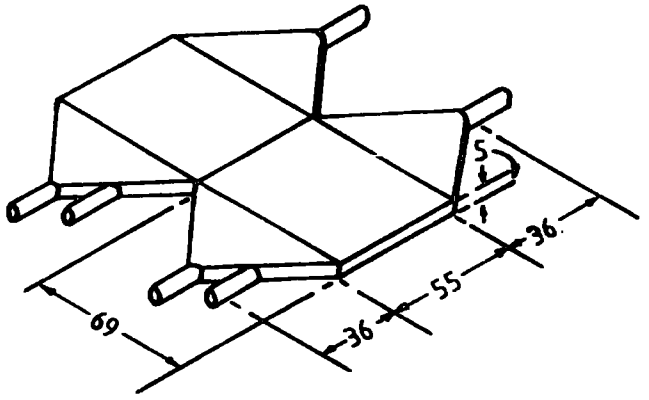

(a) The central detector (NE102A).

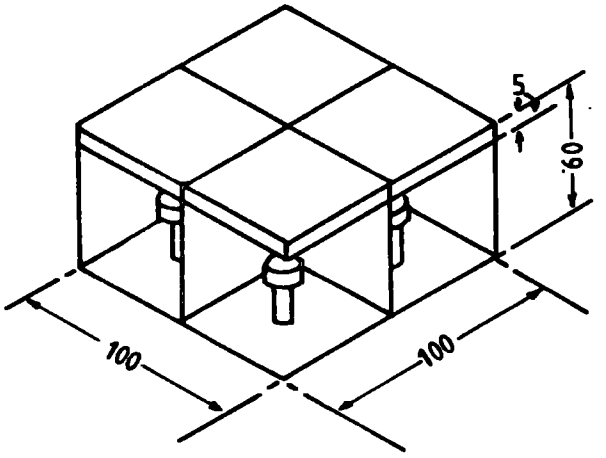

(b) A 1·0 m^2 detector (composition unknown).

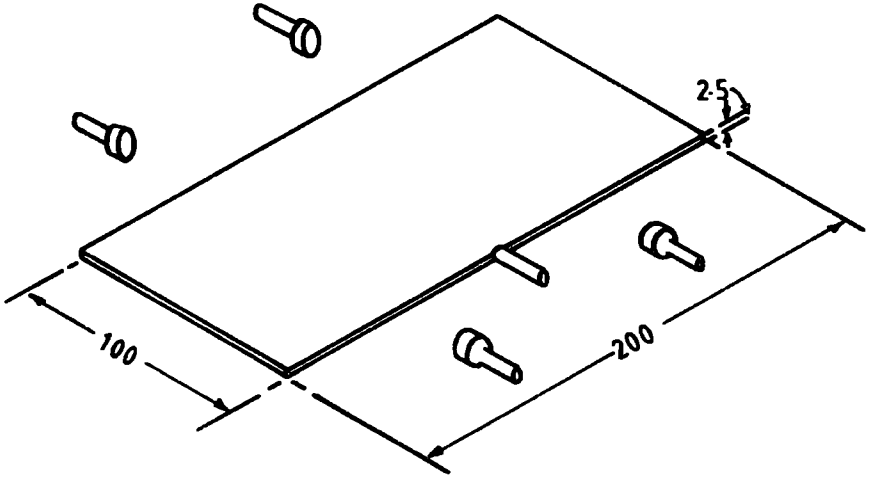

(d) A 2·0 m^2 detector (NE110).

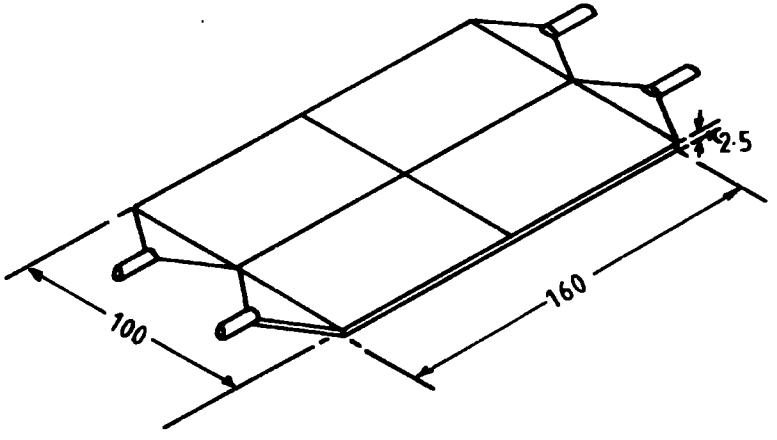

(c) A 1·6 m^2 detector (NE102A)

Figure 3.2 The Array Plastic Scintillation Counters.
(After Smith, 1976)

The third group can be divided into three subgroups having areas of $1.6m^2$, $1.2m^2$ and $0.8m^2$. Each of the detectors has a thickness of 2.5 cm and is made of the same material used for the central detector. There is only one detector in the first and the third subgroups while there are two detectors in the second one. All of these detectors are viewed by Philips 53 AVP photomultiplier tubes.

Concerning the fourth group, it contains six detectors which are the backbone of the array. They are characterised by an area of $2.0m^2$ and consist of a single piece of NE110 plastic scintillator of thickness 2.5 cm. As mentioned before, they provide both density and timing pulses which are obtained from each detector by using four 5" diameter EMI 9579B photomultiplier tubes and one 2" diameter Philips 56 AVP tube respectively.

Each plastic detector is enclosed in a wooden weather proofed box containing also the photomultiplier tubes. The E.H.T. unit and the head amplifer, described in detail by Smith (1976), are mounted on one edge of the box. These boxes rest on iron frames. Both the box and the frame are inside a wooden weather proofed hut.

3.3 The Liquid Scintillation Counters

In the array, there are 10 liquid scintillation counters each having an area of $0.26m^2$. At two places in the array, two of these detectors are connected together using a mixer which will be described later, to give detectors of $0.52m^2$.

In each of these 10 counters, there are 53 litres of liquid scintillator giving a scintillator thickness of 20 cm. This liquid consists of 91% Medicinal Paraffin and 9% Shellsol 'A' mixed with about 33 grams of P. Terphenyl and 0.55 grams of POPOP. This mixture was prepared by adding the P. Terphenyl to the Paraffin and heating both up to about $90^{\circ}C$ till the P. Terphenyl was completely dissolved. Then

the mixture was heated again together with the POPOP up to 70°C. After dissolving the POPOP, the mixture was left to cool before adding the Shellsol.

These detectors are located near the centre of the array as shown in Figure 3.1. Five of them have their positions on the roof of the Physics Department, two including a double one, are placed on the parapet of the roof and one is located in the laboratory near to the Magnetic Spectrograph. Each of the two detectors which are on the parapet is raised off that parapet by two wooden supports about 10 cm thick, while each of the other detectors is resting on an iron frame about 53 cm above the roof level. On the top of each detector, there is an aluminium weather proofed cover of a conical shape to prevent any possible damage due to the rain. One of the single liquid scintillation counters is shown in Figure 3.3.

The liquid in each detector is viewed by a single E.M.I. 9530 5" diameter photomultiplier tube facing the surface of the liquid. Consequently, the response of these detectors is very uniform over all the detector area. Figure 3.4 illustrates the base circuit of this tube which is of the high current type in order to achieve good linearity for big pulses. This tube operates with positive E.H.T. fed to its anode through a charge sensitive amplifier (C.S.A.) placed in the laboratory (3.4.2). The cable which takes the E.H.T. to the tube is also used to carry the tube's pulse to the input of the C.S.A. The pulses obtained at the anode of this tube are negative and characterised by an exponential decay time constant of about 200 ns The linearities of the used tubes were tested using a pulsed L.E.D. capable of generating phototube pulses similar to those produced as a result of the passage of real cosmic ray particles through the scintillation counters. Two filters acting as analyser and polariser

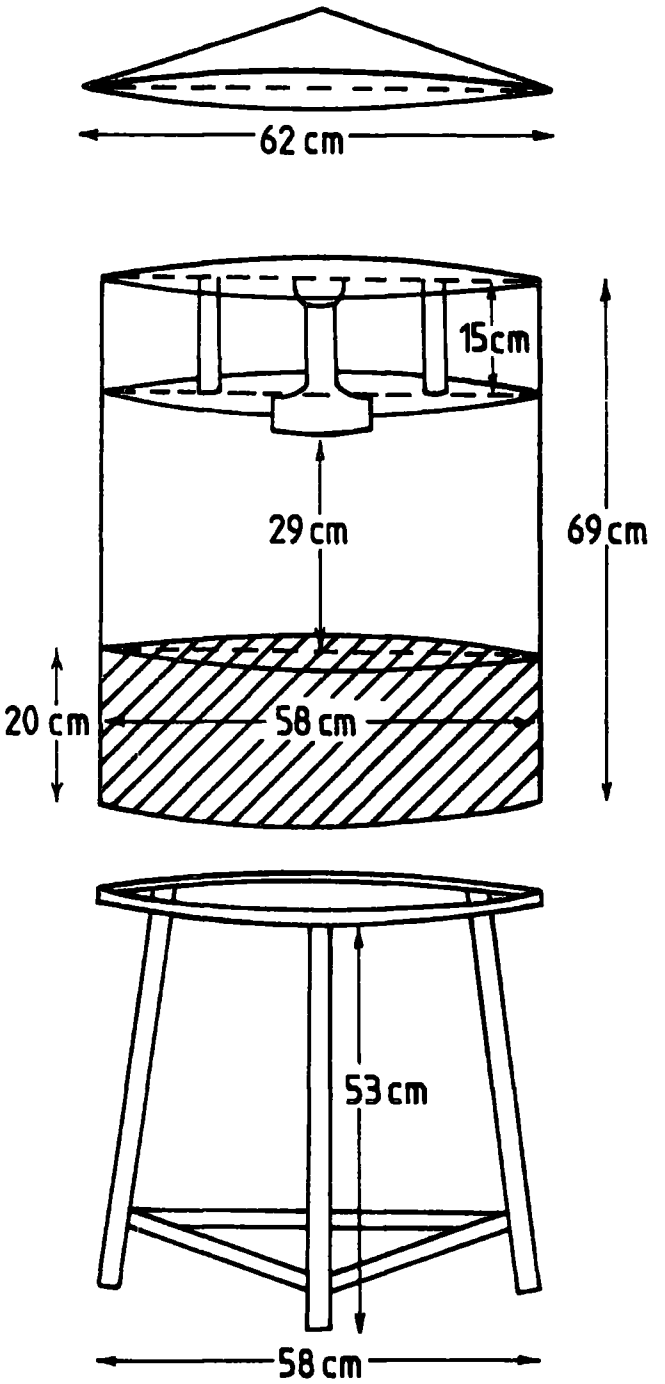

Figure 3.3 Liquid Scintillation Counter Arrangement.

(a) Weatherproofed Aluminium Cover.

(b) The Counter.

(c) Iron Frame.

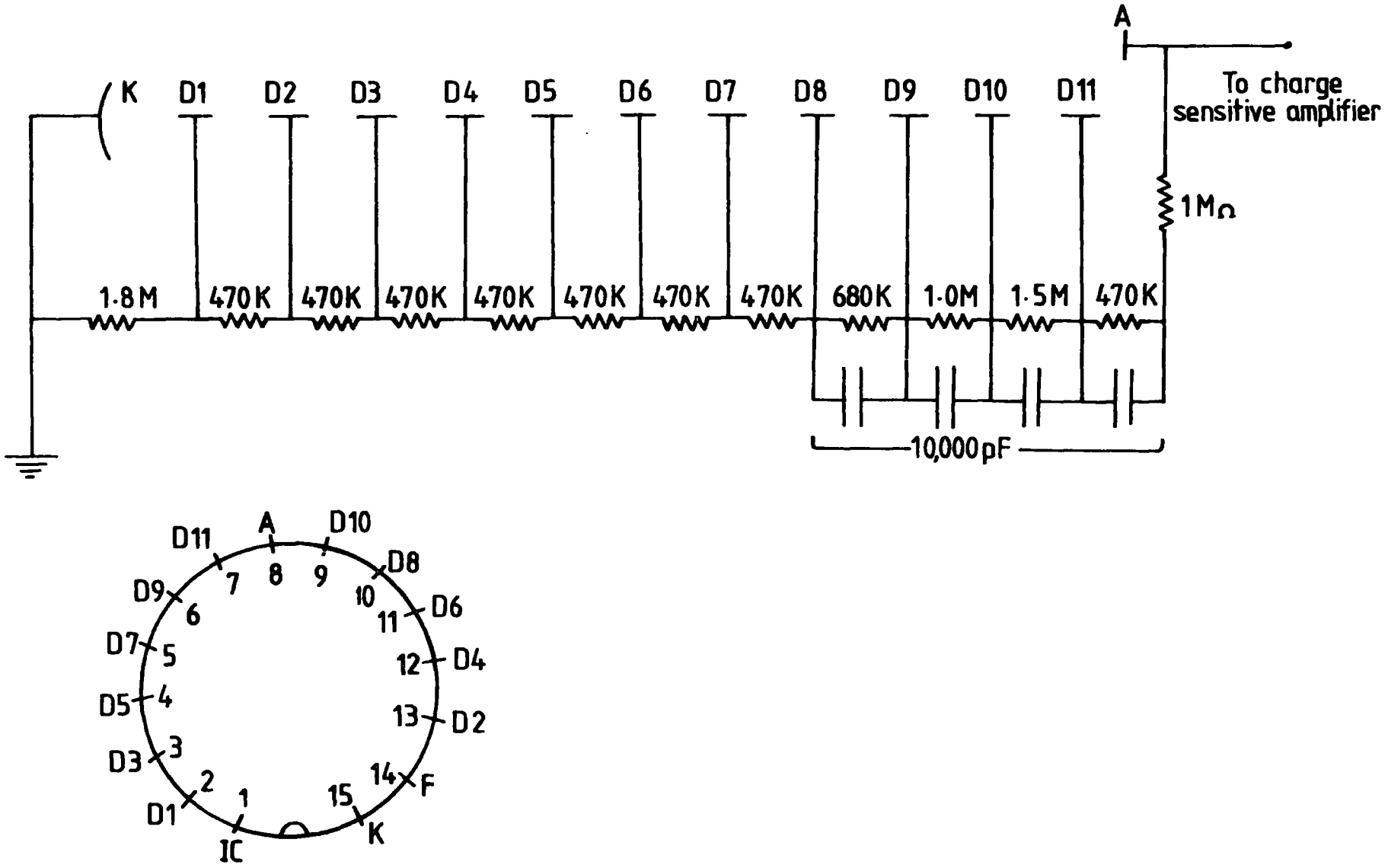

Figure 3.4 The Base Circuit For The Liquid Scintillation Counters' Photomultiplier Tubes.

were placed between the L.E.D. and the tested tube. By changing the angle θ between the planes of polarisation of these two filters the intensity of the light coming from the L.E.D. and falling on the photocathode of the tube would be altered following an intensity $\alpha \cos^2\theta$ law. The output pulses of the C.S.A. through which the E.H.T. was fed to the tested tube, were taken to an oscilloscope to measure their maximum heights. The nonlinearity of the C.S.A., which will be described later in this chapter, was taken into consideration in this test. Figure 3.5 shows the results obtained for one of the photomultiplier tubes which operates on an E.H.T. of about 1.01 kv. From this figure, it is clear that for this E.H.T. value, the tube is quite linear.

The high voltage required to run the ten photomultiplier tubes used for the liquid scintillation counters, is supplied by an E.H.T. unit which is set to 2.0 kv in the laboratory. The output of this unit is connected to the inputs of two potential distribution units such that each of the ten output voltages goes to one of the tubes via a charge sensitive amplifier. One of these two units is shown in Figure 3.6. By adjusting the resistance of each of the five resistor chains, each tube was supplied with a suitable operating voltage. The 0.1 μF capacitors are used to prevent any electrical signal passing from one charge sensitive amplifier to the other.

A calibration of the liquid scintillation counters was carried out to determine the E.H.T. which should be supplied to each photomultiplier tube to give the tubes near identical responses. For this purpose, a pulse height analyser (P.H.A.) was used. The easiest quantity to be measured when a particle distribution is obtained on the P.H.A. is the peak or the mode of the distribution rather than its mean. However, the mean pulse height is the parameter which varies in proportion to the

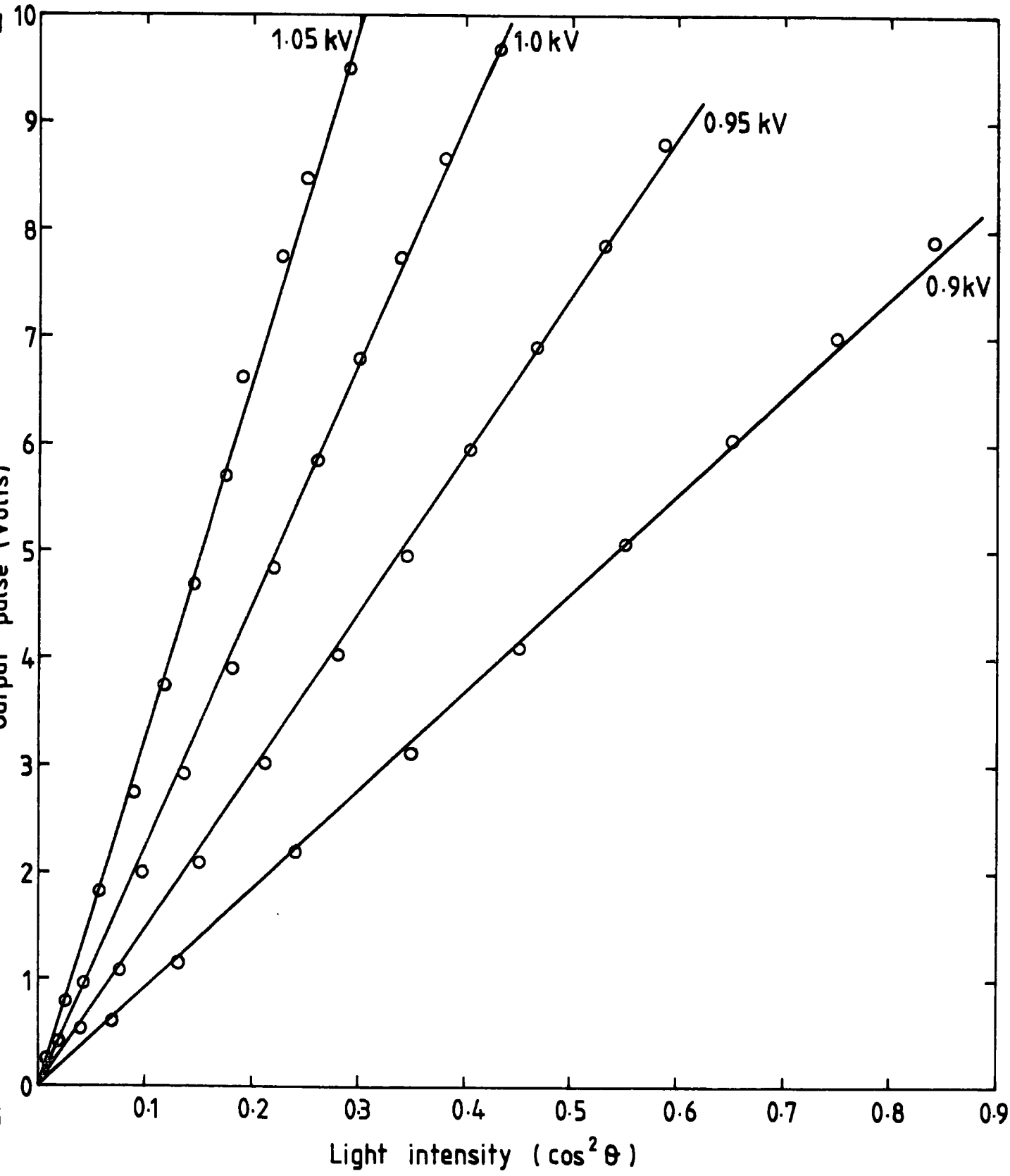

Figure 3.5 The Linearity Of A Liquid Scintillation Counter's Photomultiplier Tube.

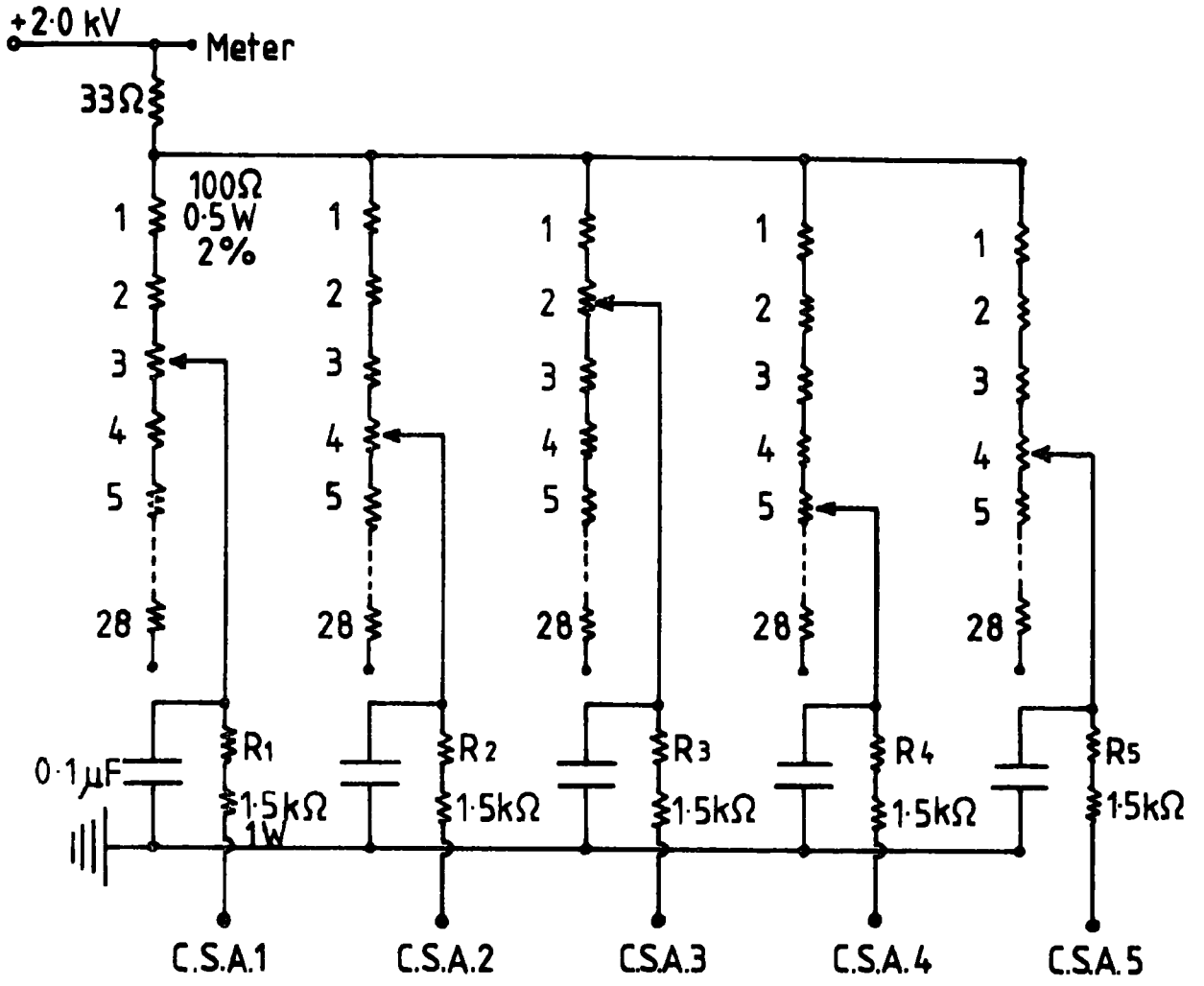

Figure 3.6 The Potential Distribution Unit.

number of the particles passing through the detector, hence the detectors were always calibrated on the mode and the ratio mean to mode was calculated initially from one distribution. The chosen value of the mode of the particle distribution for particles crossing the detector in a near vertical direction was 50 $\pm$ 10 mv.

For one detector, the distribution of the output pulses of the C.S.A. connected to its photomultiplier tube was obtained twice, namely when the particles were traversing the detector in almost a vertical direction and also when they were coming from all directions. It was found that the mode of the vertical distribution was shifted by 6% towards smaller pulse heights with respect to the second one.

The first distribution, the nearly vertical one, was obtained using an ancillary scintillator telescope. This telescope consisted of two small plastic detectors, one being placed on the top of the liquid counter and the other below it where a vertical line passed through the whole system. The positive E.H.T. needed to run each of these small detectors was provided through a C.S.A. The outputs of these two C.S.A's were discriminated above a chosen threshold level. The output standard logic signal of each discriminator was fed to the input of a coincidence unit such that its output was used to open a gate on the Analogue to Digital Converter (A.D.C.) of the P.H.A. Thus the pulse height distribution of the tested liquid scintillation counter was built up on the screen of the P.H.A. By measuring the mode of this distribution, the detector was easily calibrated.

Since as mentioned before, the C.S.A. connected to the tube under calibration has a non linear relation between its charge input and output voltage, then the mean of the previously obtained distribution could not be used to present the pulse height due to a single particle crossing the detector in almost a vertical direction. The true

representation should be the mean of the distribution of the charge packets from the photomultiplier tube itself and which are the inputs to the C.S.A. Owing to the presence of the E.H.T. accompanying the tube pulses, it was not possible to get this distribution directly on the P.H.A. So the method used was to deduce this required distribution from the already obtained one by using the calibration curve of the C.S.A. (Figure 3.9). The contribution of two and more particles to the distribution was considered to find a more true distribution of the tube's pulses for single particles passing through the detector in a near vertical direction. The mean of the final distribution was calculated and the ratio mean to mode was found to be 1.1.

It was found that the value of the input voltage to the C.S.A. corresponding to the mode of the nearly vertical distribution of the C.S.A's output pulses was the same as the mode value of the distribution of the photomultiplier tube's pulses obtained when single vertical particles traversed the detector. Therefore, it was decided to calibrate each of the detectors on the mode of the outputs from the charge sensitive amplifier for particles coming from all directions, shift that mode by 6% to the left, find the corresponding input voltage and then multiply it by the calculated ratio of 1.1. The resultant quantity was taken as the value of the pulse height obtained at the anode of the photomultiplier tube when a single particle crossed the detector roughly in a vertical direction.

3.4 The Electronic Instrumentation

The following sections describe the electronic processing of the pulse heights produced at the plastic and liquid scintillation counters of the array in order that subsequently the parameters characterising each recorded shower event could be deduced. These parameters are the arrival direction of the shower, the shower size

and the core location of the shower. To produce these parameters, the primary data must be coded and stored in a form which enables the pulses from the timing and the density detectors to be interpreted in terms of time measurements and particle densities respectively when the stored data are analysed afterwards. The Durham array is on-line to an IBM 1130 computer which achieves a quick coding and storing of each event as well as avoiding the use of any photographic technique for the purposes of data recording. The data are primarily stored on a magnetic disc in binary form.

3.4.1 The Timing Pulses

As was mentioned before, the $2m^2$ detectors are used with the central detector to generate the array fast timing pulses. These pulses which are negative of 5ns width and semi-gaussian shape, enable the direction of arrival of each shower event to be calculated when they are converted to analogue form using Time to Amplitude Converters (T.A.C's). The timing pulse coming from the central detector is chosen to be the reference for all the other timing pulses since it is always the first to arrive to the laboratory for all shower angles. Accordingly, this pulse is used to start all of the T.A.C's and subsequently each T.A.C. is stopped afterwards by a timing pulse from one of the other timing detectors. The heights of the outputs of these T.A.C's, which are positive rectangular pulses of 5μs width, are directly proportional to the difference in time between the arrival of the 'start' and 'stop' pulses. Therefore, for a detector through which the shower front passes first, the corresponding T.A.C. output is expected to be smaller than those connected to particle detectors through which the shower front passes later. Care must be taken to eliminate the delay effect of the cables as well as the electronic circuits in order to deal only with genuine time difference. This has been explained in detail by Smith, (1976).

The block diagram of the array electronics is shown in Figure 3.7. It can be seen that the timing pulses are amplified and discriminated, using fast amplifiers and fast discriminators, before going to the T.A.C's.

3.4.2 The Density Pulses

The density pulses from each plastic detector's set of photomultiplier tubes are summed and amplified using pre-amplifiers, described by Smith (1976), before entering the laboratory. In the case of the liquid detectors, the charge coming to the laboratory from each photomultiplier tube goes to the input of a corresponding charge sensitive amplifier, which integrates the output signal current of the detector. The E.H.T. required to operate the tube passes through a resistor of 100 KΩ and then to the input of the amplifier which is connected to the anode of the tube. A big capacitor is used to isolate the E.H.T. from the rest of the amplifier. The input and output impedances of the C.S.A. are about 50 Ω and a few ohms respectively. The schematic diagram of one of these C.S.A's is shown in figure 3.8. In this amplifier a capacitor is used to feed back the output to the input stage. The voltage of the output pulse v_{out}, is proportional to the input charge Q_{in} which in turn is proportional to the area of the input pulse according to the following equation

$$V_{out} = \frac{Q_{in}}{c_F} = \frac{1}{c_F} \int I_{in}\, dt = \frac{1}{c_F R_{in}} \int V_{in}\, dt = \frac{1}{c_F R_{in}} \text{Area}_{in} \qquad 3.1$$

where c_F is the feed back capacitor.

In other words, V_{out} is proportional to $V_{in} W_{in}$ where W_{in} is the width of the input pulse. But since the widths of the pulses coming from the photomultiplier tube and going to the C.S.A. are constant, then V_{out} will be proportional to the input voltage V_{in} only. Therefore, the C.S.A's were calibrated and the relationship between the input voltage

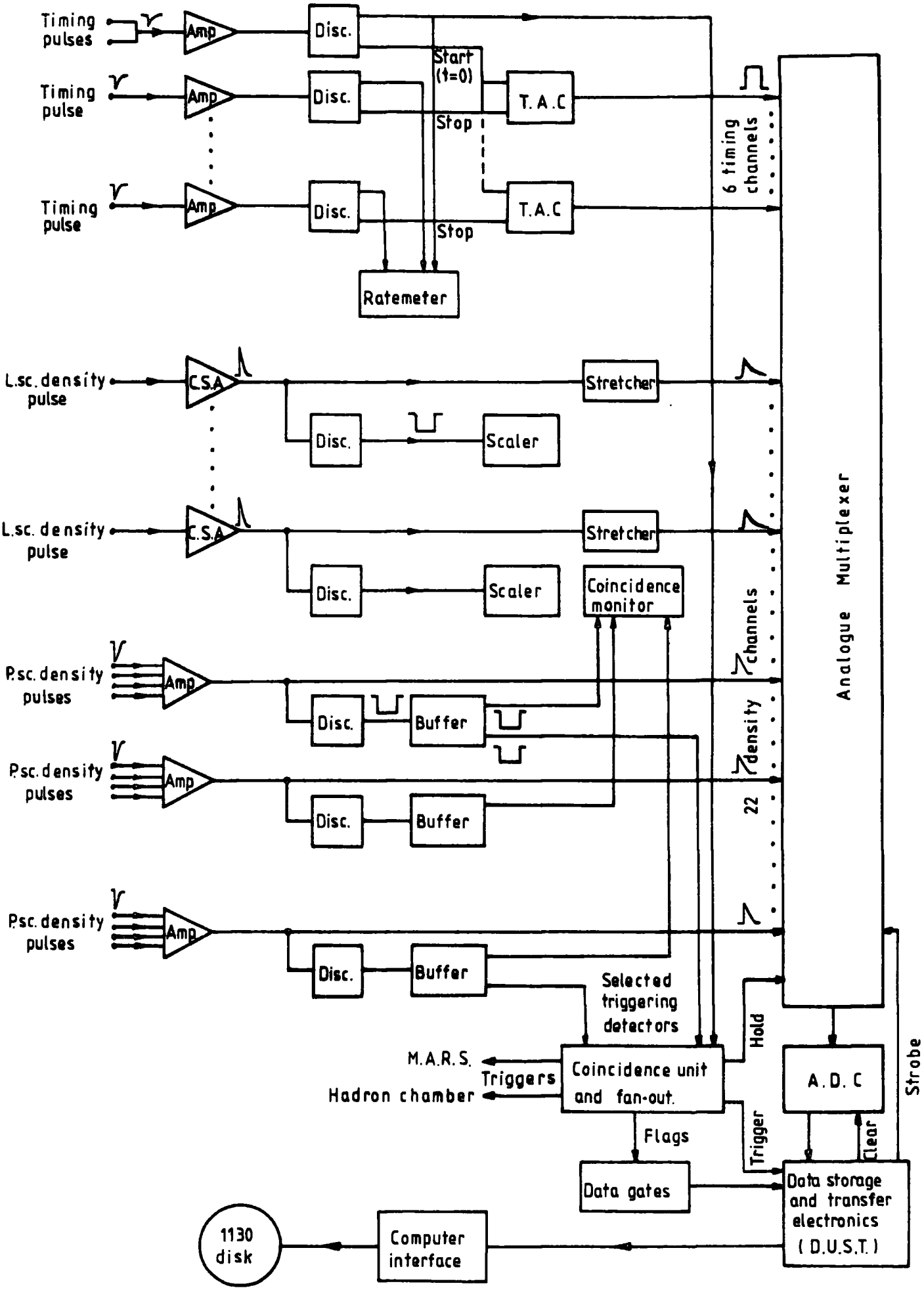

Figure 3.7 Block Diagram Of The Array Electronics.

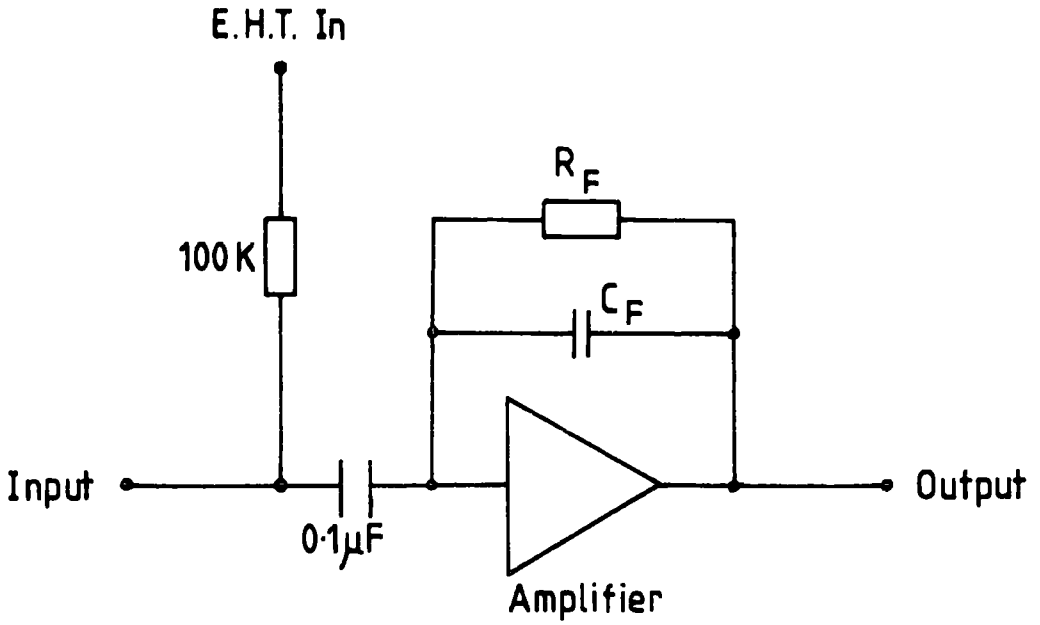

Figure 3.8 The Schematic Diagram Of The Charge Sensitive Amplifier.

V_{in}, and the corresponding output voltage, V_{out}, was found. This calibration was done when the output pulses were connected to a 50 Ω terminator and the results are represented in Figure 3.9. It can be seen that the relation between V_{in} and V_{out} is not linear for a V_{out} value up to 1v after which it tends to be linear. The decay time constant of the output pulses is about 5μs.

As was mentioned earlier, the array contains two double liquid scintillation detectors each consisting of two of the single ones combined together using a mixer. This mixer sums the output pulses of the two corresponding charge sensitive amplifiers to give a common output pulse. The mixer accepts input pulses up to a maximum of 10 volts and has a 50 Ω input impedance. It comprises two inverting amplifiers such that by connecting its output pulses to a 50 Ω terminating resistor, the overall gain of the circuit is about 0.95. The output has the same decay time constant as that of the input. Figure 3.10 illustrates the mixer.

Each output of the head amplifiers used with the plastic detectors, and each output of the C.S.A's of the single liquid detectors and of the mixers of the double ones, is connected to the input of a discriminator. There are three discriminator units each containing eight independent discriminators. The circuit diagram of one of these discriminators is shown in Figure 3.11. The basic element of this circuit is a μA710 high speed comparator. The required discriminator level can be achieved by adjusting the variable resistor connected to the base of the first transistor and hence the potential on the non-inverting input of the 710. The discrimination level for the pulses of the central detector is chosen to be of the order of 400 mv while that for each other plastic detector is about 200 mv. For the liquid detectors, the level is chosen to be about 50 mv. The output pulses of the discriminators

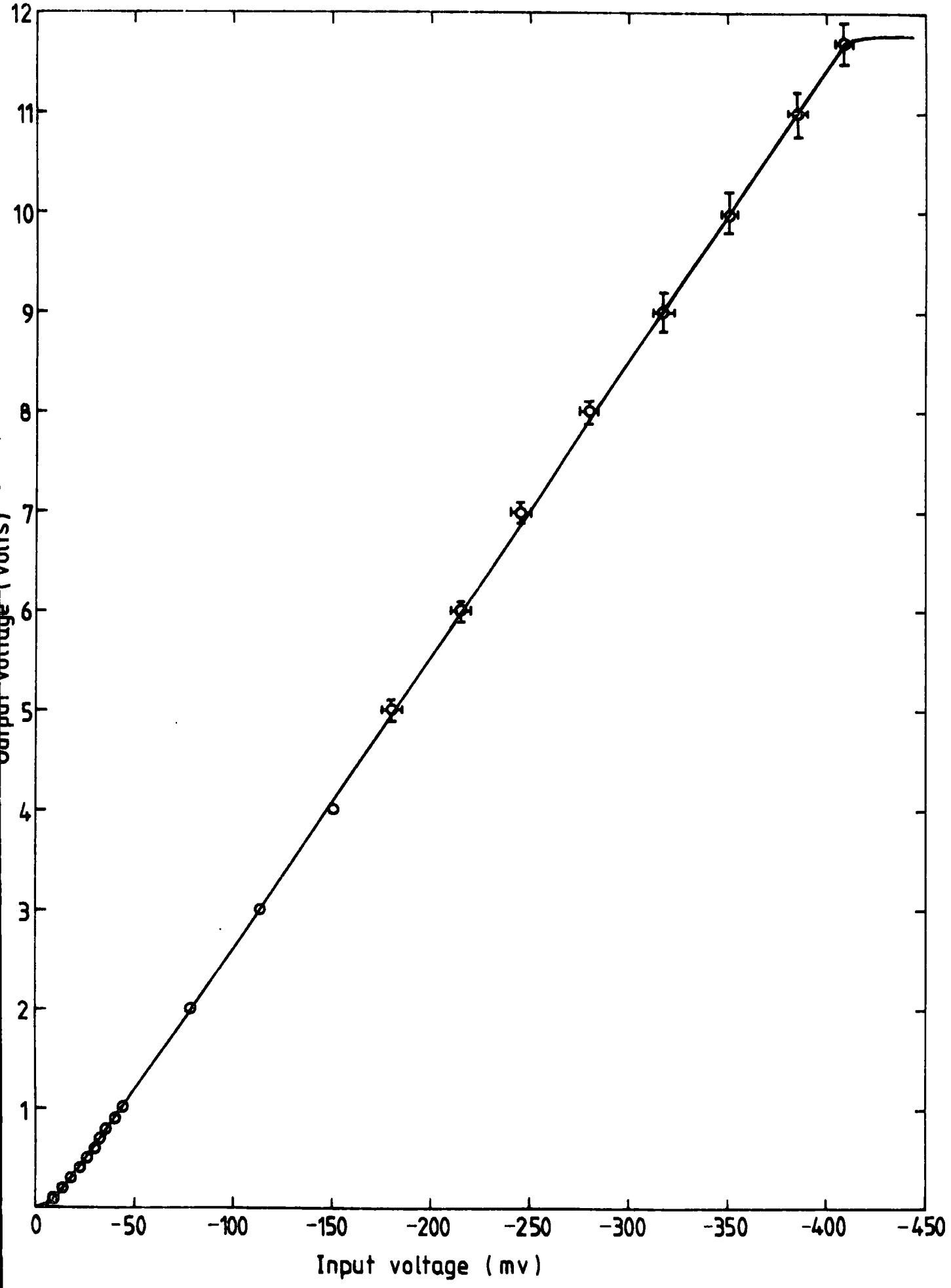

Figure 3.9 The Calibration Curve Of The Charge Sensitive Amplifier.

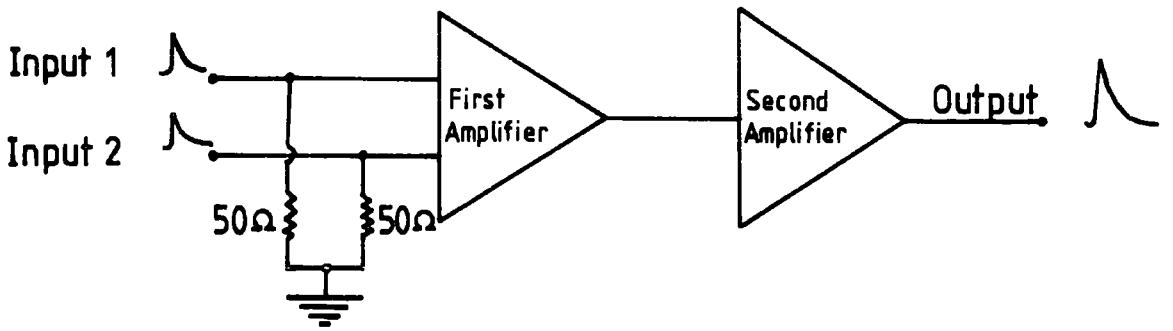

Figure 3.10 The Schematic Diagram Of The Mixer.

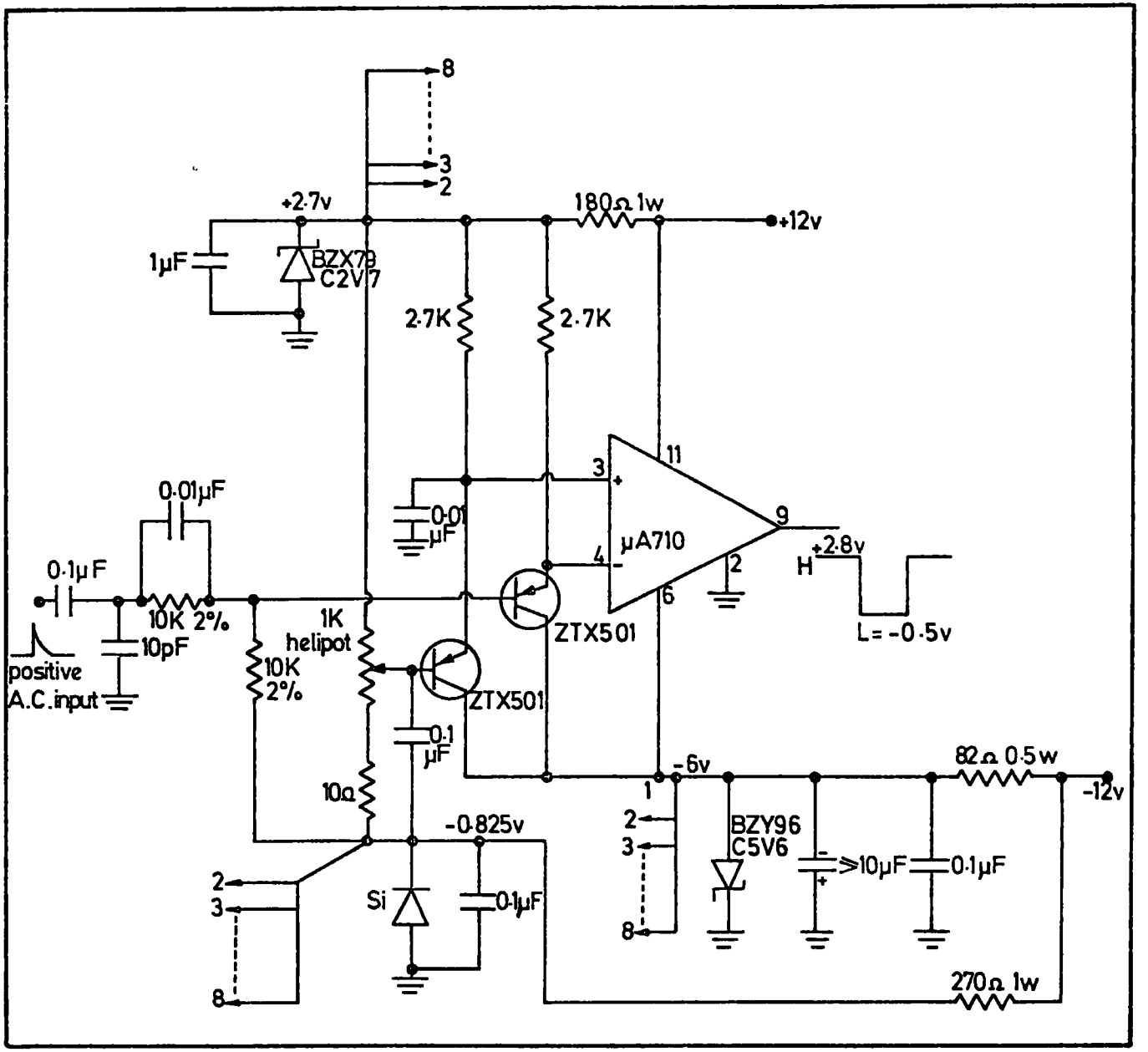

Figure 3.11 The Octal Discriminator.

are used to monitor the counting rate of each detector. The outputs of the unit to which the pulses of the central detector and the $2m^2$ detectors are connected, are also used to drive a coincidence unit such that its output triggers both the array and the spectrograph or in other words establishes the shower events. This output is produced 3μs after the arrival of the central detector's timing pulse in the laboratory.

The schematic diagram of one of the eight discriminators in the unit used for the liquid detectors is given in Figure 3.12. This figure shows that the inputs to the discriminator are also connected to a stretcher which lengthens the output pulses of the corresponding C.S.A. or mixer such that the output has a decay time constant of about 50μs. The stretcher is needed since it is found that when an event is established, the Analogue Multiplexer (described later on) which temporarily stores the shower data would otherwise store a C.S.A's or a mixer's pulse height smaller than the true value owing to the shortness of the pulse. The eight stretchers required for the eight liquid detectors are contained in one double width unit. Figure 3.13 is the schematic diagram of a stretcher which has a 50 Ω input impedance and the calibration curve of a stretcher is shown in Figure 3.14.

In the cases of the plastic detectors, the input pulses to the discriminators are taken directly to the Analogue Multiplexer (A.M.) since they are wide pulses of 20 μs decay time constant. As said before, the shower data are stored within this multiplexer for a short time before being converted into a binary form which is then permanently stored. The multiplexer consists of a Master unit and three Slave units. Each of these units has one master input and seven other inputs. Therefore, by the use of these four units, a total of 32 pulse heights can be temporarily stored. In order to hold the data within all of

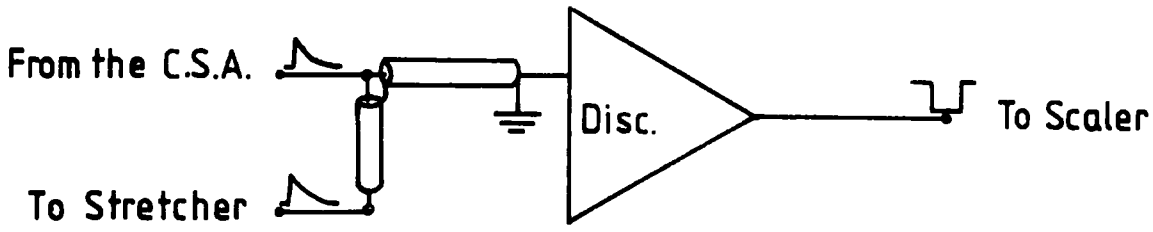

Figure 3.12 The Schematic Diagram Of The Discriminator.

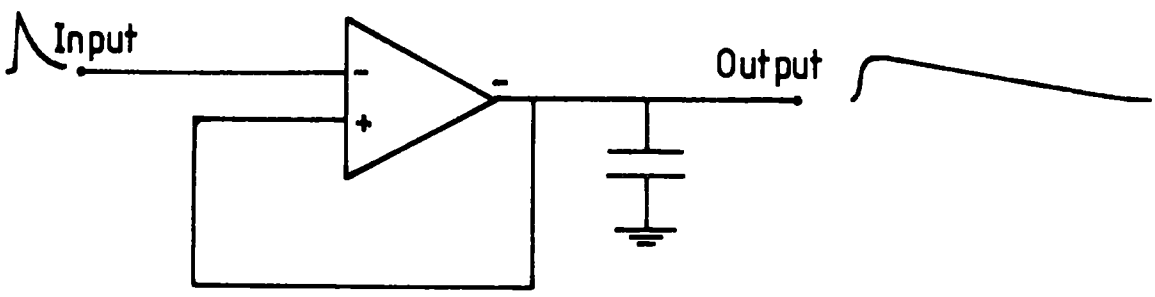

Figure 3.13 The Schematic Diagram Of The Stretcher.

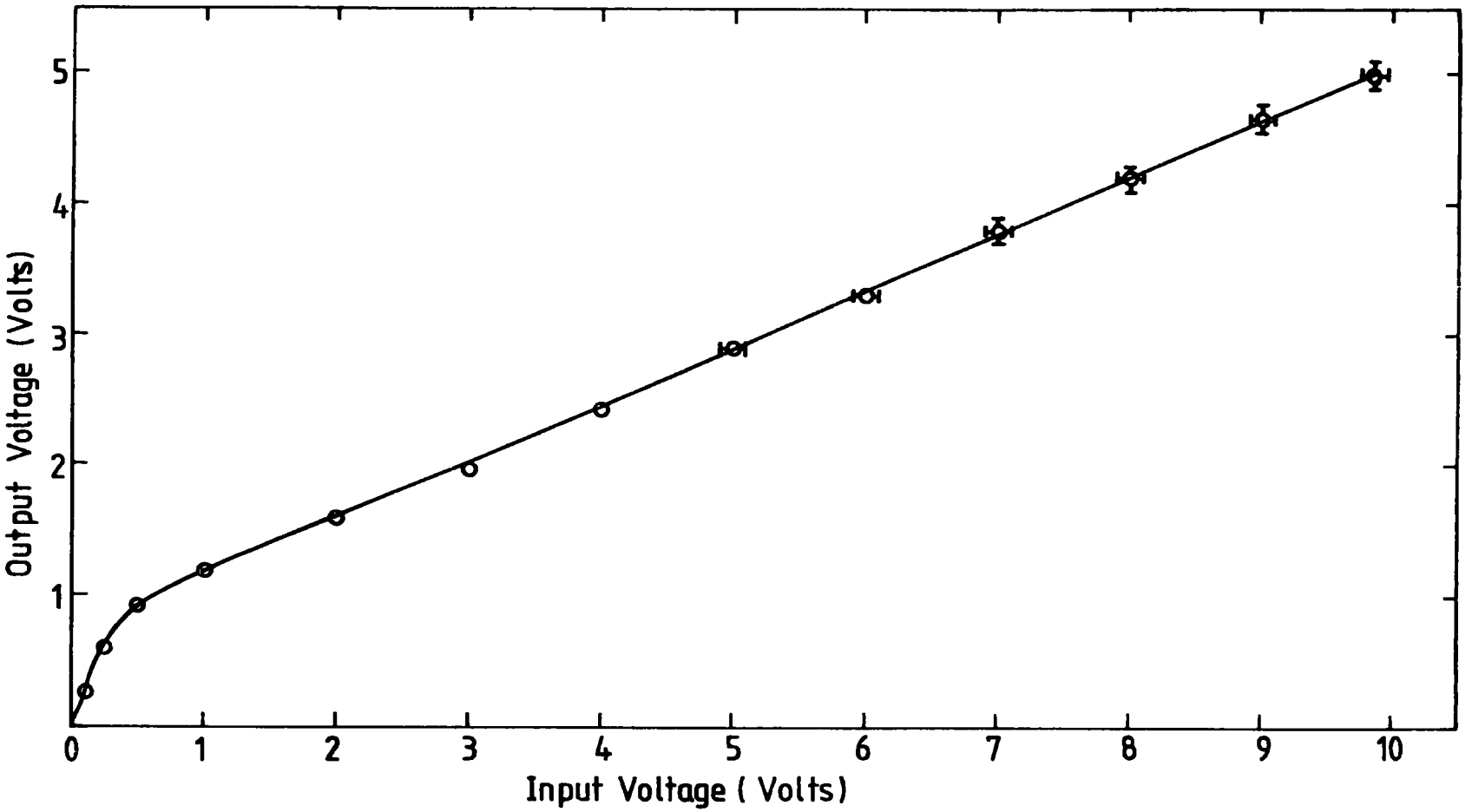

Figure 3.14 The Calibration Curve Of One Of The Eight Stretchers.

these units, a 'hold' command is generated by sending the previously mentioned coincidence output pulse to the master input of the Master unit. The Master and the first two Slave units are used for the storage of the data of the plastic detectors while the third Slave unit is used for the data of the liquid counters. The operation of this unit is shown schematically in Figure 3.15. Each input of the first three multiplexer units has an impedance of 50 Ω and accepts pulses of height ranging between 0v and 10 v. The outputs of these units are rectangular voltage pulses having a width of 4 μs and produced with a gain of 0.4. Each of the eight inputs of the fourth unit has a 1 k Ω impedance and accepts pulses with heights in the range from 0v up to 5v. Its outputs are similar to those of the other three units except that the gain with which they are produced is about 0.8.

The 32 pulse heights held in the Master and Slave units are then routed sequentially through a single output to the input of an Analogue to Digital Converter (A.D.C.). This A.D.C. has 1024 channels, operates at 50 MHz and converts its input analogue signals into binary numbers such that the magnitude of each number is proportional to the height of the corresponding input. Thus, the dynamic data are digitised.

In order to interpret and analyse each recorded air shower event, it is necessary to have a certain amount of information to identify the event and the conditions under which it was stored. Consequently, for each event the relevant information, known as the 'static' data, are stored together with the dynamic data. The static data are assembled in devices called Data Gates (D.G.). These gates consist of:

1. An Event Header which identifies the beginning of the data for every recorded event.
2. A Run Number to be used for each particular series of data collection.

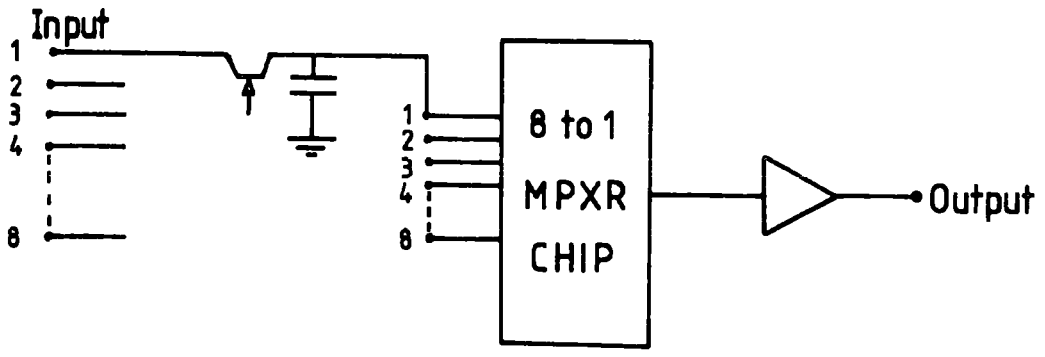

Figure 3.15 The Schematic Diagram Of The MPXR.

3. An Event number to identify individual events.
4. A Trigger Mode Data Gate which records the mode of triggering of the data storage cycle.
5. An Operational Unit Data Gate which informs the computer analysis programme which of the detectors were working when each event was recorded.
6. A Clock which allows real time information to be stored and thus the time of the event's collection is known.
7. Event End Data Gate which announces the end of the data contained in an event.

Thus by the use of the Analogue Multiplexer together with the A.D.C. and with the Data Gates which supply binary information, all the required air shower data will be in the digital form.

In addition to the generation of the 'hold' command for the Analogue Multiplexer, the output pulse of the coincidence unit is also directed into two other devices. These devices are a flip-flop to set the appropriate trigger-mode data-gate and the master control device, D.U.S.T. to initiate a data storage cycle.

The Digital Unit for Storage and Transfer (D.U.S.T.) controls the order in which the shower data are coded and stored in a temporary buffer memory. Whenan event is established and while the particle density and the fast-timing data are being stored in the Analogue Multiplexer, the output pulse of the coincidence unit generates a 'start cycle command' as it enters D.U.S.T. According to this command, the Shower Event Scaler is increased and D.U.S.T. begins to read in the first six Data Gates. Afterwards, this unit sends a strobe pulse to the Multiplexer to release the first pulse height which goes to the A.D.C. where it is digitised. The digitised data enter D.U.S.T. to be stored in the memory. D.U.S.T. then sends a clear signal to clear the A.D.C. output scaler followed by

a second strobe pulse to the Multiplexer for the second pulse height and so on until all the A.M.'s data are digitised and stored in the memory. The A.D.C. is cleared again so that it can receive the data of the next event. By the same time, the A.M. has automatically cleared itself waiting for the next 'hold' command. Finally, D.U.S.T. reads in the last Data Gate and becomes ready for the next start cycle command.

Once the memory becomes full, after the storage of the eleventh event, D.U.S.T. informs the on-line IBM 1130 to read out all the stored data and to write them on a magnetic disc where they may remain for a few days after which they are transferred to the larger IBM 370/168 computer to be analysed. After the memory has been emptied, more shower data can be acquired.

Since three separate core stores are used in the laboratory and only one cable is connected from the laboratory to the IBM 1130, an interface was constructed to enable just one core store to be emptied at a time, the others being temporarily restrained until the previous one has completed its dumping cycle.

More detailed information about the Data Gates, D.U.S.T. and the computer interface, is given by Smith (1976).

3.4.3 The Daily Checks on the Experiment

Checks were carried out daily to ensure that all the Array electronics was working correctly. The single counting rates, above the chosen discrimination threshold of each of the liquid scintillation counters and of the plastic scintillation detectors were monitored. A monitor was also used to check the coincidence rates between selected pairs and groups of the scintillation counters.

All the Analogue Multiplexer channels which acquired data during a day's run were checked. For the events recorded each day, histograms of the pulse heights stored from each multiplexer channel were obtained

by the IBM 1130 computer. These histograms were useful in that they pointed to various faults in the data collection electronics that occurred from time to time.

3.5 The MARS Spectrograph

Since the MARS spectrograph has been described in some detail elsewhere (Ayre et al., 1972 and Thompson et al., 1972), only a very brief description will be given in this section. The physical dimensions of the spectrograph as well as the positions of the detectors in the instrument are shown in figure 3.16. Briefly, MARS was a multilayer solid iron magnetic spectrograph which consisted of five levels of particle detectors separated by four rectangular blocks of iron. These magnets were used to bend the track of the cosmic ray particle traversing the spectrograph and the amount of bending was a measure of the momentum of that particle. The function of the detectors was to define and locate the particle's trajectory. Two types of detectors wereused in MARS, plastic scintillators and neon flash-tubes. The spectrograph comprised two separate halves known as the blue and red sides, the former being through the eastern side of the magnet block.

Figure 3.16 shows that the top level of MARS contained a tray on either side of the spectrograph called measuring trays. These trays consisted of eight layers of flash-tubes. The layers were separated from each other by aluminium sheets which formed the electrodes. In each layer, there were 89 tubes each having a length of 2m and a diameter of about 0.55 cm. The flash-tubes were filled with neon gas and when a charged particle passed through any of the tubes, the gas in the tube was ionized. The application of a high voltage pulse within $\sim$ 3μs across that tube caused a discharge along it and in such cases the tube was said to have flashed. Since there was very little absorber above the top of the spectrograph, the flash-tubes of the top measuring trays

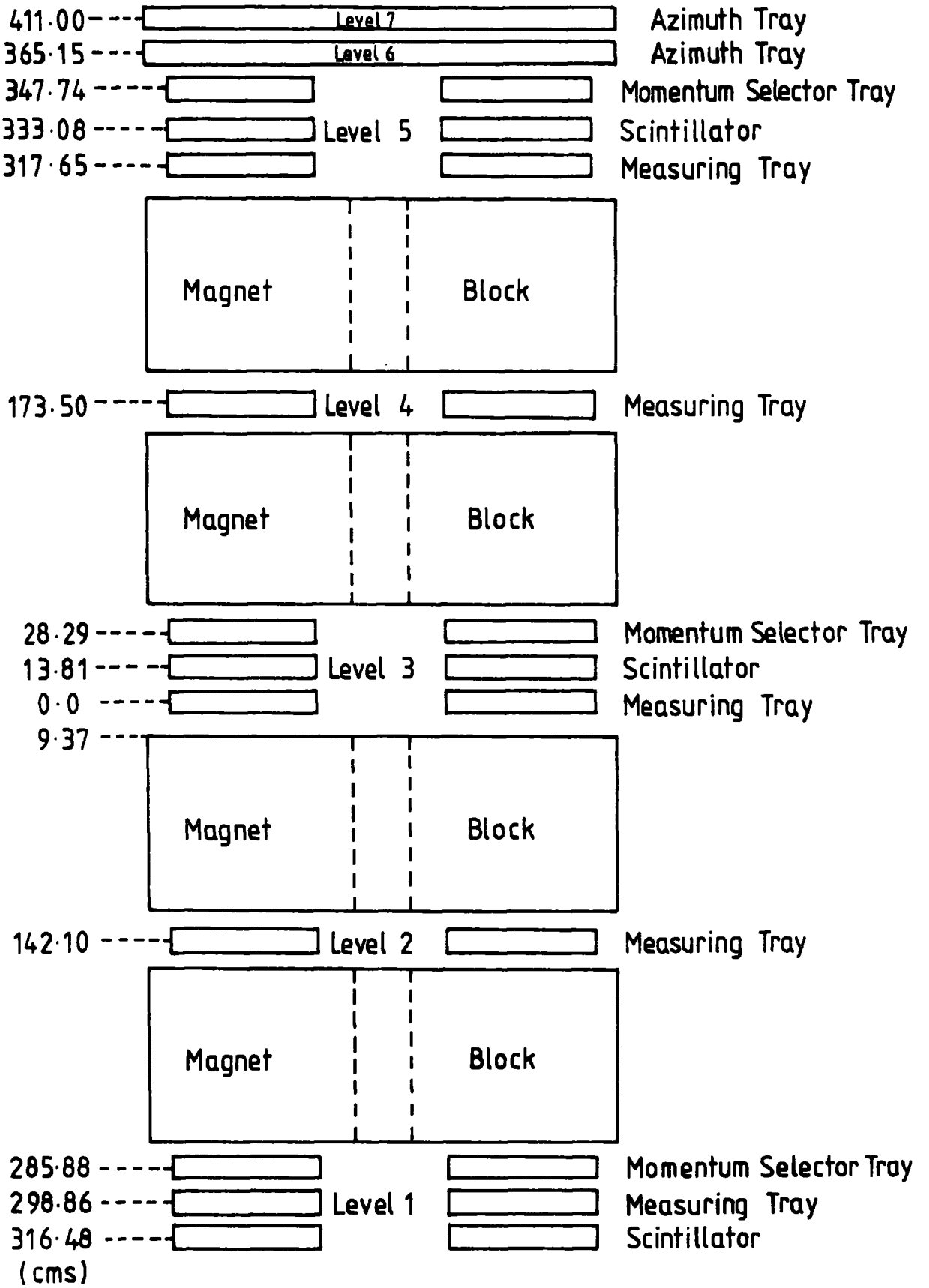

Figure 3.16 The Relative Positions Of The Various Detectors In MARS.
(After Wells, 1972)

were mainly discharged as the consequence of the passage of electrons rather than muons through the trays. Consequently, the trays were used for the measurement of the electron density in the recorded air shower event.

The whole system was designed to operate automatically. The flash-tubes of the blue side measuring trays were digitised. The method used being that of Ayre and Thompson (1969). Briefly, a small brass probe connected via a resistor to the input of an integrated circuit electronic memory, was placed in front of each of the flash-tubes. The discharge of the tube was followed by the appearance of a voltage pulse at the input of that memory. The information from the flash-tubes was sent to an IBM 1130 computer where it was stored on a magnetic disk to be transferred subsequently to magnetic tape in order to be analysed on a larger IBM 370 computer.

The flash-tubes of the red side measuring trays were not digitised but they were photographed, each time the spectrograph was triggered, using two cameras viewing the trays through a system of mirrors. Front silvered mirrors were used and the cameras viewed the tubes from a distance of about 4.25 m. Each of the cameras used a 135 mm focal length lens set at its maximum aperture of f/1.8 and had an open shutter viewing the flash-tube trays in a darkened laboratory. Immediately after each event, a clock, event number, the date and the direction of the magnetic field were illuminated in the field of view of the cameras. After each run, the film was removed and developed, and the camera reloaded.

CHAPTER FOUR

THE DATA ANALYSIS

4.1 Introduction

The previous Chapter showed how the array data of each recorded event are coded and stored on a magnetic disc on an IBM 1130 Computer. The present Chapter is concerned with the analysis programme which is used for the interpretation of these data. Before the data are analysed they are transferred from the magnetic disc to a magnetic tape as well as a 'private disc' and stored in the archives of the Northumbrian Universities' Multiple Access Computer (N.U.M.A.C.) until they are required to be analysed.

4.2 The Purpose of the Analysis

The analysis is carried out in order to obtain all possible information about the air shower parameters. Such parameters are: the direction of arrival of the shower front, the shower core position, and the shower size.

The analysis is executed using the N.U.M.A.C. computer. Before starting the analysis the raw data, which are in the form of channel values as initially collected on the IBM 1130, are divided into groups according to the different run numbers present and are then stored in separate files. Each of these files is analysed depending on the amount of the data available for each event. The broad lines of the analysis programme can be summarised in the following order:

1. Data calibration and conversion into useful quantities.
2. Calculation of the shower arrival direction.
3. Calculation of the core location and shower size.

4.3 The Analysis Programme

The following sections describe the features of the present analysis programme. This programme uses a minimisation package (4.4) in which a theoretical description of the structure of the air shower is fitted to the quantities observed by the array detectors. In order to fulfil this purpose the available raw data must be converted into useful calibrated quantities.

4.3.1 The Modifications of the 1976 Analysis Programme

The analysis programme written by Smith (1976) was modified for the present data analysis as follows:

1. The calibration coefficients of the detectors and the calibration curve for each multiplexer channel were introduced thus allowing a more accurate conversion of the stored channel values into actual densities at the detectors. For the liquid scintillation counters, the curves combining the calibration curve of each C.S.A. and that of the corresponding stretcher channel were also introduced.
2. For each detector an estimate of the minimum and maximum recordable channel values were calculated by binning up the stored channel values for that detector. A typical distribution is shown in Figure 4.1. At high channel values, the piling up of saturated measurements can be clearly seen allowing a reliable estimate of the saturation level of the detector. The calculated minimum and maximum channel values were fed to the analysis programme. If a stored channel value was found to be equal to or less than the minimum value or if it is equal to or greater than the maximum value, the detector was considered to have a zero particle density or to be saturated respectively.

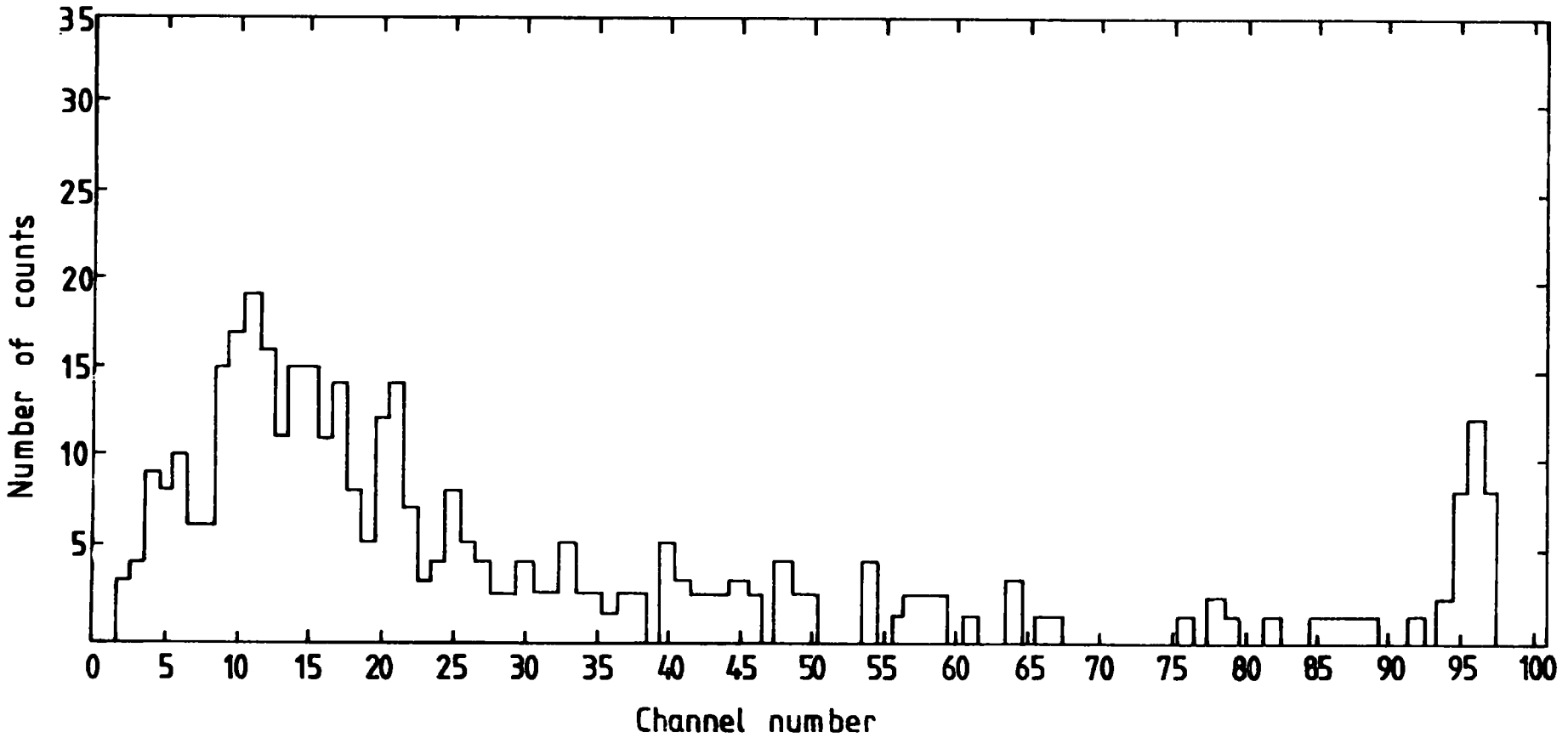

Figure 4.1 A TYPICAL A.D.C. CHANNEL DISTRIBUTION (BIN SIZE = 10).

3. The programme was also modified to allow for overwriting the data gate information such that if a certain detector was operating during a particular run and for any reason it was required to be switched off for the data analysis, this could be achieved using an added subroutine.

4. In the 1976 version of the analysis programme, the co-ordinates of the central detector were chosen as those of the starting point to the minimisation routine. In the current version, the mean co-ordinates of any saturated detectors are used as the co-ordinates of the starting point. If there are no saturation measurements, the co-ordinates of the detector which measures the maximum density are taken as those of the starting point. The present method gives a more accurate start to the minimisation programme and hence yields a quicker search for the actual co-ordinates of the shower core.

4.3.2 The Analysis Procedure

On entering the present analysis programme, subroutine HEADER is called to put in the head title. The calibration curves of the multiplexer-A.D.C. for all the array detectors, as well as those of the C.S.A.-stretcher for the liquid detectors are then read in by calling subroutine RDCL and RDCLI respectively. The minimum and maximum recorded channel values are also read in by subroutine MAXMIN. This is followed by calling subroutine SWRD by which the new Data Gate information is read in and printed out. Subroutine CALRD is then called to read in the calibration coefficients for both the plastic and the liquid detectors. For each of the plastic detectors, this coefficient represents the mean of the voltage distribution at the output of the head amplifier for single and almost vertical particles per square metre. For the liquid detectors, each of these coefficients is the mean of the

distribution of the input voltage to the C.S.A., when single and nearly vertical particles cross that detector, multiplied by the area of the detector.

The programme afterwards calls the controlling subroutine CONTROL which instructs the way of calling the analysis routines depending on the analysis codes. These codes are read from a single line file in which both the run number and the event number of the last analysed event are stored in order to avoid analysis duplication. When CONTROL is entered, an internal clock is started to monitor the used Central Processing Unit (C.P.U.) time. The analysis codes are then read and a title page is printed. This is followed, if it is the beginning of the analysis of a data file, by calling subroutine FLAGO which summarises the flag combinations, or in other words the Trigger Modes, in the file. This subroutine is one of the newly added subroutines. According to the analysis codes, several degrees of analysis can be executed. These are either a quick summary of the data contained in the data file, a summary and data print out without minimisation or a full analysis. A flow chart of the routines used in the present analysis programme is illustrated in Figure 4.2.

If full analysis is required, the programme summarises all the data in the input file. This is done by calling subroutine SUMARY which produces a table showing the runs present, the number of the events in each of these runs and the whereabouts in the data file of the first and the last events in each run. This subroutine also checks the presence of runs which contain less than 11 events, adds these runs to the previous run and prints out a corrected summary table. SUMARY calls another subroutine ADDER such that, if the data file contains more than one run, this subroutine finds the total number of events in the whole data file and prints out the combined runs summary table. Then subroutine

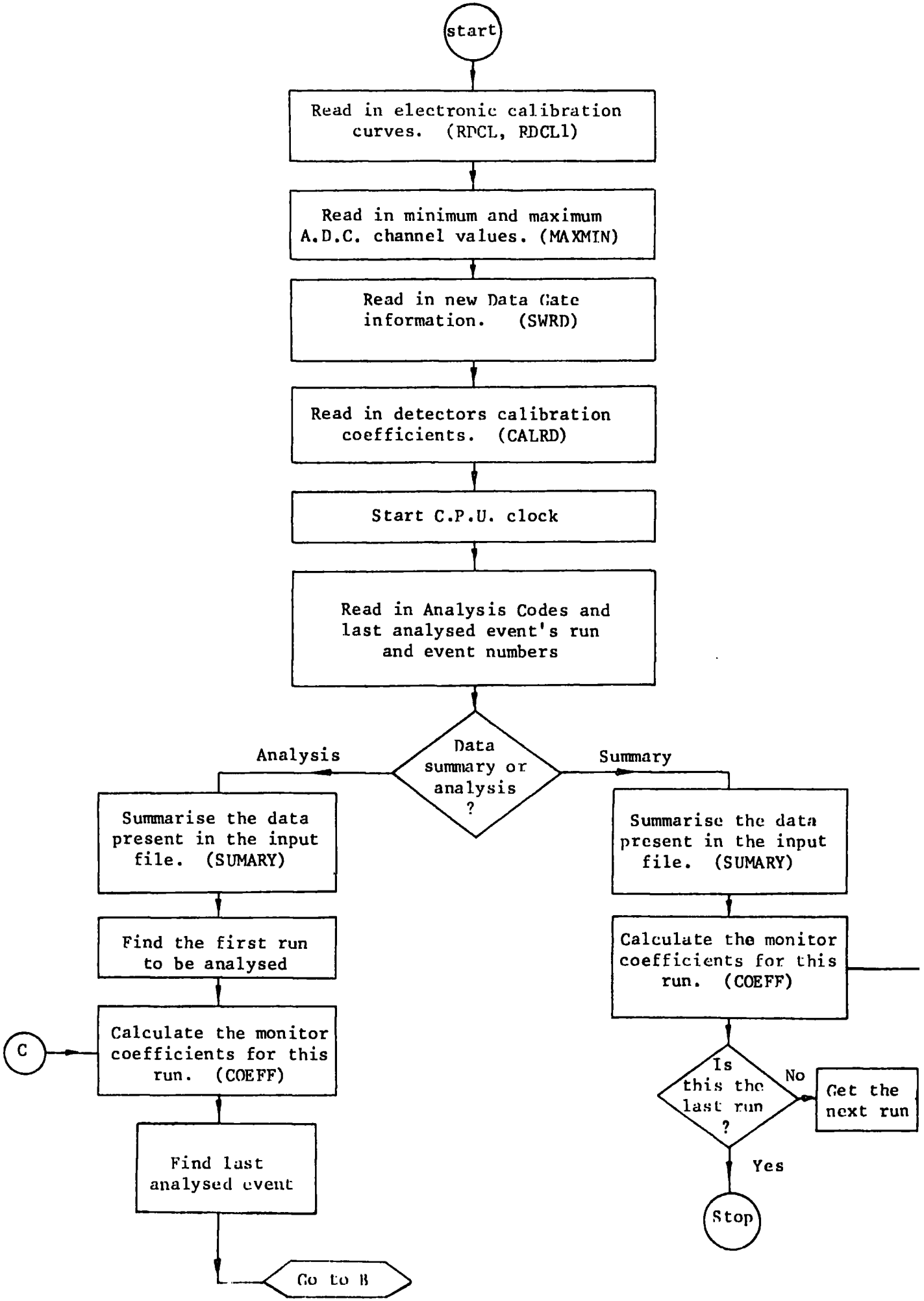

Figure 4.2 The Current Analysis Programme Flowchart.

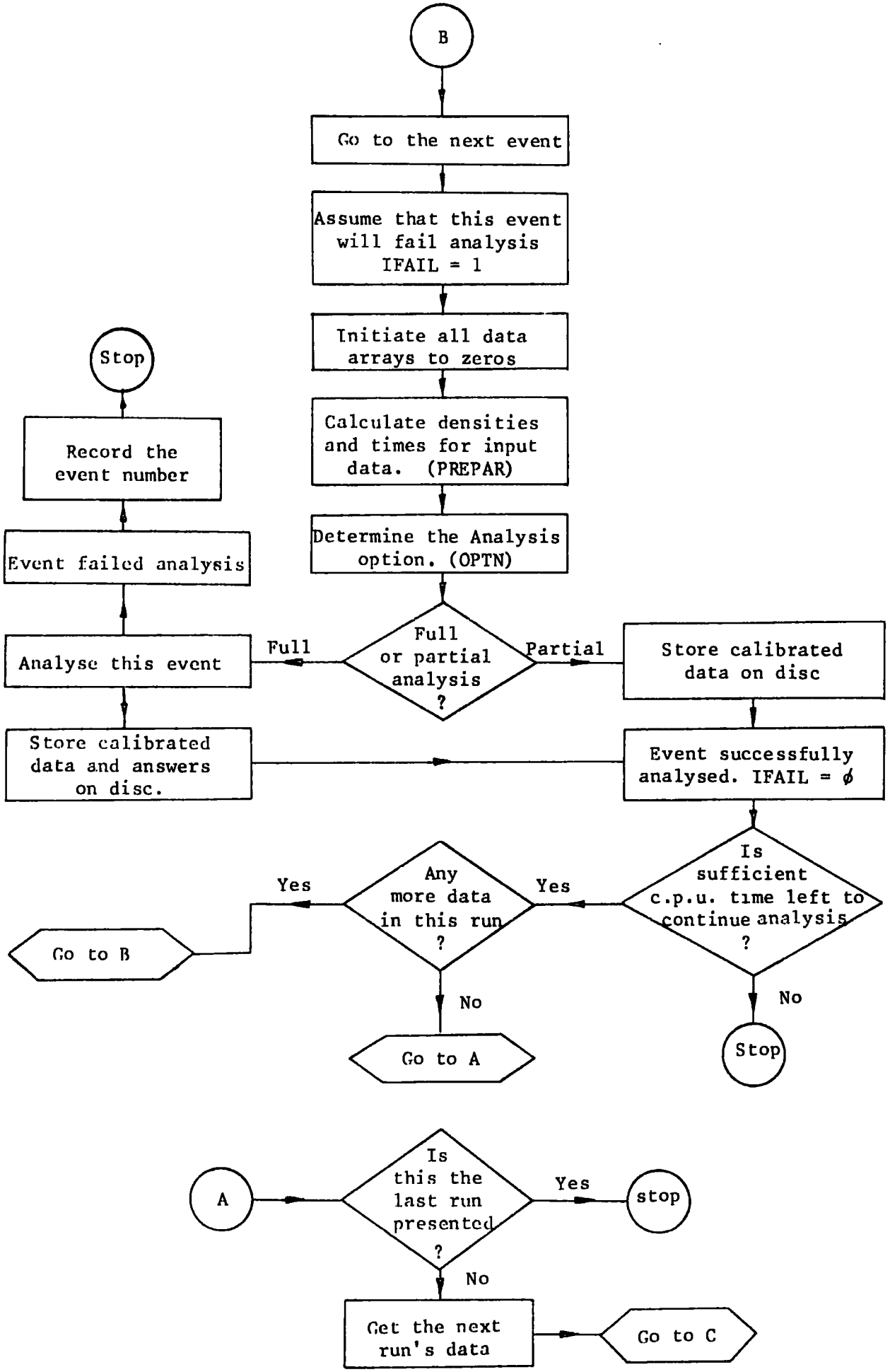
B
Go to the next event
Assume that this event will fail analysis IFAIL = 1
Initiate all data arrays to zeros
Calculate densities and times for input data. (PREPAR)
Determine the Analysis option. (OPTN)
Full or partial analysis ?
Full
Partial
Analyse this event
Store calibrated data and answers on disc.
Store calibrated data on disc
Event successfully analysed. IFAIL = ϕ
Event failed analysis
Record the event number
Stop
Is sufficient c.p.u. time left to continue analysis ?
Yes
No
Stop
Any more data in this run ?
Yes
No
Go to B
Go to A
A
Is this the last run presented ?
Yes
stop
No
Get the next run's data
Go to C

READ is called which reads into an internal array the data on the source file and decodes the Trigger Mode and Operational Units Data Gate information. If the data are impure, READ prints a message telling so and indicating the reason for the impurity. This reason could be either out of sequence run numbers or event numbers, the failure of the A.D.C. to be cleared at the end of the last acquisition cycle of the previous event, the picking up of the A.D.C. between events or the incorrect reading of the data from the input file. This subroutine also prints a message showing the total number of events to be analysed in that file. The analysis is terminated if the source file contains no data such a situation being caused by rubbing out the file or its being full of zeros.

Following the data summary, subroutine COEFF is called which displays histograms of the input data and calculates the mode, mean and standard deviation on the mean for each of the multiplexer channels. These values are printed out and stored to be used later on.

After evaluating the previous statistical quantities, CONTROL calls subroutine ANALYZ. This routine is the one which calls all the routines required for the various analysis options and where the analysis remains until the chosen C.P.U. time limit is reached. A previous routine has found the location in the data file of the last analysed event . ANALYZ then begins the analysis from the next record in the data file. The first step in the analysis demands the conversion of the input data stored in the internal array from being in integer form, the form delivered to D.U.S.T. by the A.D.C. into relative times of arrival of the shower front at the array timing detectors and into particle densities as observed by each density detector. For this purpose, ANALYZ calls subroutine PREPAR which is a totally modified version of the 1976 one such that all the subroutines called are new ones. At the beginning

PREPAR calls subroutine DATGATE in order to alter the Data Gate information, if required, to the information read previously by subroutine SWRD. Then PREPAR checks the presence of data for each operative detector by testing if the mean value of its data distribution as calculated by subroutine COEFF is higher than a particular channel value, chosen to be 20. The failure of any detector to pass this test causes the termination of the programme. This test is carried out on both timing and density detectors.

On a successful completion of the previous test, PREPAR works out the previously calculated means of the timing detectors T.A.C. distributions in nanoseconds since these means are related to the time delays caused by pulse propagation into cables and through laboratory electronics. This is done just for the switched on detectors and in two steps. First, PREPAR calls subroutine CAL which finds the pulse height to each multiplexer channel which corresponds to each of these means using the multiplexer– A.D.C. calibration curves. Secondly, subroutine CALTAC is called to convert these pulse heights into nanoseconds using precalculated slopes of each T.A.C. calibration curve. The same two steps are executed again for the event's timing data of the same detectors. This is followed by calling subroutine PHYTM which checks that each detector has produced a timing value which lies within physically reasonable limits and works out the relative time of arrival of the shower front at that detector. This is done by subtracting from the timing value observed by that detector, the corresponding cable and electronic delay obtained from the mean of the detector's T.A.C. distribution for that run. The resultants for the useful timing detectors are used by the minimisation routines in calculating the direction of arrival of the shower. Figure 4.3 shows the form of a T.A.C. distribution.

As for the density data, PREPAR starts by calling subroutine

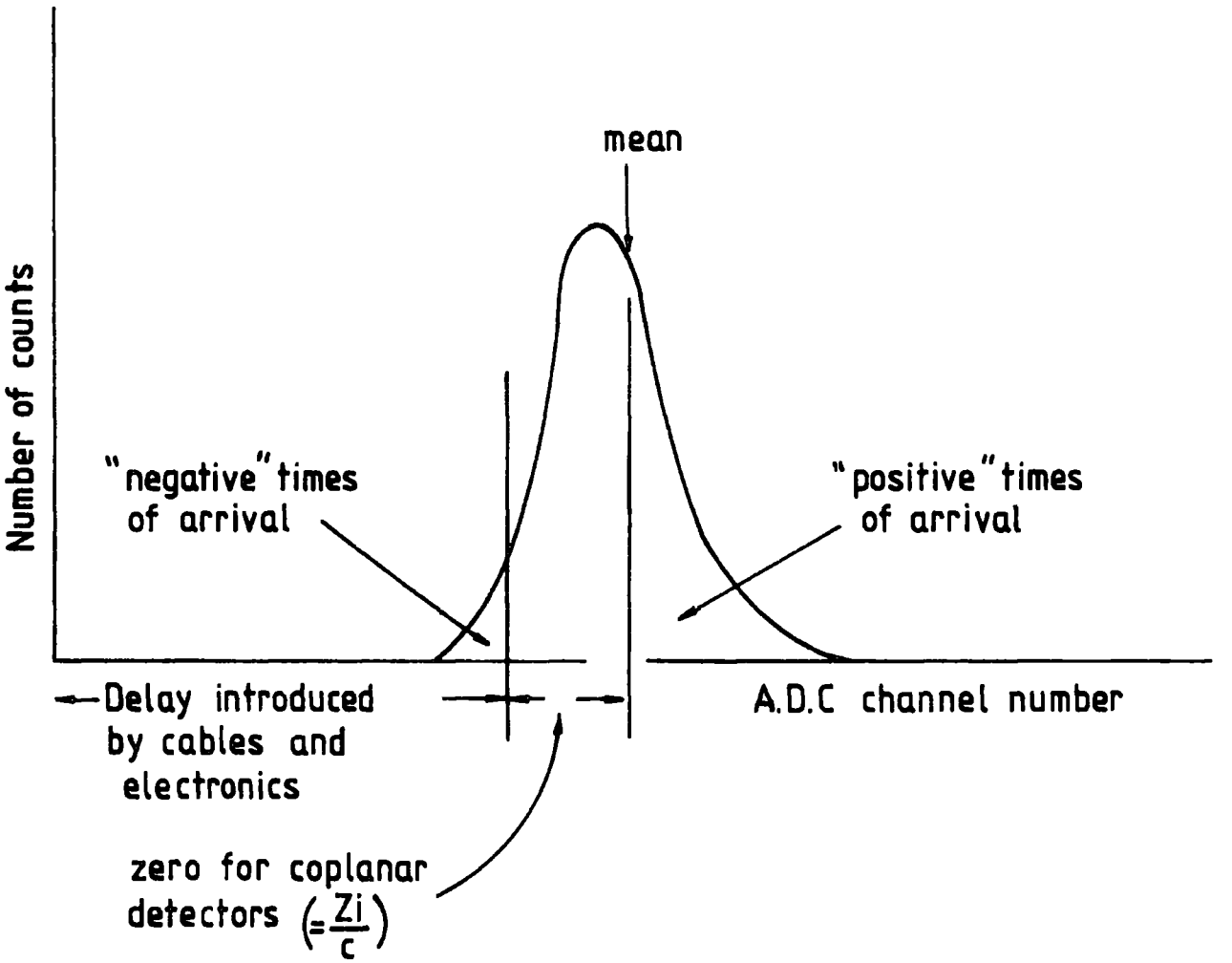

Figure 4.3 Schematic Diagram Of A T.A.C. Distribution.

MAXMN to check the presence of any saturated detectors. This is followed by converting the event's density data, which are in the form of A.D.C. channel values, into numbers of particles per square metre. To achieve this, subroutine CAL is called first to determine the pulse height to each multiplexer input which corresponds to the stored channel value using the multiplexer - A.D.C. calibration curves. PREPAR then calls subroutine CALDEN which, for the plastic detectors, divides the detector's pulse height calculated in CAL by the detector's calibration coefficient. For the liquid detectors, CALDEN calls another subroutine CALI where the C.S.A. - stretcher calibration curves are used in order to obtain the pulse height to each C.S.A. which corresponds to the pulse height determined by CAL. CALDEN then divides the CALI resulting pulse height obtained for each liquid detector by the corresponding calibration coefficient. Thus, the density in particles per square metre measured at each of the array density detectors is obtained.

Both the calculated values of the relative times of arrival of the shower front at the timing detectors and those of the densities (m^{-2}) observed by the density detectors are printed out. For each detector's calibrated data, the decoded Data Gate information is also printed out. This information indicates whether or not the detector is switched off and shows if any timing detector is to be eliminated when the minimisation procedures are carried out. It also specifies any density detector which is saturated and which is therefore excluded from taking part in calculating the shower size and the core location. Next, the errors on the observed densities are determined for use in the minimisation routines. Each of these errors is calculated as the result of dividing the square root of the quadrature sum of the Poissonian error (Regener,1951) and the detector's response error on the number of the particles passing through the detector by the area of the detector.

Now that the calibrated data observed by all the useful timing and density detectors have been obtained, the next step is the calculation of the arrival direction of the shower, the core position and the shower size using the minimisation routines. In order to accomplish this, the number of useful detectors as well as the co-ordinates of the starting point to the routines must be known. PREPAR counts the number of useful timing and density detectors to be used in the subroutine which identifies the analysis option to be chosen. There are four possible ways to analyse an event. These different options, which are illustrated in table 4.1, depend mainly on the amount of data present. Concerning the co-ordinates of the starting point, they are calculated according to the new method mentioned in the previous section.

Returning to ANALYZ, the subroutine which determines the most appropriate analysis way matching the available data, is called. Since all the information required for the data minimisation is obtained, ANALYZ calls the minimising routines for a full analysis of the event. When the analysis is completed, the answers are written out. Both the calibrated data and the analysed answers are then stored on a private disc for future use together with all relevant information such as the event number, the run number, the trigger mode and the decoded data gates. This is followed by checking the time to see if there is still sufficient C.P.U. time for more events to be analysed. If not, the programme stops.

In fact, the most reliable option amongst the four mentioned is option number four since it requires the presence of sufficient timing as well as density data. So, the results deduced when option four is chosen are those to be used for future calculations.

TABLE 4.1

THE ANALYSIS OPTIONS

Analysis Option	Meaning	# Relative Times	# Densities
1	Insufficient data for analysis. No analysis done.	< 2	< 5
2	Insufficient timing data for full analysis. Three parameter (x_c, y_c, N) fit to the density data, θ assumed to be 0° and ϕ assumed to be 180°	< 2	≥ 5
3	Timing data used to calculate (θ, ϕ).	≥ 2	< 5
4	Full analysis. Timing data used to calculate (θ, ϕ). Density data used to calculate (x_c, y_c, N)	≥ 2	≥ 5

4.4 The Method of Array Data Minimisation

The minimisation routines represent the basis of the analysis programmes. These routines consist of the C.E.R.N. programme MINUIT (James and Roos, 1971) in which several internal checks are used in order to achieve correct execution of the suitable function. If, after the pre-chosen number of tries (16,000), MINUIT fails to converge, it will stop such that the parameter values deduced from the last attempt will be returned.

Concerning the minimisation procedure used to obtain the arrival direction of the shower front, the timing data measured by the useful timing detectors are fitted to a plane in three dimensions using a least squares technique based on a numerical minimisation approach. The minimisation method includes the minimisation of the following function:

$$F_1 = \sum (t_{iobs} - t_{icalc})^2 \qquad 4.1$$

where t_{iobs} and t_{icalc} are the observed and calculated relative times of the shower front arrival at a particular detector i and where the summation is made over all the useful timing detectors.

After completing the timing data fitting, no matter whether it was successful or not, and provided that there is a sufficient number of useful density detectors, the analysis continues by fitting a selected shower structure function to these density data by minimising the weighted least squares function

$$F_2 = \sum \frac{(\rho_{icalc} - \rho_{iobs})^2}{\xi^2_{iobs}} \qquad 4.2$$

where ρ_{icalc} and ρ_{iobs} are the calculated and observed densities (m^{-2}) at a detector i and $\xi_{i\ obs}$ is the error on the observed density at this detector as calculated in the previous section. The summation is also over all useful density detectors.

The structure funciton which is used in searching for the core location is based on that of Catz (1975) since this was obtained using scintillation counters. The Catz function is given by

$$\rho(N,r) = 0.0157N \frac{Exp(-r/120)}{(r+1)^{1.62}} \qquad 4.3$$

where ρ is the density of particles (m^{-2}) at a radial distance r metres from the core of a shower having a size N. Only one modification has been made to this function: to use (r+2) instead of the original (r+1) term since it has been found that the use of the modified function gives a better fit to the data than the original Catz function (see Appendix A).

At this stage of the analysis both the core location and the shower size are minimised together as independent variables. Figure 4.4 represents all the quantities printed out by the programme when an event is analysed using option 4. An explanation of all these quantities is also shown.

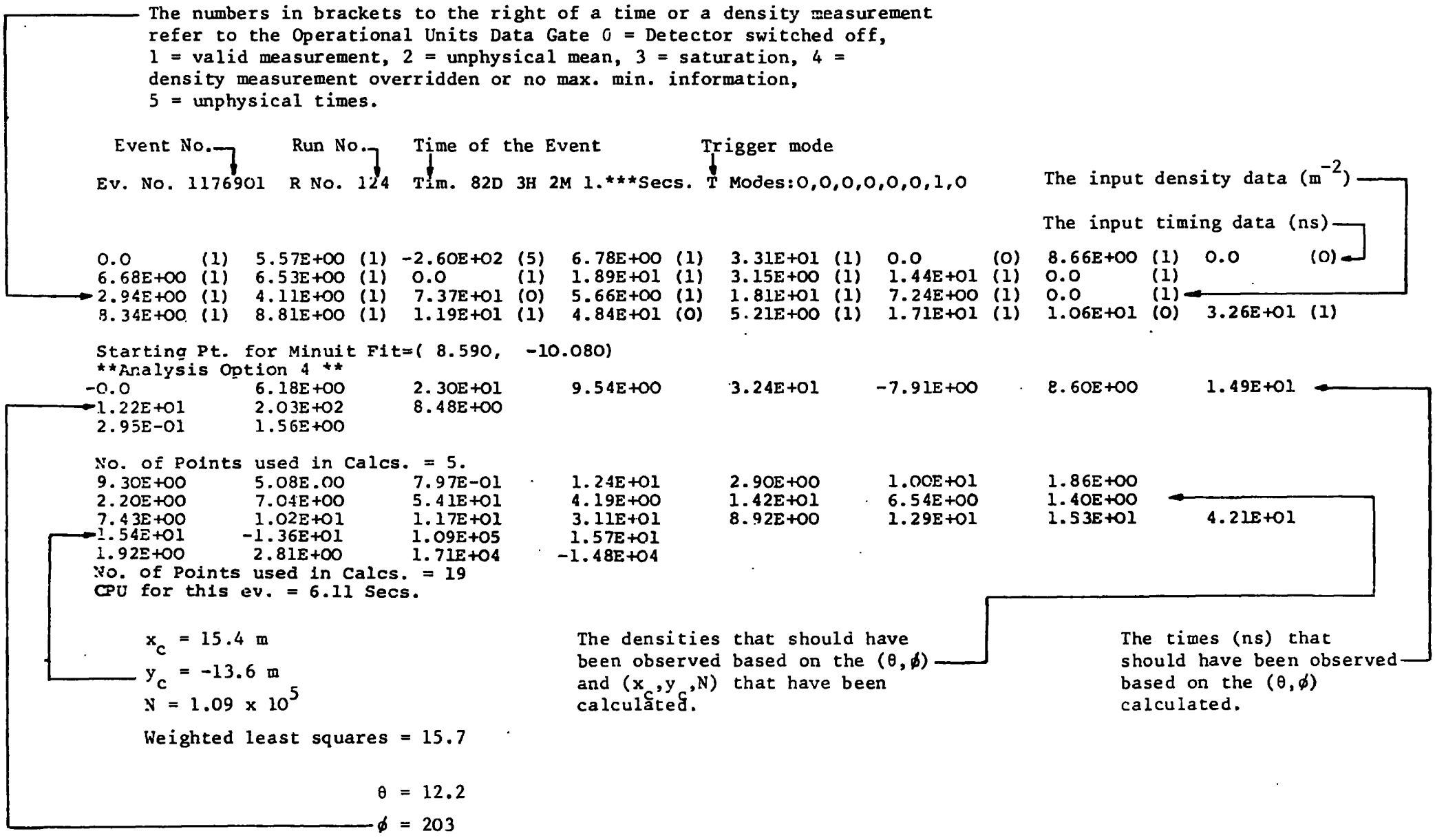

Figure 4.4 A Typical Option 4 Analysed Event

CHAPTER FIVE

DATA SIMULATION

5.1 Introduction

It has been seen in the previous chapter how the analysis programme, through the minimisation routines, determines the location of the core of each recorded shower. This chapter is concerned with studying the effect of inclusion of the liquid scintillation counters as useful density detectors, when the minimisation routines calculating the core positions are executed, on the accuracy with which the core positions are determined. The study has been carried out by using a programme which simulates data similar to the real data and analysing these simulated data with and without the consideration of the liquid detectors. In each case, the displacement of each resultant core location from the true generated one indicates how accurate the analysis programme calculates the shower core position.

In this chapter, a study has also been carried out to find the effect of the inclusion of the liquid detectors on the shower size value resulting from data analysis.

5.2 The Simulation Programme

On first entry to the simulation programme, several tasks and initialisations are performed. Internal variables and clocks have to be reset and started for the random number routines. At this point, the programme reads in data supplied by the user to determine parameters such as shower size spectrum slope, the position of the break point if any, or input shower size specified and index for the angular distribution of the incident showers. The user may also specify maximum ground area for simulation as well as details of detector characteristics and laboratory discrimination levels.

When all the necessary information has been obtained, the simulation programme begins to generate extensive air showers by calling the main

subroutine EASGEN. On entering this subroutine, the simulation codes are read from a single line file which indicates how many showers are required to be simulated and accepted by the array and shows the chosen event and run numbers for these showers. The number of the successfully accepted showers is also stored in that file. EASGEN continues by calling subroutine SPEKY which either selects a shower size from the spectrum defined earlier or considers that the shower has the prechosen fixed size. This is followed by a selection of the shower's zenith angle, θ, and azimuthal angle, ϕ, according to the previously read information. EASGEN then calls subroutine CORE to select the location of the shower core.

It is necessary to determine whether the generated shower succeeds in triggering the array. To do this, subroutine TRIGRA is called which calculates the densities (m^{-2}) measured at the triggering detectors, converts these densities to the corresponding pulse heights at the multiplexer inputs and compares these heights with the detector discrimination levels. The densities are obtained in two steps. First the radial distance from the shower axis to each of the triggering detectors has to be determined. Secondly according to a chosen structure function, the corresponding density is obtained. The function used in this programme is that represented by equation 4.3 with the mentioned modification (paragraph 4.3.2). From each density ρ, the mean number of particles ($\rho A \cos\theta$) is calculated. The actual number of particles observed at each detector is then deduced by selecting an integer number, n, from a Poissonian distribution defined by the parameter $\rho A \cos\theta$. Using the integer number, n, the pulse height to the multiplexer input is calculated by calling subroutine VOLTDT where a value of that height is picked up from the detector's pulse height distribution resulting from the passage of the n particles through the detector. The pulse height for each of the triggering detectors is checked to see if it is

greater than the corresponding discrimination level or not. The failure of any of those detectors to produce a pulse height above that minimum acceptable limit, means that the shower has not been able to trigger the array and that another shower has to be generated. On the other hand, if all the triggering detectors have succeeded in passing the previous test, the programme considers the shower as an acceptable one. In this case, TRIGRA calls subroutine VLTCH to convert the obtained pulse heights to the corresponding A.D.C. channel values using the Multiplexer-A.D.C. calibration curves. The programme then calculates the channel values for the rest of the plastic detectors in the same manner described above. The liquid detectors are treated in the same way except that an extra calibration curve is added to account for the nonlineariety of both the C.S.A. and the stretcher.

Concerning the timing data, subroutine TRIGRA starts by calculating the relative time of arrival of the shower front at each of the operating timing detectors using the previously selected values of the angles θ and ϕ. The calculation of the corresponding A.D.C. channel value is done according to the following procedure. At first, subroutine TACLE is called which adds to the obtained relative time of the shower arrival, the cable and electronic time delay which was found to be on average of the order of 200 ns. A 5 ns measurement error is then added to this result. This time value is then converted to the corresponding pulse height at the multiplexer input using the precalculated slope of the T.A.C. calibration curve. Finally, subroutine VLTCH is called to obtain the corresponding A.D.C. channel value using the multiplexer-A.D.C. calibration curve for that detector.

The next step is to check if any of the density detectors are saturated. For this purpose, the A.D.C. channel value obtained for each density detector is checked against the detector's predetermined maximum recordable channel (paragraph 4.3.1). If the A.D.C. channel value is greater than this, it is regarded as being a saturated measurement.

On returning back to EASGEN, subroutine WRITS is called by which the obtained channel values for both the timing and the density detectors are stored in a sequential file on magnetic disc together with other relevant information such as the event and run numbers, the trigger mode and the data gate information. These simulated data are stored in the same order and with the same format as is used for storing the real data. WRITS also stores in a line file the event and run numbers, the trigger made, the angles θ and ϕ, the core co-ordinates and the shower size of the generated shower such that the initial parameters of the simulated data can be compared with those resulting from the analysis of these data later on.

Now, the number of the accepted showers is tested to see if it is less than the total number required to be generated and accepted. If it is less, EASGEN checks the C.P.U. time. If the pre-chosen time limit is reached, the number of the successful showers are printed out together with the total number of the generated ones after which the programme stops. In the case of having sufficient time to continue, EASGEN carries on generating more showers until either the chosen time is totally consumed, or the required accepted showers are obtained.

Thus data are simulated and stored for later analysis. Figure 5.1 shows a flow chart for the simulation programme and figure 5.2 illustrates the simulated A.D.C. channel distribution which corresponds to the distribution previously obtained in chapter four (figure 4.1).

5.3 The Effect of the Liquid Scintillation Counters on the Accuracy of the Core Location Determination

As mentioned earlier, the aim of carrying out the data simulation is to study how the presence of the liquid detectors affects the accuracy with which the analysis programme locates the shower core of each recorded event. For this purpose, data were simulated such that

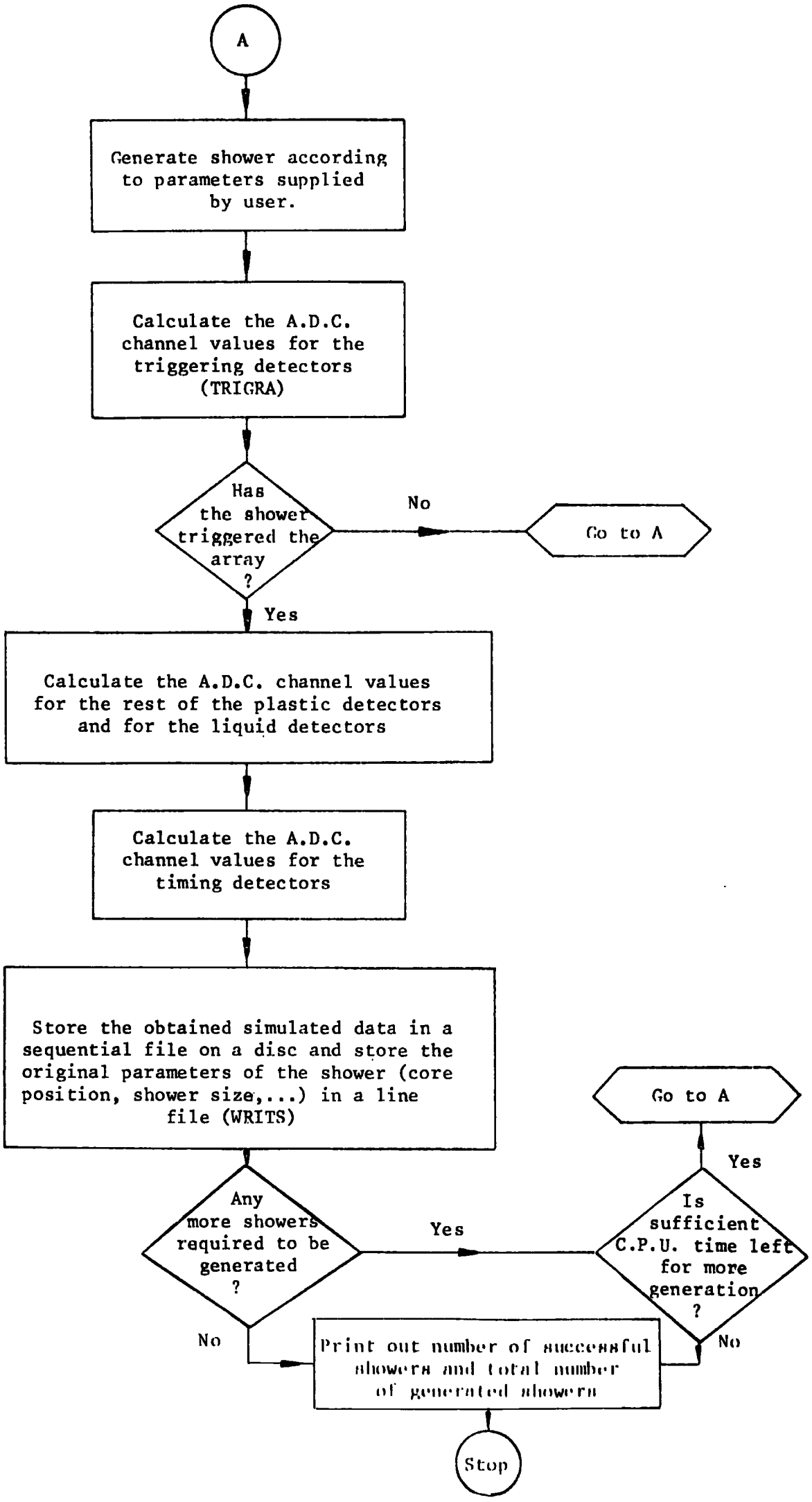
A
Generate shower according to parameters supplied by user.
Calculate the A.D.C. channel values for the triggering detectors (TRIGRA)
Has the shower triggered the array ?
No
Go to A
Yes
Calculate the A.D.C. channel values for the rest of the plastic detectors and for the liquid detectors
Calculate the A.D.C. channel values for the timing detectors
Store the obtained simulated data in a sequential file on a disc and store the original parameters of the shower (core position, shower size,...) in a line file (WRITS)
Any more showers required to be generated ?
Yes
Is sufficient C.P.U. time left for more generation ?
Yes
Go to A
No
No
Print out number of successful showers and total number of generated showers
Stop

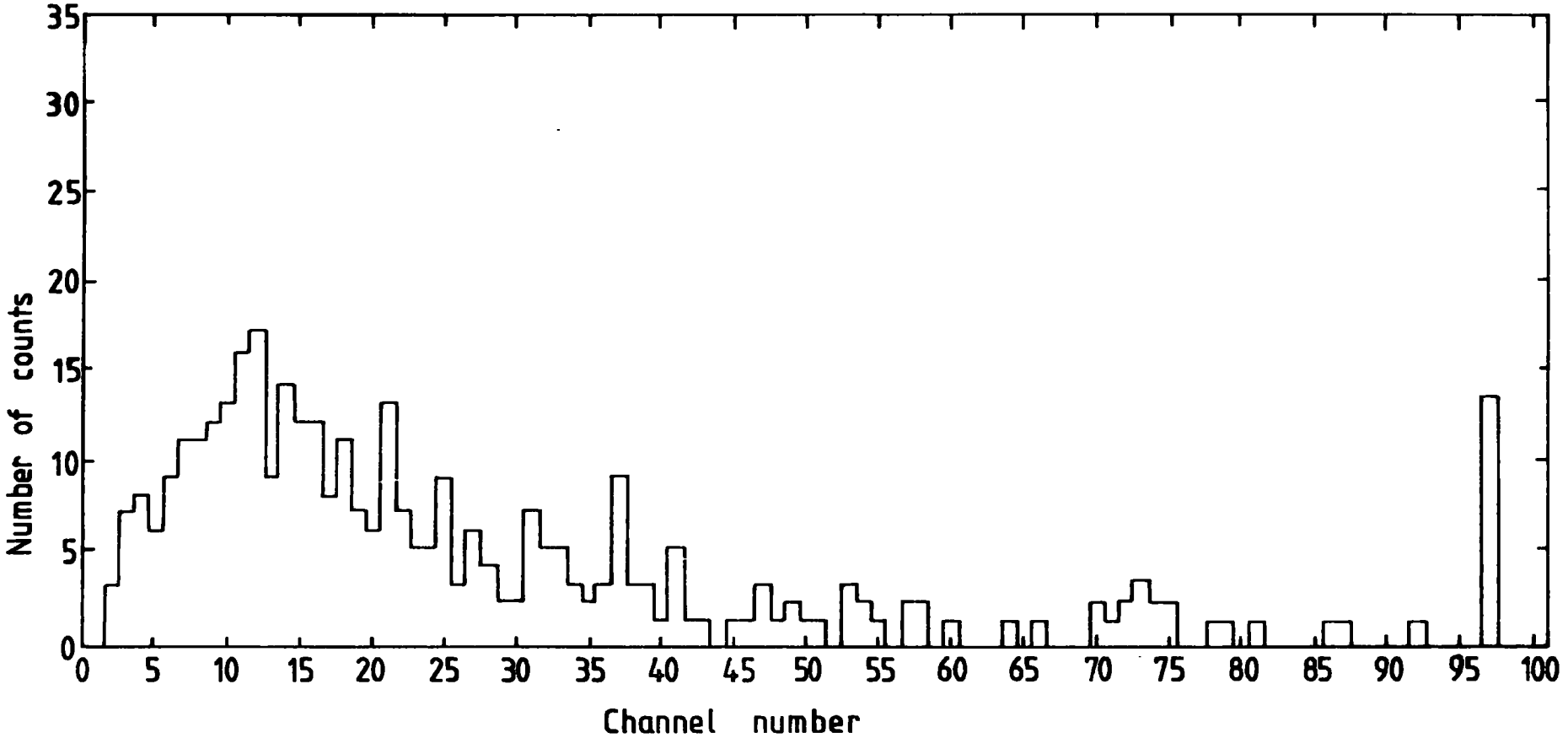

Figure 5.2 Simulated A.D.C. Channel Distribution.

the showers were generated with a fixed chosen shower size. This was done for four shower size values in the range from 5.0×10^4 to 1.0×10^6. The simulated data were then analysed twice. First, the liquid counters were eliminated from the calculation of the shower core position. Then the data were reanalysed with those counters considered as useful density detectors when the minimisation routines responsible for determining the core location were carried out.

In each case, the core position of each analysed event was compared with the corresponding simulated one and the core displacement was deduced. This displacement was calculated according to the following equation:

$$\text{core displacement} = \sqrt{(X_S - X_A)^2 + (Y_S - Y_A)^2} \qquad 5.1$$

Where X_S, Y_S are the core co-ordinates of the simulated shower and X_A, Y_A are those resulting from the shower analysis. The events for each of the four shower size values, with which showers were generated, were then divided into four groups according to the radial distance value of the simulated cores. For each group, the core displacement histogram was obtained. The resultant histograms are shown in figures 5.3, 5.4, 5.5 and 5.6. For each pair of these histograms (without and with the consideration of the liquid detectors), the number of the events for which the core displacements lay within a displacement range of 0 to 2m, 0 to 3m, and 0 to 5m were calculated. The percentages of these numbers of the total number of events present in each histogram were plotted as a function of shower size. The resultant curves are shown in figure 5.7 (a), (b) and (c). This figure shows that when the liquid detectors were not included in the analysis of events which were

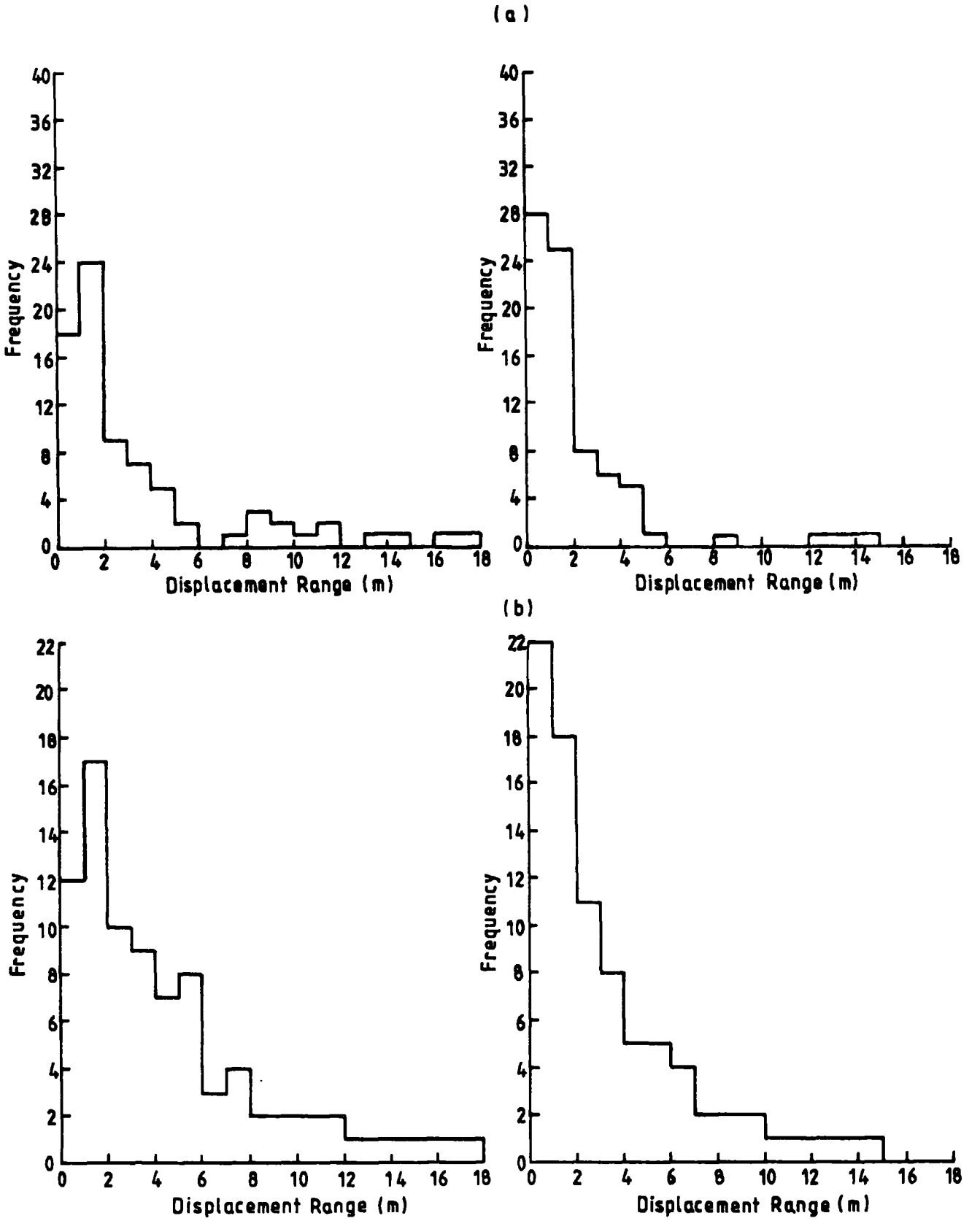

Figure 5.3 The core displacement histograms resulting from the analysis, without and with the consideration of the liquid detectors, of events simulated with a fixed shower size of $5{\cdot}0 \times 10^4$ and for $0 < R_c \leq 10$ m (a) and $10 < R_c \leq 20$ m (b) where R_c is the radial distance of the simulated core. The results without and with the liquid detectors are shown on the L.H.S. and R.H.S. respectively.

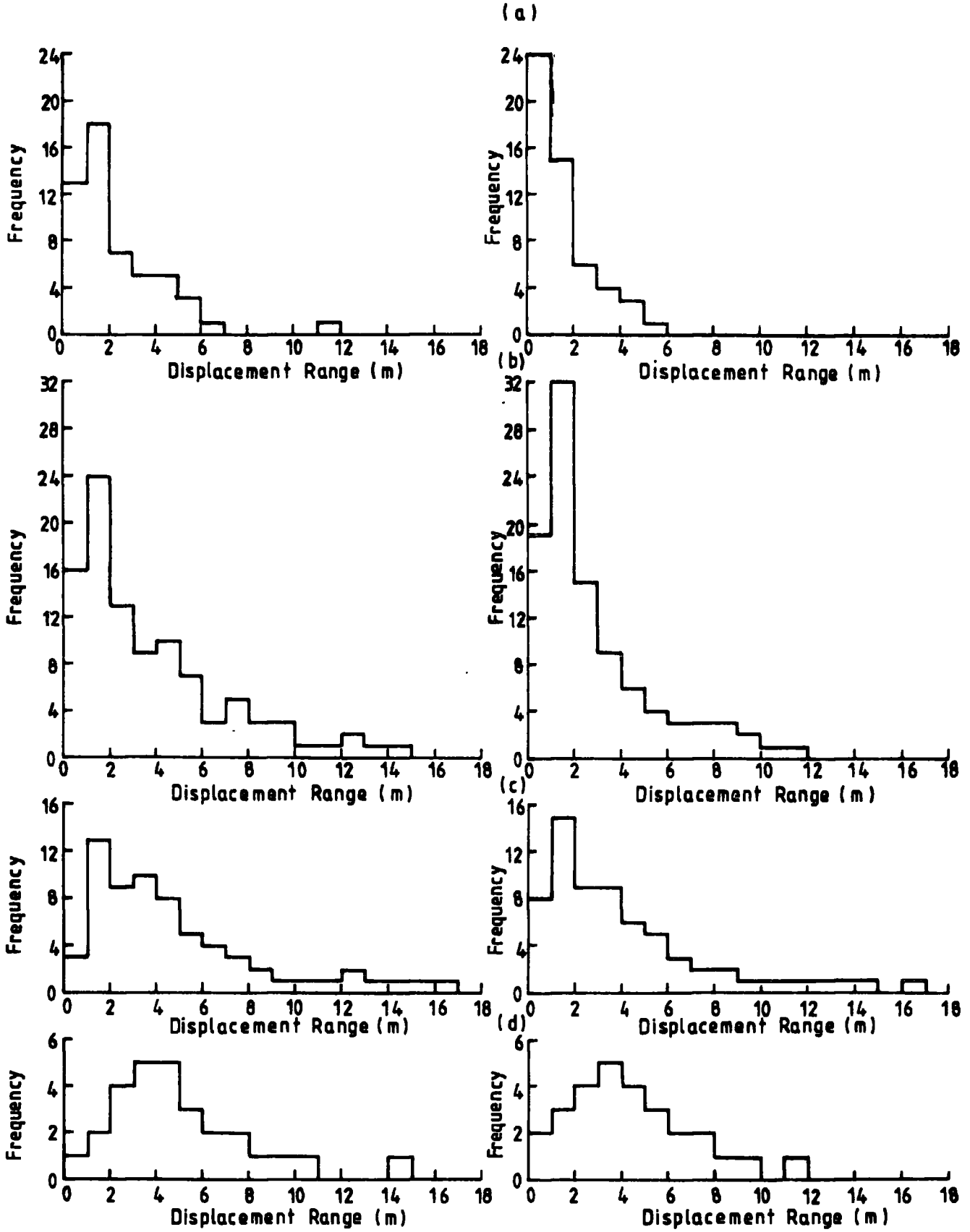

Figure 5.4 The core displacement histograms resulting from the analysis, without and with the consideration of the liquid detectors, of events simulated with a fixed shower size of 1.0×10^5 and for $0 < R_c \leq 10$m (a), $10 < R_c \leq 20$m (b), $20 < R_c \leq 30$m (c) and $30 < R_c \leq 50$m (d). The results without and with the liquid detectors are shown on the L.H.S. and R.H.S. respectively.

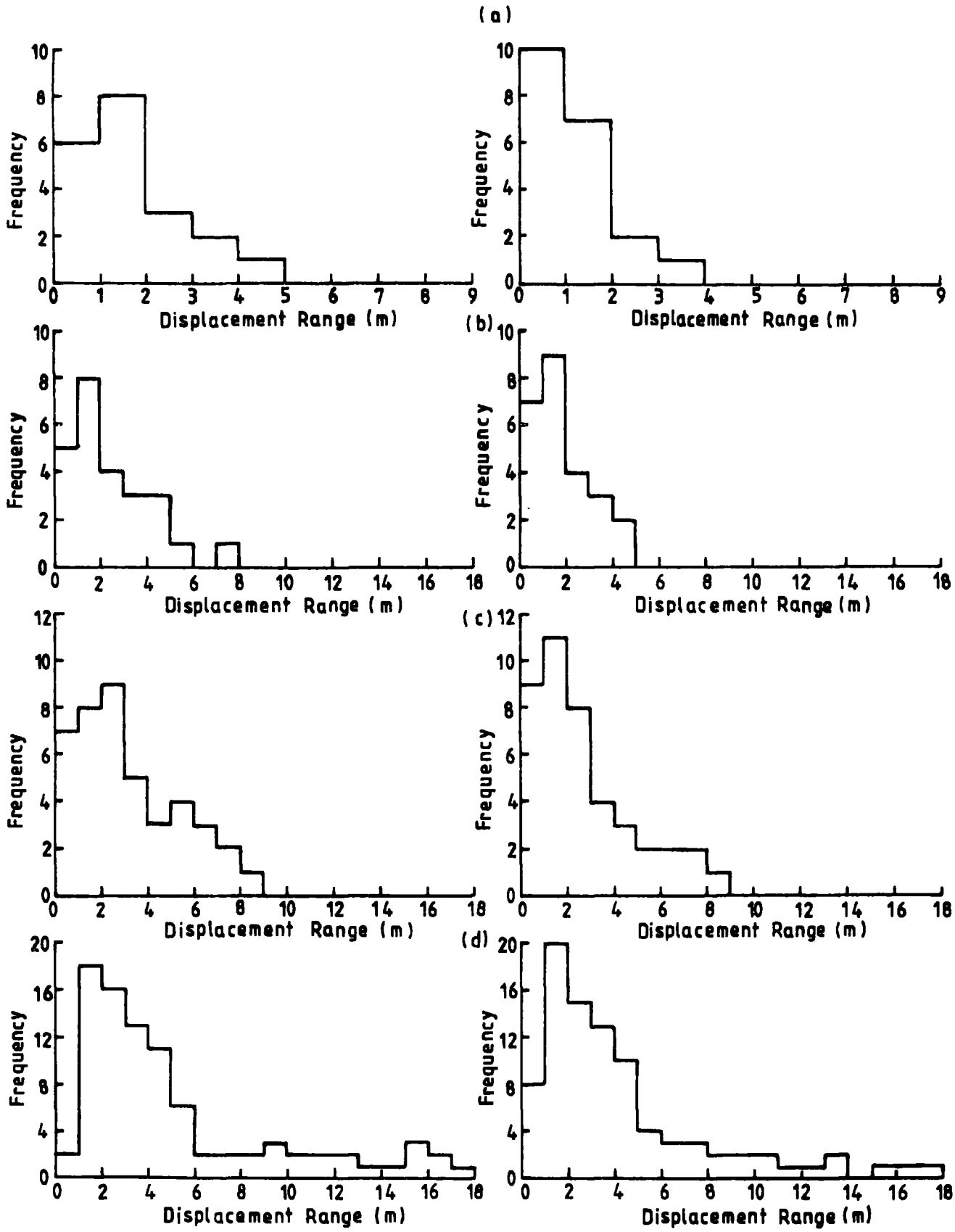

Figure 5.5 The core displacement histograms resulting from the analysis, without and with the consideration of the liquid detectors, of events simulated with a fixed shower size of 5.0×10^5 and for $0 < R_c \leq 10$m (a), $10 < R_c \leq 20$m (b) $20 < R_c \leq 30$m (c) and $30 < R_c \leq 50$m (d). The results without and with the liquid detectors are shown on the L.H.S. and R.H.S. respectively.

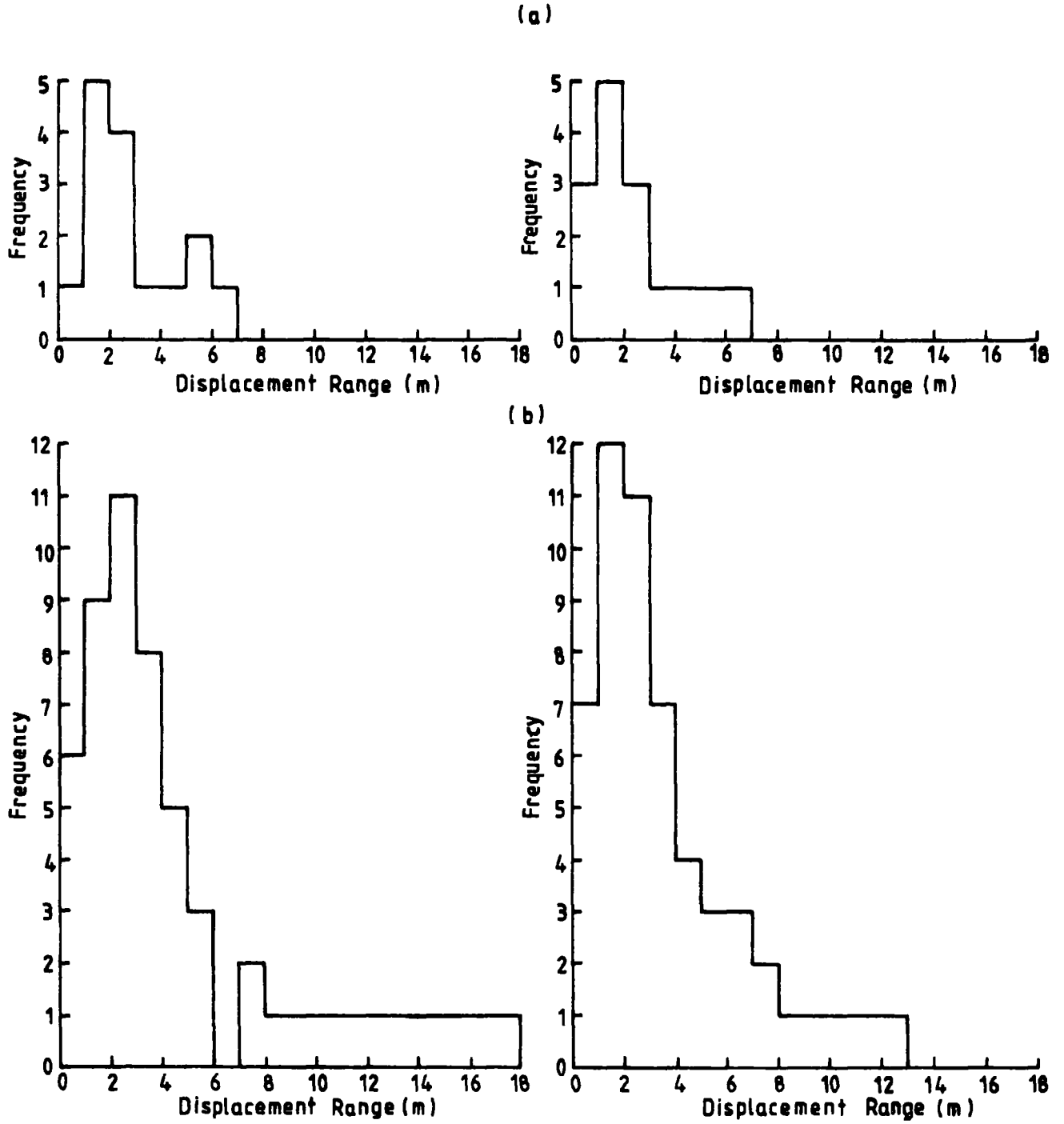

Figure 5.6 The core displacement histograms resulting from the analysis, without and with the consideration of the liquid detectors, of events simulated with a fixed shower size of $1{\cdot}0 \times 10^6$ and for $20 < R_c \leq 30$m (a) and $30 < R_c \leq 50$m (b). The results without and with the liquid detectors are shown on the L.H.S. and R.H.S. respectively.

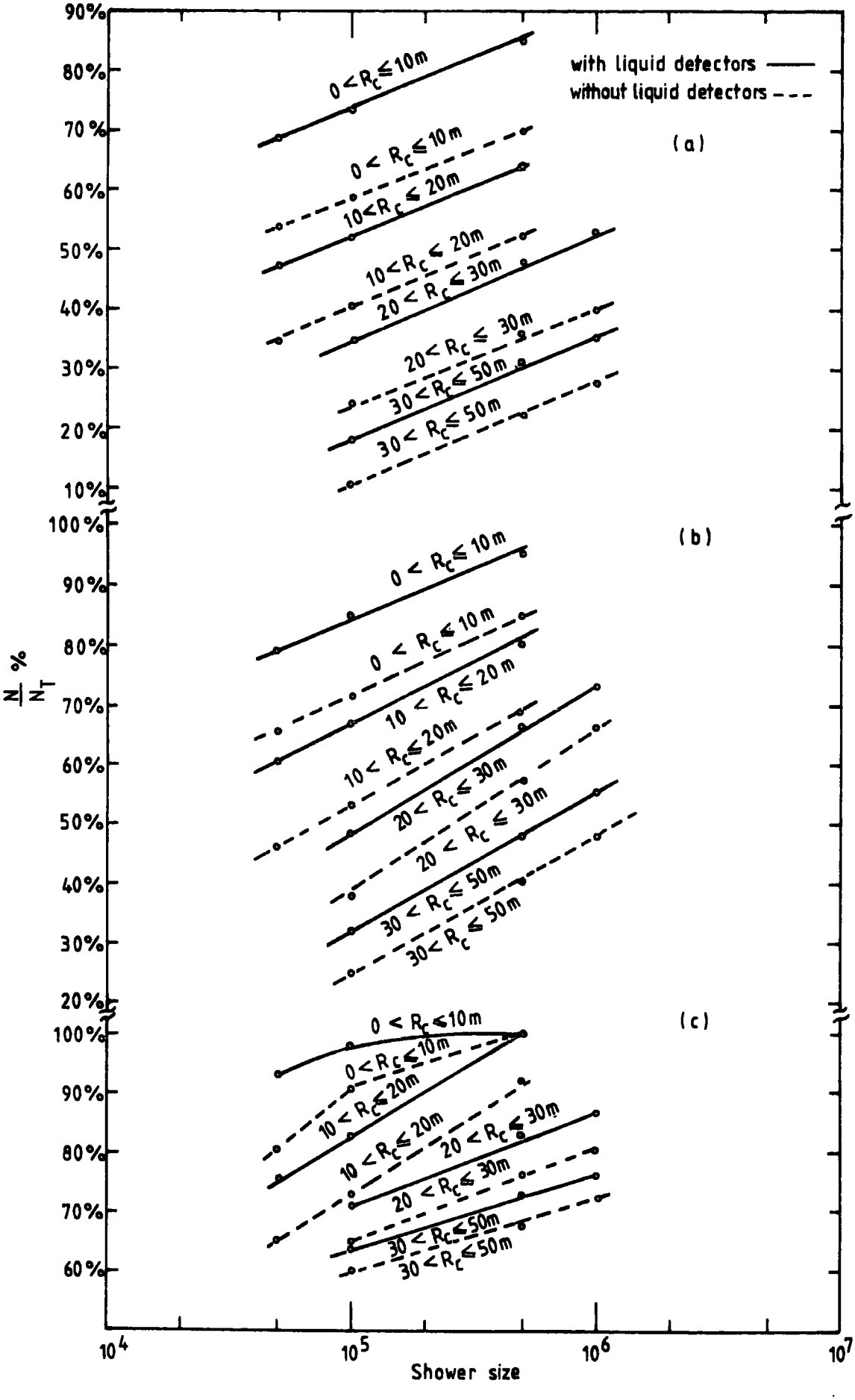

Figure 5.7 The relationship between the shower size of simulated events and $\frac{N}{N_T}$ % where N_T is the total number of events present in the corresponding histogram and N is the number of events for which the core displacements lie within displacement range of: 0 to 2m (a), 0 to 3m (b) and 0 to 5m (c). R_c is the radial distance of the simulated core.

generated with a fixed shower size of 1.0×10^5 and which had their cores simulated within a radial distance range of 10 to 20m, then 40.4%, 53.5% and 72.7% of these analysed events had core displacements in the range (a) 0 to 2m, (b) 0 to 3m and (c) 0 to 5m respectively. On the other hand, when the liquid detectors were included these percentages increased to be 52.0%, 67.4% and 82.7% respectively. A similar increase is also seen for each of the other three ranges of radial distance of the simulated cores for the above shower size. The same applies to the other values of shower size in each of the four ranges of the simulated core distances. Hence, it can be concluded that the inclusion of the liquid detectors improves the accuracy of locating the shower core.

As will be seen in the next chapter, an equation has been obtained to represent the densities (m^{-2}) observed by the liquid scintillation counters. With this equation, the effect of the interactions of photons and nuclear active particles, N.A.P., in the scintillator material of these detectors has effectively taken into account (S6.2). Therefore, in order to study the effect of the interactions on the accuracy of determining the shower core, further data simulations were carried out using the mentioned equation to simulate the densities measured by the liquid detectors. This was done for two fixed values of shower size; 1.0×10^5 and 5.0×10^5. As before, the simulated data were analysed both considering and ignoring the liquid detectors in the calculation of the shower parameters. In both cases, the core displacement of each event was determined. Figures 5.8 and 5.9 are the resultant core displacement histograms (equivalent to those shown in figures5.4 and 5.5). Similarly, for each histogram, the numbers of events for which the core displacements were found to be within ranges of 0 to 2m, 0 to 3m and 0 to 5m were deduced and the percentage of the total number of events

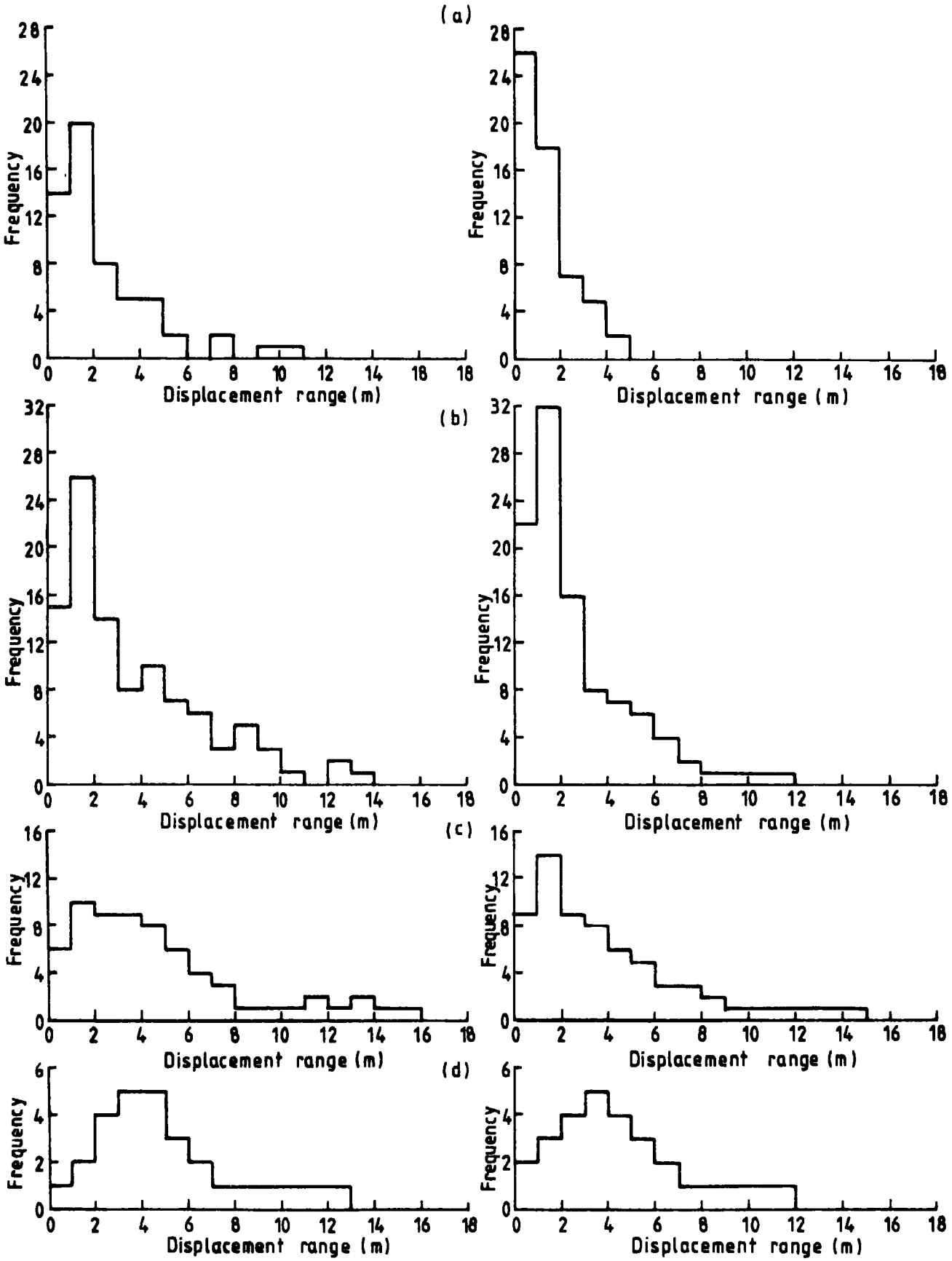

Figure 5.8 The core displacement histograms resulting from the analysis, without and with the consideration of the liquid detectors, of events simulated with a fixed shower size of $1{\cdot}0 \times 10^5$ taking into account the photon and N.A.P effect and for $0 < R_c \leq 10$m (a), $10 < R_c \leq 20$m (b), $20 < R_c \leq 30$m (c) and $30 < R_c \leq 50$m (d). The results without and with the liquid detectors are shown on the L.H.S. and R.H.S. respectively.

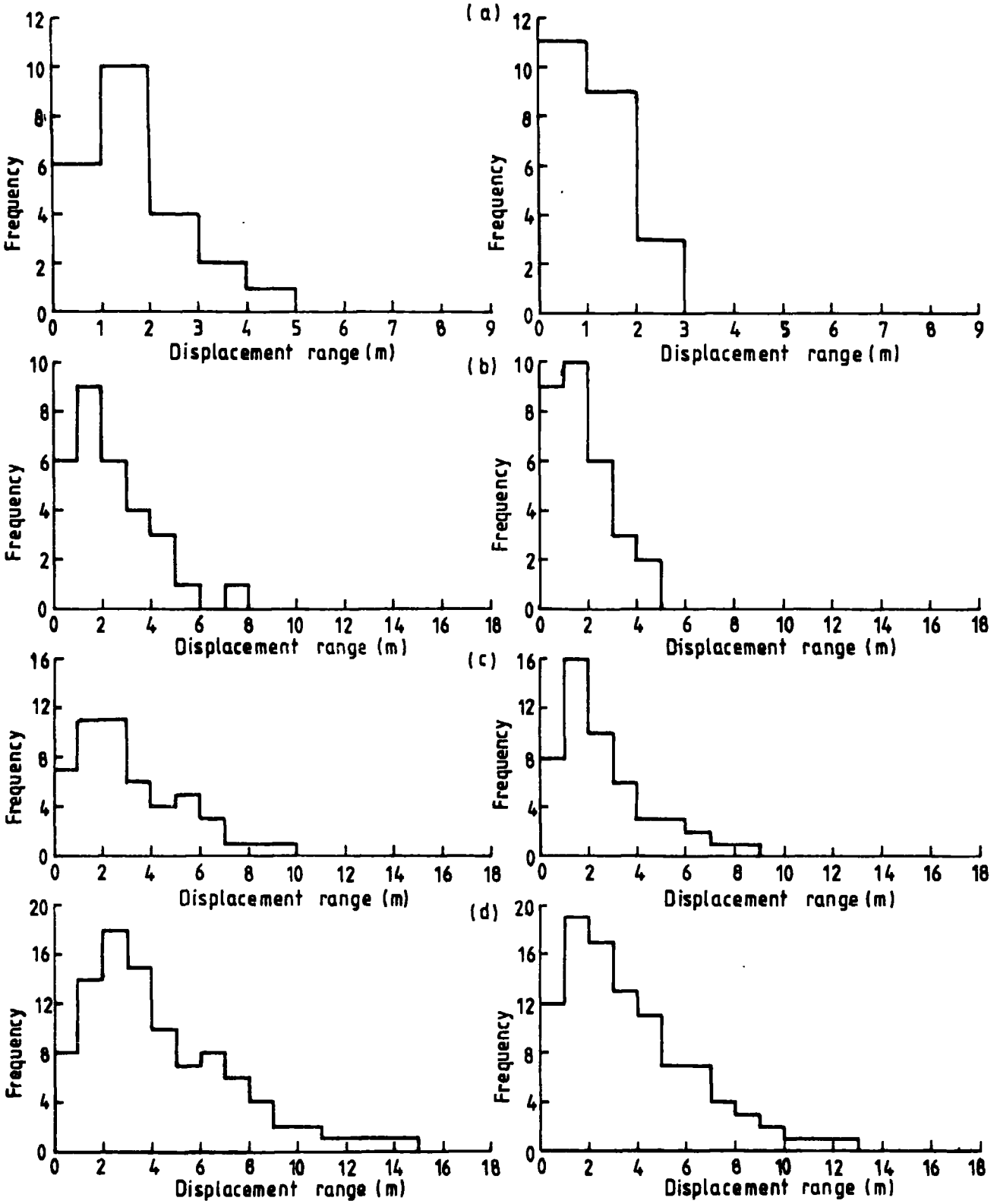

Figure 5.9 The core displacement histograms resulting from the analysis, without and with the consideration of liquid detectors of event simulated with a fixed shower size of $5{\cdot}0 \times 10^5$ taking into account the photon and N.A.P. effect and for $0 < R_c \leq 10$m (a), $10 < R_c \leq 20$m (b), $20 < R_c \leq 30$m (c) and $30 < R_c \leq 50$m (d). The results without and with the liquid detectors are shown on the L.H.S. and R.H.S. respectively.

present found, ($\frac{N}{N_T}$ %). The percentages obtained earlier when the data were simulated neglecting the effect of the photon and N.A.P. interactions (those plotted in figure 5.7) were then compared with the percentages resulting when that effect was taken into account. This comparison is shown in tables 5.1 and 5.2 for the two shower values for which data were resimulated and the tables show that in addition to the previous conclusion that the inclusion of the liquid detectors improves the accuracy of location of the shower core, consideration of effects of photon and N.A.P. gives further improvement to the accuracy when the simulated core radial distance is below 20m.

5.4 The Effect of Considering the Liquid Detectors on the Shower Size Estimated by the Analysis Programme

In order to study the effect of including the liquid detectors on the shower size calculated by the analysis programme, a comparison was made between the mean values of shower size resulting from the analysis of the simulated data ignoring these detectors and including them in the analysis. This was done for the two sets of simulated data, both when the photon and N.A.P. effects were neglected and when they were taken into account. Tables 5.3 and 5.4 show the result of the comparison for all events independent of the simulated core radial distance, R_c, and for only those events which had those cores generated within ten metres of the central detector respectively. It is clear from the first table that the overall mean shower size obtained from data analysis had nearly the same value in all cases. On the other hand the second table shows that for the events which had $R_c \leq 10$m, inclusion of the liquid detectors increases the resultant mean shower size slightly. Although the statistics are poor the indications are that the increase is greater when the effect of photon and N.A.P. in the liquid scintillation counters are considered by way of the modified structure function.

Table 5.1

Comparison between the values of $\frac{N}{N_T}$ % obtained from the analysis of data simulated with a fixed shower size of 1.0×10^5 when the liquid scintillation counters (L.Sc.) were not considered and when they were considered.

a: results obtained for data simulated while the photon and N.A.P. effect was neglected.

b: results obtained for data simulated with the consideration of that effect.

R_c is the radial distance of the simulated core.

(a)

Displacement Range (m)	$0<R_c\leq 10$m		$10<R_c\leq 20$m		$20<R_c\leq 30$m		$30<R_c\leq 50$m	
	L.Sc.out	L.Sc.in	L.Sc.out	L.Sc.in	L.Sc.out	L.Sc.in	L.Sc.out	L.Sc.in
0 to 2	58.5%	73.6%	40.4%	52.0%	24.2%	34.9%	10.7%	17.9%
0 to 3	71.7%	84.9%	53.5%	67.4%	37.9%	48.5%	25.0%	32.1%
0 to 5	90.6%	96.1%	72.7%	82.7%	65.2%	71.2%	60.7%	64.3%

(b)

Displacement Range (m)	$0<R_c\leq 10$m		$10<R_c\leq 20$m		$20<R_c\leq 30$m		$30<R_c\leq 50$m	
	L.Sc.out	L.Sc.in	L.Sc.out	L.Sc.in	L.Sc.out	L.Sc.in	L.Sc.out	L.Sc.in
0 to 2	58.6%	75.9%	40.6%	53.5%	24.6%	35.4%	10.7%	17.9%
0 to 3	72.4%	87.9%	54.5%	69.3%	38.5%	49.2%	25.0%	32.1%
0 to 5	89.7%	100%	72.3%	84.1%	64.6%	70.8%	60.7%	64.3%

Table 5.2

Comparison between the values of $\frac{N}{N_T}\%$ obtained from the analysis of data simulated with a fixed shower size of 5.0×10^5 when the liquid scintillation counters (L.Sc.) were not considered and when they were considered.

a: results obtained for data simulated while the photon and N.A.P. effect was neglected.

b: results obtained for data simulated with the consideration of that effect.

(a)

Displacement	$0<R_c\leq 10$m		$10<R_c\leq 20$m		$20<R_c\leq 30$m		$30<R_c\leq 50$m	
Range (m)	L.Sc.out	L.Sc.in	L.Sc.out	L.Sc.in	L.Sc.out	L.Sc.in	L.Sc.out	L.Sc.in
0 to 2	70%	85%	52%	64%	35.7%	47.6%	22.5%	31.5%
0 to 3	85%	95.0%	68%	80%	57.1%	66.7%	40.5%	48.3%
0 to 5	100%	100%	92%	100%	76.2%	83.3%	67.4%	74.2%

(b)

Displacement	$0<R_c\leq 10$m		$10<R_c\leq 20$m		$20<R_c\leq 30$m		$30<R_c\leq 50$m	
Range (m)	L.Sc.out	L.Sc.in	L.Sc.out	L.Sc.in	L.Sc.out	L.Sc.in	L.Sc.out	L.Sc.in
0 to 2	69.6%	87%	50%	63.3%	36%	48%	22.5%	31.6%
0 to 3	87%	100%	70%	83.3%	58%	68%	40.8%	49%
0 to 5	100%	100%	93.3%	100%	78%	86%	66.3%	73.5%

Table 5.3

Comparison between the overall mean values of shower size resulting from the analysis, without and with the consideration of the liquid scintillation counters, of data simulated with fixed shower size of 1.0×10^5 and 5.0×10^5.

a: results obtained for data simulated while the effect of photon and N.A.P. interactions was neglected.

b: results obtained for data simulated with the consideration of that effect.

Simulated shower size	(a)		(b)	
	without L.Sc.	with L.Sc.	without L.Sc.	with L.Sc.
1.0×10^5	$[8.33 \pm 1.66] 10^4$	$[8.38 \pm 1.53] 10^4$	$[8.35 \pm 1.61] 10^4$	$[8.40 \pm 1.58] 10^4$
5.0×10^5	$[4.47 \pm 0.92] 10^5$	$[4.49 \pm 0.79] 10^5$	$[4.48 \pm 0.77] 10^5$	$[4.50 \pm 0.76] 10^5$

Table 5.4

Comparison between the mean values of shower size resulting from the analysis, without and with the consideration of the liquid counters, of data simulated with a fixed shower size of 1.0×10^5 and for $o<R_c \leq 10m$

a: results obtained for data simulated while the photon and N.A.P. effect was neglected.

b: results obtained for data simulated with the consideration of that effect.

(a)		(b)	
without L.sc.	with L.sc.	without L.sc.	with L.sc.
$[8.4 \pm 1.2]10^4$	$[8.6 \pm 1.0]10^4$	$[8.4 \pm 1.1]10^4$	$[9.2 \pm 1.13]10^4$

However, it can be seen that in all cases, the mean shower size obtained analysing the simulated data is always less than the initial shower size for which the simulations were carried out.

CHAPTER SIX

RESULTS AND INTERPRETATION

6.1 Introduction

Chapter four described how the array data were analysed in order to obtain the various parameters of the recorded showers. The analysis was carried out whilst one of the liquid scintillation counters and one of the plastic detectors were eliminated from the calculation of these parameters. Hence, the lateral distribution of the electron-photon component of extensive air showers as measured by each of these two types of detector could be deduced. The shower parameters calculated by the analysis programme were also used in a comparison made between the distribution of the number of flash-tubes discharged in the red-side top measuring tray of the specteograph (S3.5), and the theoretically predicted distribution.

6.2 Lateral Distribution of the Electron-Photon Component

It has been found by many authors, Bray et al (1965), Shibata et al. (1965), Dake et al (1971) and Alexeyev et al (1977), that the particle densities in EAS as measured by scintillation counters are higher than those measured by either spark chambers or Geiger Müller counters placed at the same position as the scintillation counters. This has been attributed to the scintillator responding to the electron-photon cascade and to the interaction of nuclear active particles, NAP, in the scintillator material whilst both spark chambers and Geiger counters respond only to the EAS charged particles. Since the particles in the electron-photon cascade and the nuclear active component are more energetic near the shower core, the effect of the interactions of these particles in the scintillator material increases as the radial distance between the scintillation counter and the shower core decreases. Also it has been found from the work of several authors, and which was

summarised by Smith (1978), that the contribution of these interactions to the observed densities increases with increasing depth of the scintillator. This is expected since the thicker the scintillator material the greater the probability of the nuclear active particles interacting and of the photons producing electron-positron pairs by pair production.

In this research and as mentioned earlier, the array data were analysed while a liquid detector and a plastic detector were not considered by the analysis programme in the calculation of the shower parameters. These two detectors were chosen to be detector number 7 and detector number 41 respectively (see figure 3.1). The depth of the liquid in the liquid counter is 20 cm and the thickness of the plastic detector is 5 cm. For each analysed shower which was found to have an apparent value for the zenith angle, θ, of $\leqslant 30^{o}$ and an accepted core radial distance, R_c, $\leqslant 50$ m, the densities observed by these two detectors were determined, by the analysis programme, and their radial distances from the shower core were calculated.

Figures 6.1 and 6.2 show the lateral distributions of the electron-photon component measured by the two detectors and the experimental results are plotted together with the best fit curves. By comparing the two figures, it is clear that the lateral distribution curve obtained by the liquid counter is higher and also somewhat steeper than that measured by the plastic detector. This is expected since the first detector is thicker than the second. The equation representing the best fit curve for the results of the liquid scintillation counter is given by

$$\rho_{det.} = \rho_o \times \left(\frac{r + 3}{r + 1}\right) \qquad 6.1$$

where ρ_{det} is the particle density (m^{-2}) measured at the detector, ρ_o is the density given by the equation which represents the modified Catz lateral structure function used for the minimisation routines (S4.4) and r is the radial distance (m) between the detector and the shower core.

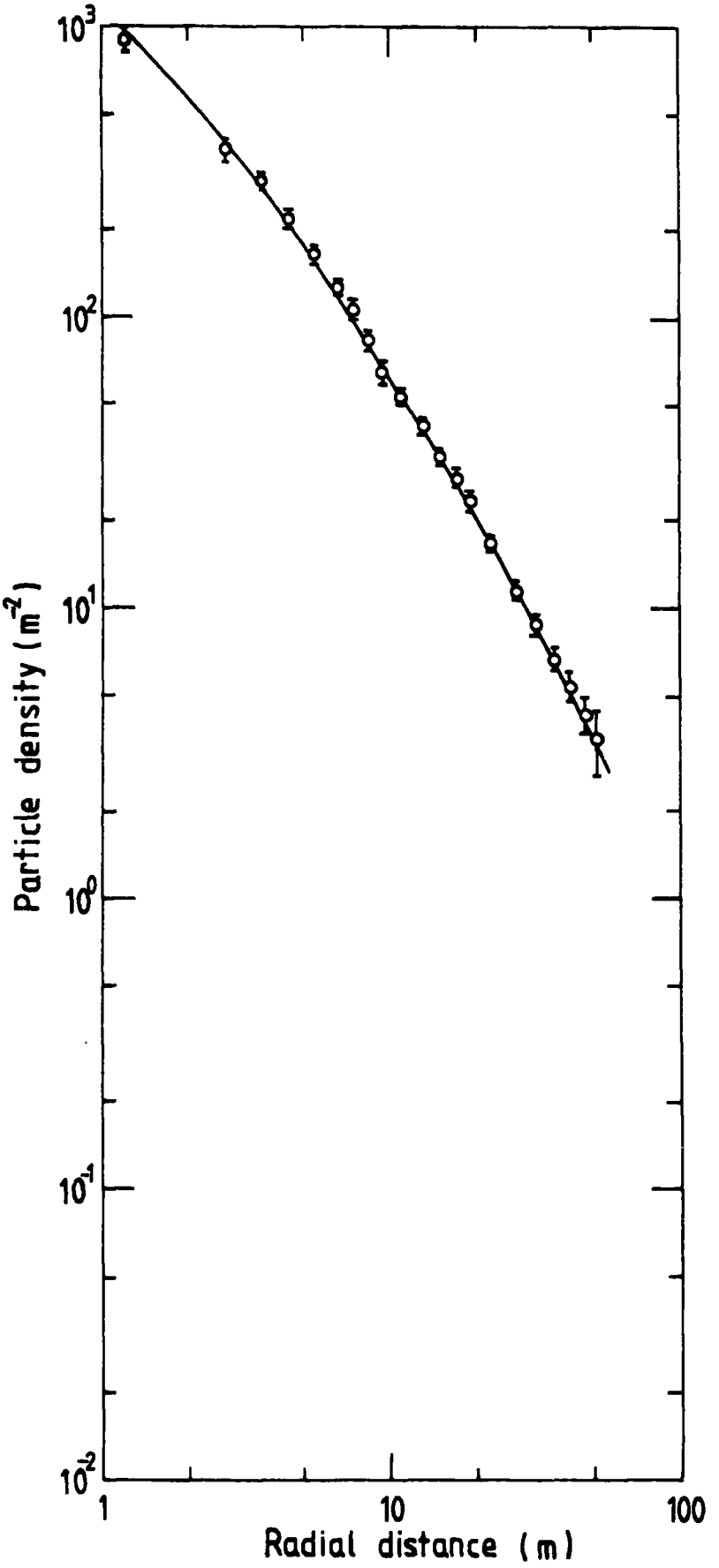

Figure 6.1 Lateral distribution of the electron-photon component of E.A.S., normalised to $N = 2{\cdot}1 \times 10^5$, as measured by the liquid scintillation counter, 7, (20 cm thick). The solid curve represents the best fit equation.

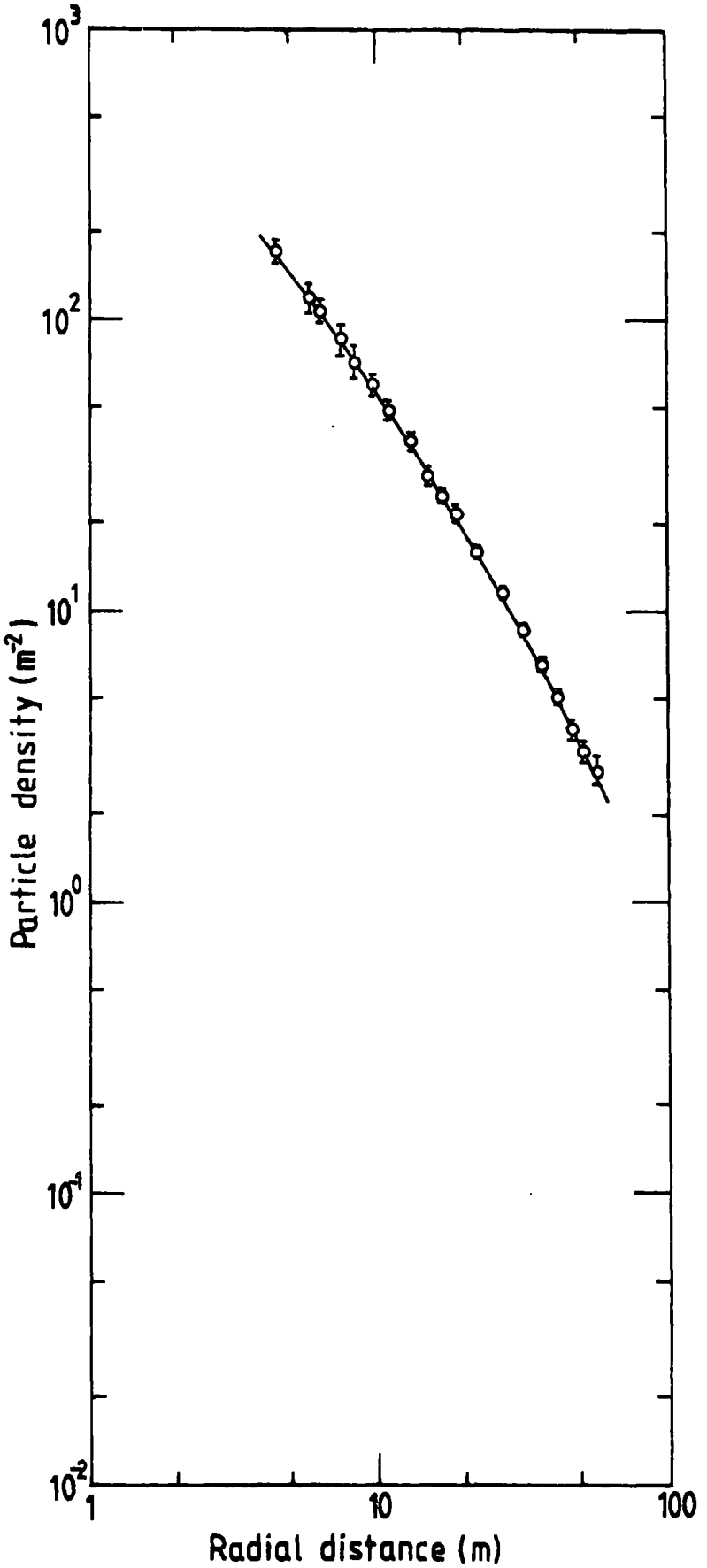

Figure 6.2 Lateral distribution of the electron - photon component of E.A.S., normalised to $N = 2{\cdot}1 \times 10^5$, as measured by the plastic scintillation counter, 41, (5 cm thick). The solid curve represents the best fit equation.

The term $\frac{r + 3}{r + 1}$ represents the mentioned effect of the interactions of photons and nuclear active particles in the scintillator material and can be written as 1 + A where $A = \frac{2}{r + 1}$. Table 6.1 illustrates the relationship between the value of the detector's radial distance r and the corresponding value of A. This table shows that the contribution of the interactions of photons and NAP to the density observed by the detector decreases as r increases since for r = 1m the density measured is 100% higher than that given by the modified Catz function while for r = 20 m the density is only about 10% higher.

For the plastic detector, the best fit curve was found to be represented by an equation of the form,

$$\rho_{det} = \rho_o \times \left(\frac{r + 1.4}{r + 1}\right) \qquad 6.2$$

Similarly, the term showing the effect of the interactions of photons and NAP, $\frac{r + 1.4}{r + 1}$, can be written as 1 + B where $B = \frac{0.4}{r + 1}$. In this case the increase in the density due to these interactions is less than that observed for the liquid detector such that this increase is only 0.8% at r = 50 m and reaches 20% at r = 1 m.

The results obtained for the two detectors are plotted again in figures 6.3 and 6.4 together with the lateral distribution structure functions deduced from various experiments. In these figures, the error bars on the present results are not shown in order to avoid confusion. By comparing all the curves and data shown in the two figures, it is clear that the Hasegawa function (2.3) is the steepest function amongst all those presented. If the other lateral distribution curves are arranged in descending order, it can be seen that for radial distances below 20 m the highest and steepest one is that represented by the results obtained at Moscow for liquid scintillation counters having a thickness of 30 cm (2.5.5). Next, come the present results for the liquid counter, 7, in which the depth of the liquid is 20 cm. These

TABLE 6.1

The relationship between the radial distance (m) of the liquid scintillation counter, 7, and the contribution of the interactions of photons and NAP to the observed particle density.

Radial distance r(m)	$A:(\frac{2}{r+1})$
1.0	1.0
2.0	0.67
5.0	0.33
10.0	0.18
15.0	0.13
20.0	0.10
30.0	0.06
40.0	0.05
50.0	0.04

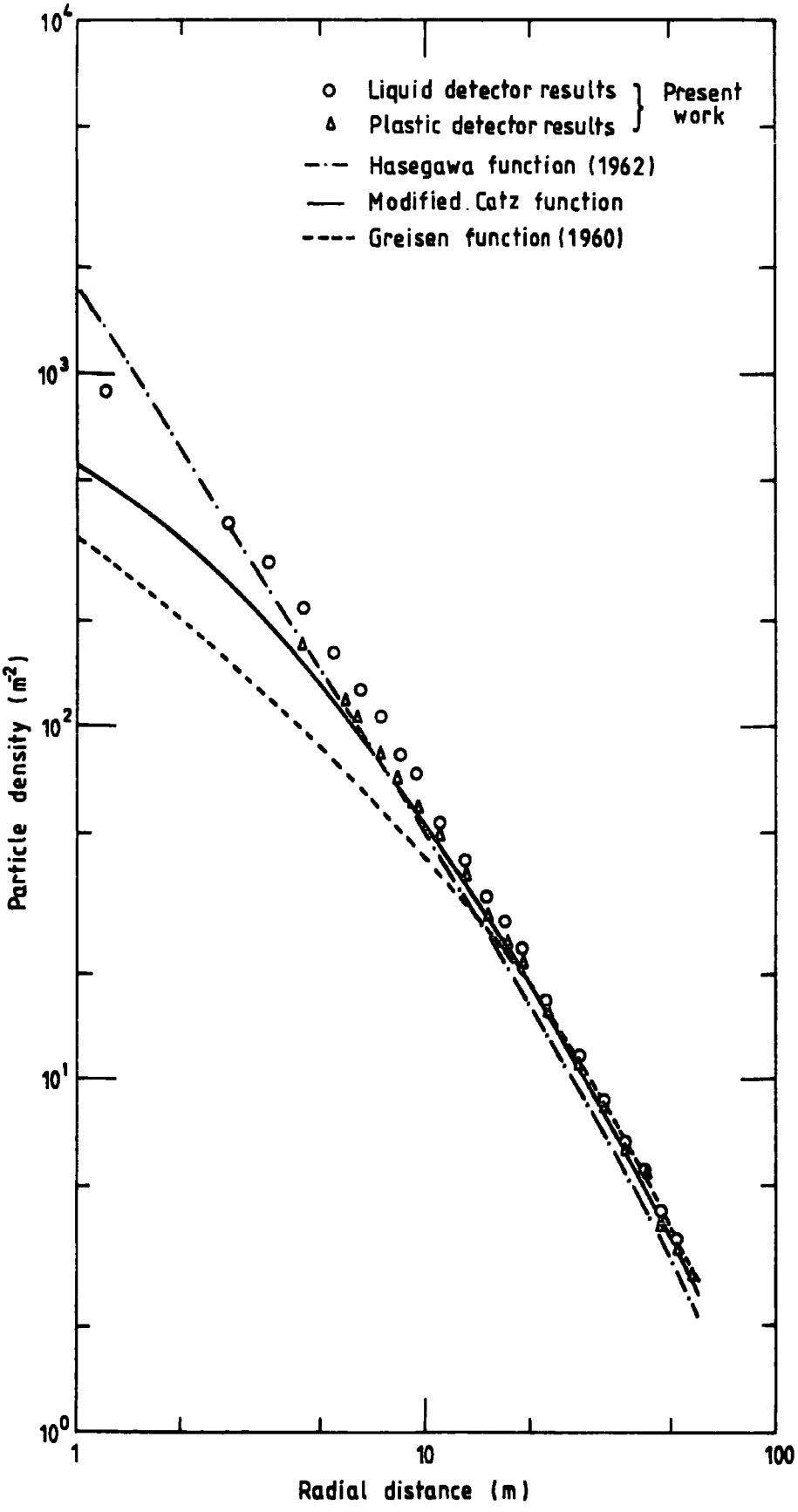

Figure 6.3 Comparison between the present results obtained by the liquid and the plastic detectors, 7 and 41, and the air shower lateral structures due to several authors, normalised to $N = 2{\cdot}1 \times 10^5$.

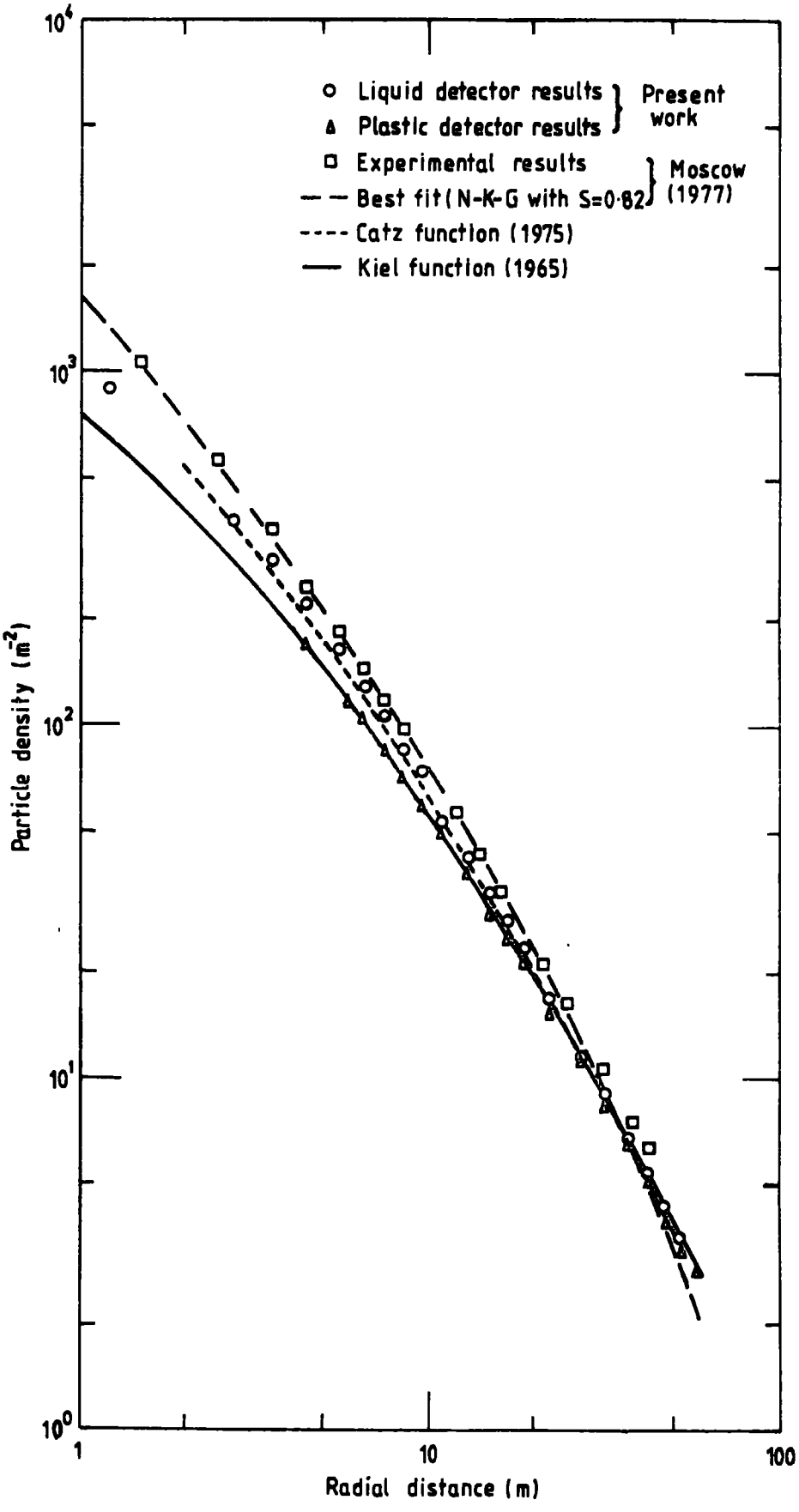

Figure 6.4 Comparison between the present results obtained by the liquid and the plastic detectors, 7 and 41, and the air shower lateral structures deduced from various experiments, normalised to $2{\cdot}1 \times 10^5$.

are followed by the Catz function (4.3) deduced for the particle densities as registered by liquid counters which were about 12 cm thick (S2.5.4). Below this function are the present results recorded using the plastic detector, 41, which has a thickness of 5 cm, as well as the Kiel lateral distribution function (2.5) obtained for plastic detectors of a similar thickness and which, as seen, agrees well with the present results. The next curve is that representing the modified Catz function (S4.4) which has been deduced for thinner scintillation counters. Finally comes the lateral distribution function of Greisen (1960) which is to be expected since this function is only for the charged particles in the EAS.

Therefore, it may be concluded from the previously mentioned two figures, that apart from the Hasagawa function, there is a good agreement between all the other lateral distribution functions and the present results if the thickness of the detectors used in each case is taken into account.

6.3 The Comparison Between the Experimental Data Obtained by the Top Measuring Tray of MARS and the Theoretical Predictions

In order to carry out this comparison, it was required to find which of the eight layers of tubes in the red-side top measuring tray was most suitable. For this purpose, the efficiency of the tubes in each layer, the probability of each tube being discharged as a consequence of the passage of a particle through its internal volume, was investigated and the results are shown in table 6.2 It can be seen from this table that the tubes in layers 4 and 6 were the most efficient. Therefore for each recorded shower event of zenith angle $\theta \leqslant 30^{\circ}$ and which had fallen at a radial distance $\leqslant 50$ m, layers 4 and 6 were scanned to know how many tubes were discharged in each. The histogram of the shower size of these events resulting from the analysis programme was then obtained (figure 6.5). The events having shower size values

TABLE 6.2

The Efficiency of the Red-Side Top Measuring Tray of the Spectrograph

Layer	1 (top)	2	3	4	5	6	7	8
Layer Efficiency %	53.3	57.0	54.6	57.1	45.3	58.3	56.2	55.7
Tube Efficiency %	82.6	88.3	84.5	88.4	70.2	90.3	87.0	86.3

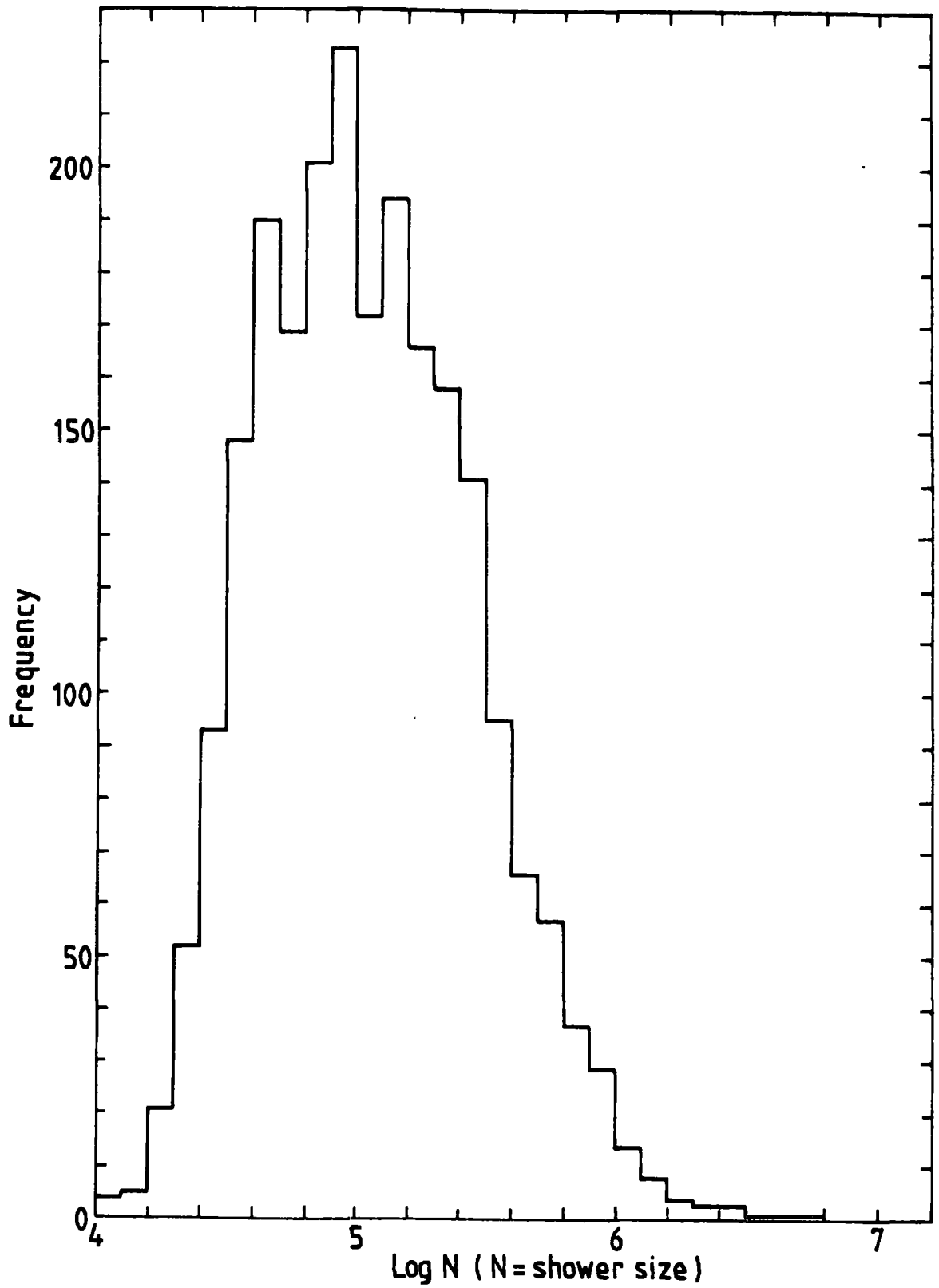

Figure 6.5 Histogram of the shower size values resulting from the analysis of the scanned events.

in the range from 1.0×10^4 to 1.0×10^6 were divided into four groups, each containing nearly the same number of events, and the actual mean of the shower size for each group was calculated. The ranges of shower sizes, N, of the events in these groups were as follows:

$1.0 \times 10^4 < N \leqslant 5.0\ 1 \times 10^4$, $5.01 \times 10^4 < N \leqslant 1.0 \times 10^5$, $1.0 \times 10^5 < N \leqslant 2.0 \times 10^5$, and $2.0 \times 10^5 < N \leqslant 1.0 \times 10^6$.

Each of these groups was in turn divided into four approximately equal subgroups according to the value of the radial distance, R_M, of the top red-side measuring tray. For each of the resultant sixteen subgroups the actual mean value of R_M was calculated and the distribution of the mean number of tubes discharged in the two scanned layers was then obtained.

The calculated actual mean values of the shower size and of the top measuring tray radial distance were used to deduce the corresponding theoretical distributions. Owing to the fact that both the flash-tubes of the top measuring tray and the Geiger Müller counters respond only to the charged particles in the EAS, the Griesen structure function (equation 2.1) was considered suitable for calculating the particle density (m^{-2}) corresponding to the evaluated mean shower size and mean radial distance. It is considered that the probability $p_m(n)$, that n out of a total m particle detectors, each of equal area s, are struck when the mean particle density is ρ, is represented by the following Poisson formula.

$$p_m(n) = \frac{m!}{n!(m-n)!} \left[1 - e^{-\rho s}\right]^n \left[e^{-\rho s}\right]^{m-n} \qquad 6.3$$

In this equation, each detector is considered as a separate independent one. Thus for each calculated mean particle density, the probability distribution for each layer was obtained using the above formula. This was done for n ranging from 1 to 89 (the total number of the layer tubes) and where each tube was considered as a separate detector of area S

taken to be equal to the internal diameter times the length of the tube covered by the electrode multiplied by the tube's efficiency. This efficiency was assumed to be uniform over the length of the tube. A Monte Carlo technique was used such that the actual number of tubes discharged in each of the chosen layers was selected from the corresponding precalculated probability distribution. Finally, the theoretical distribution for the mean of the number of tubes discharged in the two layers was deduced.

Figures 6.6, 6.7, 6.8 and 6.9 represent the obtained experimental and theoretical distributions. The ratio between the mean of each experimental distribution and that of the corresponding theoretical one is shown in table 6.3. It can be seen from this table that the disagreement between the experimental results and the theoretical predictions decreases with the shower size. This may be interpreted on the basis of figure 6.10 which shows the relationship between the fixed values of shower size with which data were simulated, N_{in}, (see chapter 5) and the corresponding mean values for the shower size, N_{out}, resulting from the analysis of these simulated data. According to this figure, the mean value of the shower size obtained by the analysis programme is always less than the value with which showers were generated. Also it can be seen from this figure that the mean value of N_{out} increases from $0.8\ N_{in}$ to $0.92\ N_{in}$ as the value of N_{in} increases from 5.0×10^4 to 1.0×10^6.

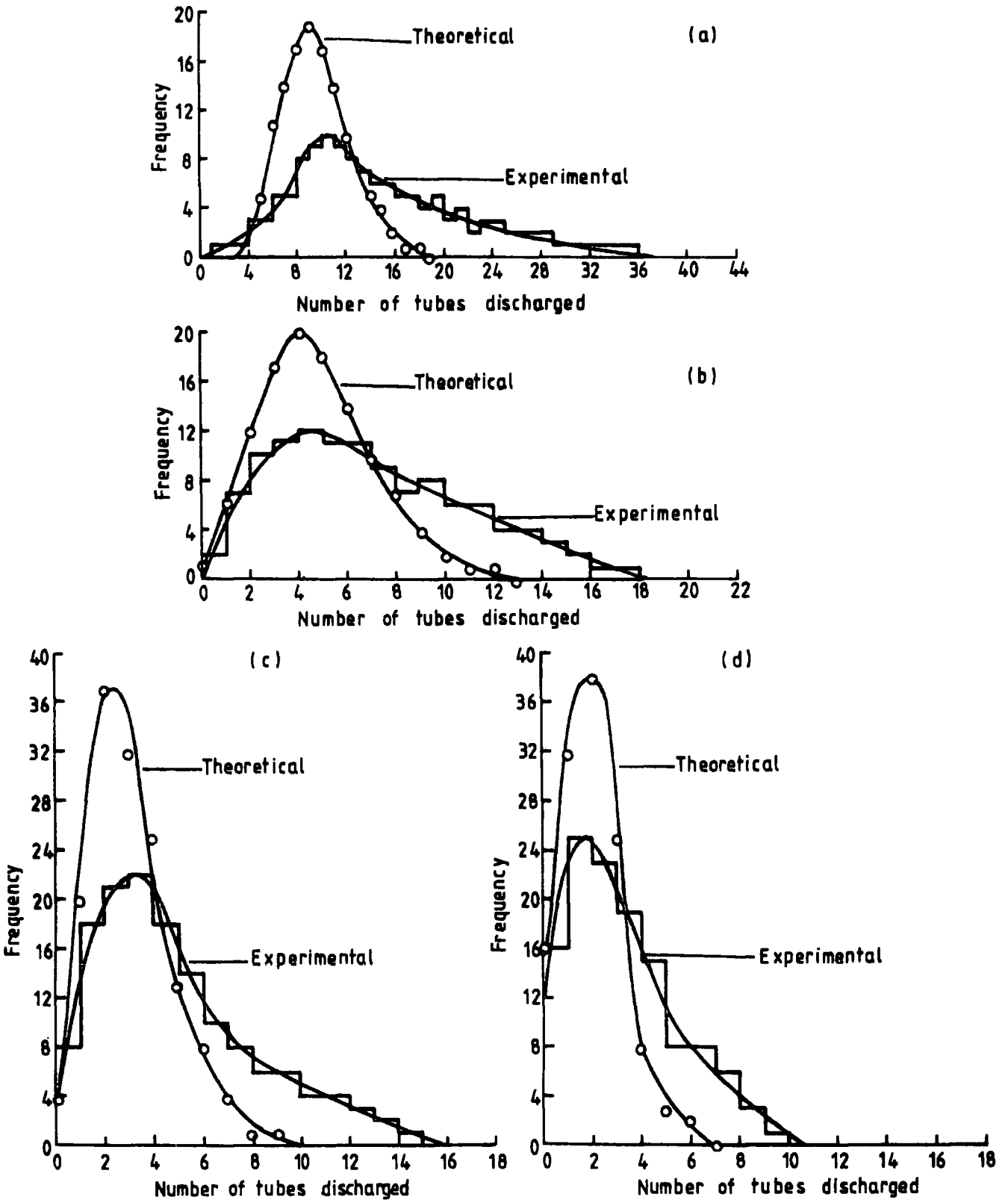

Figure 6.6 Comparison between the experimental and theoretical distributions for the number of tubes discharged in layers 4 and 6. The experimental distributions are for $1{\cdot}0 \times 10^4 < N \leq 5{\cdot}01 \times 10^4$ and for $0 < R_M \leq 10$m (a), $10 < R_M \leq 14$m (b), $14 < R_M \leq 20$m (c) and $20 < R_M \leq 44$m (d) where N is the shower size and R_M is the radial distance of the red-side top measuring tray of MARS from the shower core. For the theoretical distributions $\bar{N} = 3{\cdot}55 \times 10^4$ and $\bar{R}_M = 6{\cdot}24$m (a), $12{\cdot}04$m (b), $16{\cdot}94$m (c) and $25{\cdot}11$m (d).

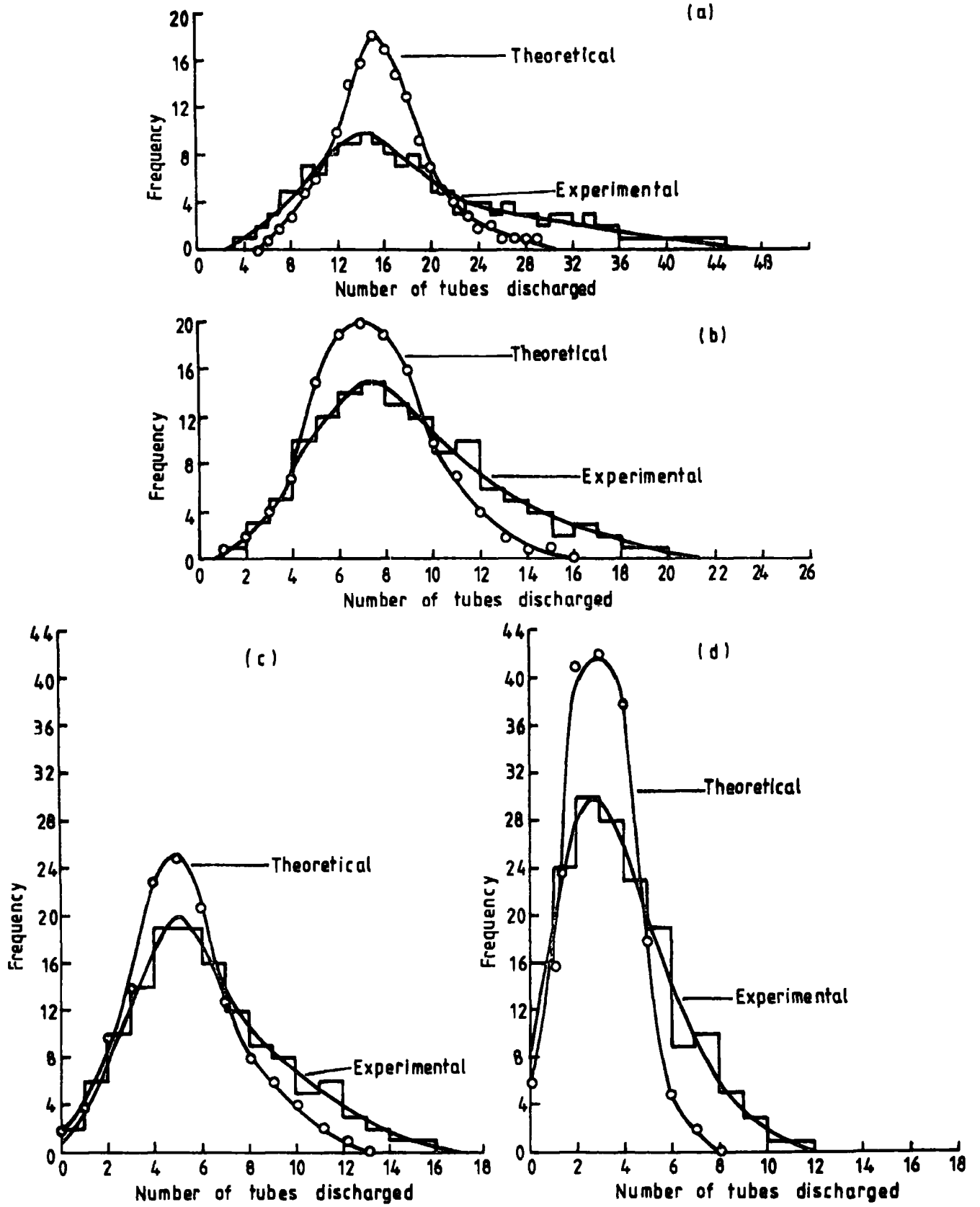

Figure 6.7 Comparison between the experimental and theoretical distributions for the number of tubes discharged in layers 4 and 6. The experimental distributions are for $5{\cdot}01 \times 10^4 < N \leq 1{\cdot}0 \times 10^5$ and for $0 < R_M \leq 12$ m (a), $12 < R_M \leq 18$ m (b), $18 < R_M \leq 24$ m (c) and $24 < R_M \leq 52$ m (d). For the theoretical distributions $\bar{N} = 7{\cdot}42 \times 10^4$ and $\bar{R}_M = 7{\cdot}83$ m (a), 15·4 m (b), 20·8 m (c) and 30·83 m (d).

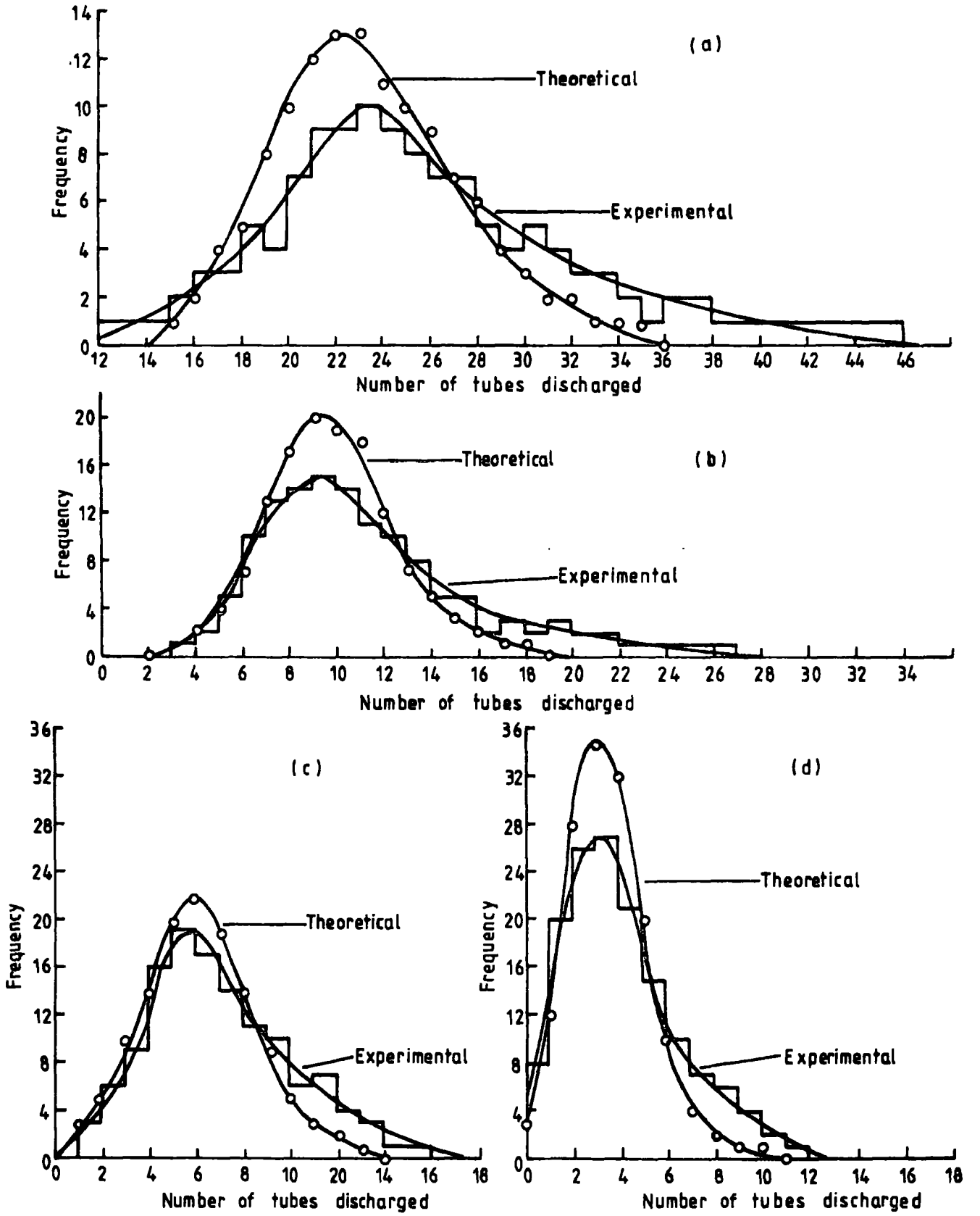

Figure 6.8 Comparison between the experimental and theoretical distributions for the number of tubes discharged in layers 4 and 6. The experimental distributions are for $1{\cdot}0 \times 10^5 < N \leq 2{\cdot}0 \times 10^5$ and for $0 < R_M \leq 16$m (a), $16 < R_M \leq 24$m (b), $24 < R_M \leq 32$m (c) and $32 < R_M \leq 54$m (d). For the theoretical distributions $\bar{N} = 1{\cdot}43 \times 10^5$ and $\bar{R}_M = 9{\cdot}71$m (a), 20·05m (b), 27·73m (c) and 39·51m (d).

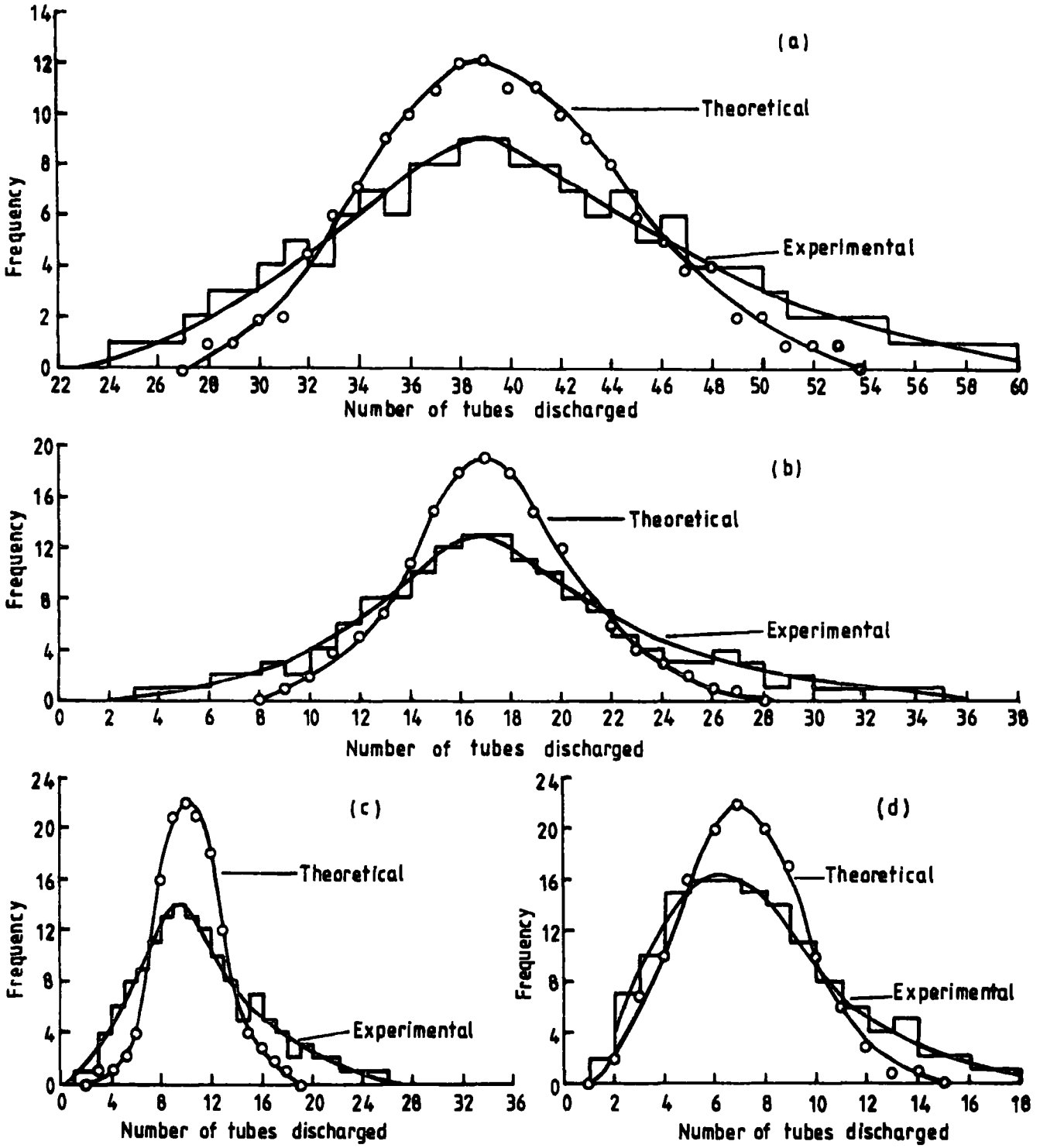

Figure 6.9 Comparison between the experimental and theoretical distributions for the number of tubes discharged in layers 4 and 6. The experimental distributions are for $2{\cdot}0 \times 10^5 < N \leq 1{\cdot}0 \times 10^6$ and for $0 < R_M \leq 22$m (a), $22 < R_M \leq 32$m (b), $32 < R_M \leq 40$m (c) and $40 < R_M \leq 58$m (d). For the theoretical distributions $\bar{N} = 3{\cdot}79 \times 10^5$ and $\bar{R}_M = 14{\cdot}85$m (a), $26{\cdot}93$m (b), $36{\cdot}14$ (c) and $45{\cdot}2$m (d).

TABLE 6.3

The ratio between the mean of the experimental distribution and that of the corresponding theoretical distribution for each of the chosen sixteen subgroups.

Ex. : Experimental Th. : Theoretical

$1.0<N\leq 5.01\times10^4$ (Ex.) $\bar{N}=3.55\times10^4$ (Th.)			$5.01\times10^4<N\leq 1.0\times10^5$ (Ex.) $\bar{N}=7.42\times10^4$ (Th.)			$1.0\times10^5<N\leq 2.0\times10^5$ (Ex.) $\bar{N}=1.43\times10^5$ (Th.)			$2.0\times10^5<N\leq 1.0\times10^6$ (Ex.) $\bar{N}=3.79\times10^5$ (Th.)		
R_M (m)	$\bar{\rho}$ (m^{-2})	Mean (Ex.) / Mean (Th.)	R_M (m)	$\bar{\rho}$ (m^{-2})	Mean (Ex.) / Mean (Th.)	R_M (m)	$\bar{\rho}$ (m^{-2})	Mean (Ex.) / Mean (Th.)	R_M (m)	$\bar{\rho}$ (m^{-2})	Mean (Ex.) / Mean (Th.)
$0<R_M\leq 10$ (Ex.)			$0<R_M\leq 12$ (Ex.)			$0<R_M\leq 16$ (Ex.)			$0<R_M\leq 22$ (Ex.)		
$\bar{R}_M$=6.2 (Th.)	12.0	1.5	$\bar{R}_M$=7.8 (Th.)	20.0	1.2	$\bar{R}_M$=9.7 (Th.)	30.6	1.1	$\bar{R}_M$=14.85 (Th.)	49.4	1.0
$10<R_M\leq 14$ (Ex.)			$12<R_M\leq 18$ (Ex.)			$16<R_M\leq 24$ (Ex.)			$22<R_M\leq 32$ (Ex.)		
$\bar{R}_M$=12.0 (Th.)	6.0	1.5	$\bar{R}_M$=15.4 (Th.)	9.2	1.2	$\bar{R}_M$=20.1 (Th.)	12.6	1.1	$\bar{R}_M$=26.9 (Th.)	21.6	1.0
$14<R_M\leq 20$ (Ex.)			$18<R_M\leq 24$ (Ex.)			$24<R_M\leq 32$ (Ex.)			$32<R_M\leq 40$ (Ex.)		
$\bar{R}_M$=17.0 (Th.)	3.9	1.5	$\bar{R}_M$=20.8 (Th.)	6.2	1.2	$\bar{R}_M$=27.7 (Th.)	7.8	1.2	$\bar{R}_M$=36.1 (Th.)	13.4	1.1
$20<R_M\leq 44$ (Ex.)			$24<R_M\leq 52$ (Ex.)			$32<R_M\leq 54$ (Ex.)			$40<R_M\leq 58$ (Ex.)		
$\bar{R}_M$=25.1 (Th.)	2.3	1.6	$\bar{R}_M$=30.8 (Th.)	3.4	1.3	$\bar{R}_M$=39.5 (Th.)	4.3	1.2	$\bar{R}_M$=45.2 (Th.)	8.9	1.1

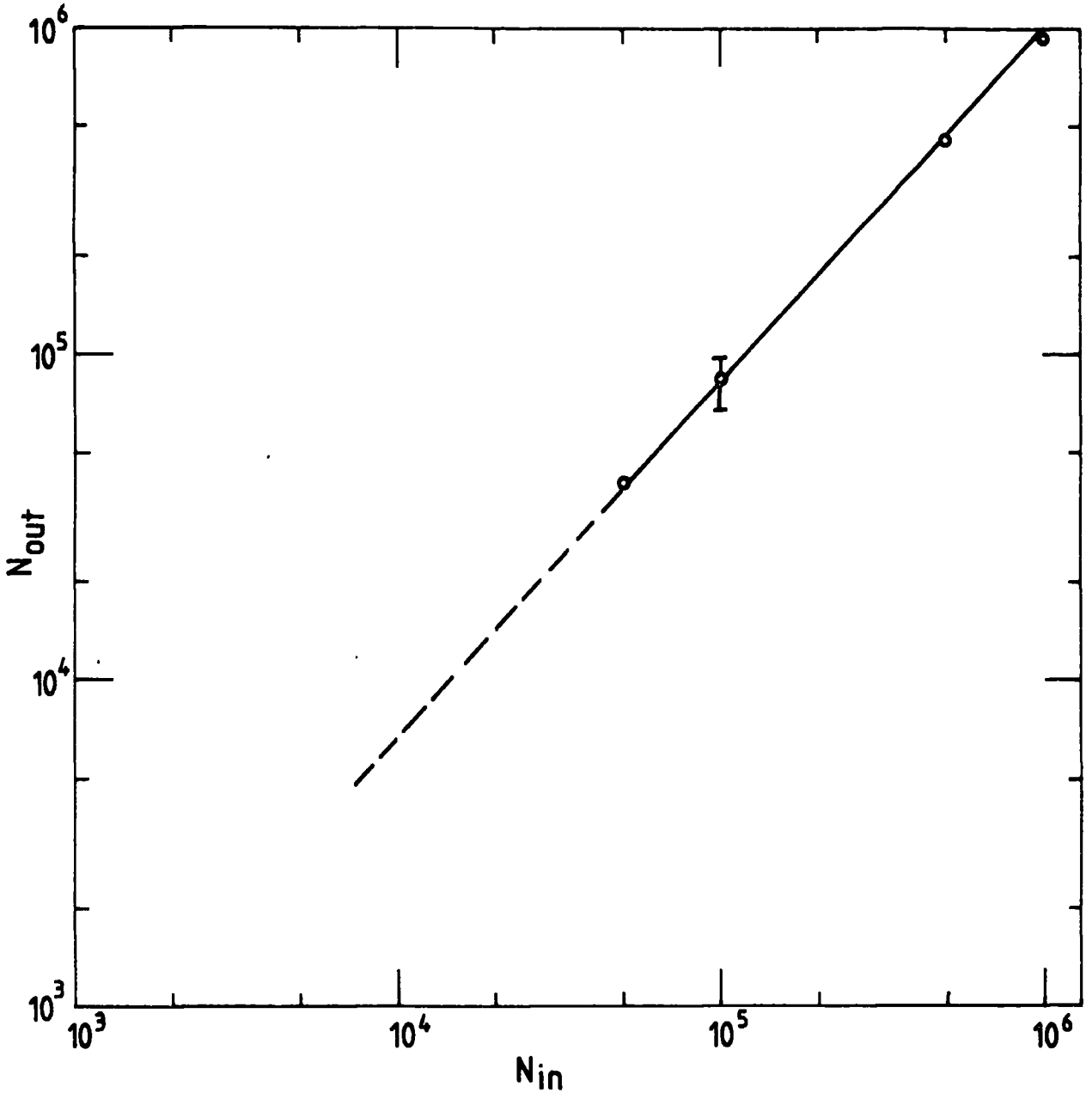

Figure 6.10 Relationship between the fixed values of shower size, N_{in}, with which data were simulated and the corresponding mean values for shower size, N_{out}, resulting from the analysis of these simulated data. The error bars represent the standard deviation on the corresponding mean value.

APPENDIX A

THE MODIFICATION TO THE CATZ FUNCTION

As has been mentioned in chapter four, a modification was made to the Catz lateral distribution structure function (4.3). The modification was to replace the original term (r + 1) by (r + 2) since with this latter function, a better fit to the data was obtained. An explanation for this can be summarised as follows:

1. 4,000 Events were analysed three times using the original Catz function to locate the shower core and determine the shower size, the liquid scintillation counters being excluded in the calculations of these parameters. For each of these events, the observed and predicted densities for all the array detectors, including the liquid counters, were calculated by the analysis programme according to the method described in chapter four.
2. For each useful event, i.e. one having a zenith angle $\leqslant 30^{o}$ and a core radial distance $\leqslant 50$ m, the radial distance from the shower core to each of the liquid detectors was found.
3. These events were then divided into groups according to the values of the radial distances.
4. For each group, the observed and predicted densities of the liquid detectors were referred to as Y and X respectively. The straight line $Y = a + bX$ was fitted to these data using the weighted least squares method where and and b were the intercept and the slope of that line.
5. The resulting values of a and b for all of these groups are listed in table A1. It was assumed that the original Catz function (4.3), according to which the predicted densities were calculated, does not make any allowance for the interactions of photons and nuclear active particles in the thick scintillator

material of the liquid detectors. As was explained in Chapter six, this effect is large at small distances from the shower core and results in a large increase of the observed density at the liquid detectors. It will also be seen that this effect decreases as the radial distance increases. Therefore, it was expected that the first data group would have a slope b greater than one and that this slope should decrease to unity as the radial distance increases. As seen from table A.1, the slope, b, for the group of largest radial distance range may not be considered far from what was expected, but the slopes,b, corresponding to the other groups, especially the first one, are lower than is to be expected

Table A.1

L.Sc. radial distance range (m)	Number of points present	a	b
0.5 to 5	742	-0.27	0.75 ± 0.03
5 to 10	1694	0.2	0.88 ± 0.02
10 to 20	5196	0.39	0.90 ± 0.01
20 to 30	3075	0.42	0.91 ± 0.01

6. Table A2 shows the corresponding results obtained for one of the plastic detectors, detector 11 (see figure 3.1), where only 1,000 events were considered.

Table A.2

Radial distance range (m)	Number of points present	a	b
0.5 to 5	32	-0.13	1.00 ± 0.05
5 to 10	53	0.1	1.05 ± 0.04
10 to 20	162	0.15	1.09 ± 0.02
20 to 30	98	0.16	1.13 ± 0.03

7. Therefore, it was concluded from the previous two tables that the original Catz function was quite suitable for data from the plastic detectors, which were used for the estimation of the shower parameters, but not so suitable for the liquid counters which were ignored in the calculations of these parameters.

8. Hence it was found that the original Catz function should be modified to obtain a better fit for the present data from the liquid detectors. This was done by replacing the original term (r + 1) by (r + 2). 400 Events were then reanalysed using the modified function while the liquid detectors were also neglected in that analysis. Similarly the liquid detectors density data (i.e.plots of the observed densities against predicted densities) were fitted by straight lines using the weighted least squares method (as described earlier in S.4). The results obtained in this case are illustrated in Table A.3

Table A.3

L.Sc. radial distance range (m)	Number of points present	a	b
0.5 to 5	75	-0.25	1.08 ± 0.o4
5 to 10	182	0.34	1.02 ± 0.03
10 to 20	518	0.33	0.97 ± 0.01
20 to 30	308	-0.25	0.94 ± 0.02

9. The comparison between tables A.1 and A.3 shows that the use of the modified function gave slopes, b, for the liquid detectors higher than those which resulted using the original function. Although the new slopes are still lower than expectation, it was concluded that the modified function could be suitable for the present data of the liquid detectors. This conclusion was based on the fact that these detectors were not included in the data analysis and that if their observed densities were considered in the determination of the core location, the gradiants of the lines fitted to their data might have the expected values.

10. This was tested by reanalysing the 400 events using the modified Catz function and including the liquid detectors into the calculations of the shower parameters. The procedures described in sections 2 to 4 were then followed to obtain the values of a and b in this case. Table A.4 illustrates the resulting values which seem to be reasonable. This was understood since it was found subsequently that the original Catz function was deduced for liquid scintillation counters

having an average thickness of about 12 cm (Hochart, 1976) and hence the previous assumption that this function neglects the effect of photon and N.A.P. interactions was not correct. This is probably the main reason for the values of b shown in table A.1 being lower than the expectations.

Table A.4

L.Sc. radial distance range (m)	Number of points present	a	b
0.5 to 5	66	0.05	1.52 ± 0.04
5 to 10	224	0.08	1.20 ± 0.02
10 to 20	646	0.06	1.10 ± 0.01
20 to 30	450	0.09	1.07 ± 0.01

11. The effect of using the modified function on the results for the plastic detectors data, when the liquid detectors were not considered and when they were considered by the analysis programme, was also studied. Table A.5 illustrates a comparison between the results obtained when the original function was used and those corresponding to the modified function for each plastic detector and for all values of radial distance (see figure 3.1). The table indicates that the use of the modified function, with or without the data from the liquid detectors, does not result in giving significant differences in the values of a and b obtained for each of the plastic detectors.

12. Thus owing to the previous study, it was decided to analyse the present data using the modified Catz function.

TABLE A.5

(#: number of points present)

Detector	Using the original Catz function (L.sc. out)			Using the modified function (L.Sc. out)			Using the modified function (L.Sc. in)		
	#	a	b	#	a	b	#	a	b
C	240	0.52	0.98 ± .02	243	0.50	0.96 ± .02	241	0.50	1.02 ± .02
11	241	0.41	1.09 ± .02	239	0.36	1.11 ± .02	245	0.32	1.10 ± .02
31	231	0.47	1.07 ± .02	234	0.51	1.07 ± .02	230	0.46	1.08 ± .02
51	248	0.38	1.02 ± .02	250	0.40	1.00 ± .02	253	0.30	1.01 ± .02
13	153	0.22	1.03 ± .03	155	0.15	0.98 ± .03	151	0.13	0.98 ± .03
33	130	0.08	0.88 ± .03	132	-0.04	0.95 ± .03	135	-0.03	0.90 ± .03
53	165	0.53	1.21 ± .03	162	0.24	1.20 ± .03	170	0.44	1.22 ± .03
32	204	0.07	0.95 ± .03	208	-0.17	0.95 ± .03	211	-0.24	0.95 ± .03
41	230	0.15	1.04 ± .02	235	-0.26	1.06 ± .02	228	0.19	1.05 ± .02
42	148	0.34	0.81 ± .03	153	0.24	0.80 ± .03	147	0.37	0.81 ± .03
52	240	-0.42	0.94 ± .02	237	-0.29	0.95 ± .02	250	0.03	0.95 ± .02
61	253	0.13	0.93 ± .02	260	0.27	0.94 ± .02	257	0.05	0.92 ± .02
62	150	-0.09	-0.93 ± .03	147	0.03	0.95 ± .03	153	0.12	0.94 ± .03

REFERENCES

(P.I.C.C.R. = Proceedings of the International Conference on Cosmic Rays)

Alexeyev, E.N., Chudakov, A.E., Danshin, A.E., Galperin, M.D., Glemba, P.Ya., Lidvansky, A.S., Sulla-Petrovsky, Yu.R., Tatian, B.B., Tizengausen, V.A., Khristiansen, G.B., Kulikov, C.V., and Sulakov, V.P., 1977, P.I.C.C.R., Plovdiv, 8, 52.

Alexeyev, E.N., Glemba, P.Ya., Lidvansky, A.S., Markov, V.Ya., Molchanova, N.I., Tatian, B.B., Tizengausen, V.A., Chudakov, A.E., Kulikov, G.V., Sulakov, V.P., and Khristiansen, G.B., 1975, P.I.C.C.R., Munich, 8, 2996.

Anderson, C.D., 1932, Science, 76, 238.

Antonov, R.A., et al., 1971, P.I.C.C.R., Hobart, 6, 2194.

Ayre, C.A., Hamdan, M.A., Hume, C.J., Nandi, B.C., Thompson, G.M., Wells, S.C., and Whalley, M.R., 1972, Nucl. Inst. and Meth., 102, 35.

Ayre, C.A., Hamdan, M.A., Hume, C.J., Stubbs, F.W., Thompson, M.G., Wells, S.C., and Whalley, M.R., 1972, Nucl. Inst. and Meth., 102, 12.

Avre, C.A., and Thompson, M.G., 1969, Nucl. Inst. and Meth., 69, 106.

Bagge, E., Böhm, E., Ftitze, R., Roose, U.J., Samorski, M., Schnier, C., Staubert, R., Thielhein, K.O., Trümper, J., Wiedecke, L., and Wolter, W., 1965, P.I.C.C.R. London, 2, 738.

Bagge, E., Samorski, M., and Stamm, W., 1977, P.I.C.C.R., Plovdiv, 8, 34.

Bennet, S., et al., 1962, J. Physc. Soc. Japan, Suppl. A III, 17, 196.

Bothe, W., and Kolhörster, W., 1929, Zeits Phys., 56, 751.

Bradt, H., et al., 1965, P.I.C.C.R., London, 2, 715.

Bray, A.D., Crawford, D.F., Jauncey, D.L., McCusker, C.B.A., Polle, P.C., Rathgeber, M.H., Ulrichs, J., Wand, R.H., and Winn, M.M., 1964, Nuovo Cimento, 32, 827.

Bray, A.D., Crawford, D.F., Jauncey, D.L., McCusker, C.B.A., Melley, D., Nelson, D., Poole, P.C., Rathgeber, M.H., Seet, S.H., Ulrichs, J., Wand, R.H., and Winn, M.M., 1965, P.I.C.C.R., London, 2, 685.

Catz, Ph., Gawin, J., Grochalska, B., Hibner, J., Hochart, J.P., Milleret, G., Stanczyk, J., and Wdowczyk, J., 1975, P.I.C.C.R., Munich, 12, 4329.

Chatterjee, B.K., et al., 1968, Can. J. Phys., 46, S136.

Clark, G., et al., 1958, Nuovo Cimento, 8, Supple. 2, Series 10, 623.

Clay, J., 1927, Proc. Roy. Acad. Amsterdam, 30, 1115.

Coconni, G. Koester, L.J., and Perkins, D.H., 1961, U.R.C.L. High Energy Physics Study Seminars, 28, part 2, U.C.I.D.

Colgate, S.A., and White, R.H., 1966, Astro. Phys. J., 143, 626.

Compton, A.H., 1933, Phys. Rev., 43, 378.

Cooper, D.A., 1974, Ph.D. Thesis, University of Durham.

Dake, S., Asayama, K., Jitsuno, K., Nishikawa, N., Sakata, M., Yamamoto, Y., and Hatano, Y., 1971, P.I.C.C.R., Hobart, 3, 948.

de Beer, J.F., et al., 1966, Proc. Phys. Soc., 89, 567.

de Beer, J.F., et al., 1968, J. Phys. A., 1, 72.

Dixon, H.E., and Turver, K.E., 1974, Proc. Roy. Soc. Lond., A., 339, 171.

Earnshaw, J.C., et al., 1967, Proc. Phys. Soc., 90, 91.

Elbert, J.W., Larson, M.O., Lowe, G.H., Morrison, J.L., Mason, G.W., and Spencer, R.L., 1975, J. Phys. A. Math. Gen., 8, 1, L13.

Elster, J., and Geitel, H., 1899, Physik Zeitschr, 1, 11.

Fermi, E., 1949, Phys. Rev., 75, 1169.

Fermi, E., 1954, Astrophys. J., 119, 1.

Geitel, H., 1900, Physik. Zeitschr , 2, 116.

Greider, P.K.F., 1973, P.I.C.C.R., Denver, 4, 2639.

Greisen, K., 1956, Prog. Cosmic Ray Physics III (North Holland Pub. Co., Amsterdam), 1.

Greisen, K., 1960, Ann. Rev. Nucl. Science, 10, 63.

Greisen, K., 1966, Phys. Rev. Lett., 16, 748.

Grigorov, N.L., Nesterov, V.E., Rapoport, I.D., Savenko, I.A., and Skuridin, G.D., 1970, Yad. Fiz., 11, 1058; Sov. J. Nucl. Phys., 11, 588.

Hasegawa. H., et al., 1962, J. Phys. Soc. Japan, 17, A III, 189.

Hess, V.F., 1912, Physik. Zeitschr., 13, 1084.

Hillas, A.M., 1970, Acta. Phys. Hung., 29, Supple. 3, 539.

Hillas, A.M., 1975, Phys. Rep., (Phys. Lett. C.), 20C, 61.

Hochart, J.P., 1976, Ph.D. Thesis, Laboratory of Cosmic Ray Physics, France.

James, F., and Roos, M., 1971, C.E.R.N. Computer 7600 Program Library, D505, D516.

Johnson, T.H., and Street, J.C., 1933, Phys. Rev., 43, 381.

Kamata, K., and Nishimura, J., 1958, Suppl. Prog. Theor. Phys., 6, 93.

Kameda, T., et al., 1965, P.I.C.C.R., London, 2, 681.

Karakula, S., 1968, See Wdowczyk, J., 1973.

Karakula, S., Osborne, J.L., and Wodowczyk, J., 1974, J. Phys. A. Math., Nucl. Gen., 7, 437.

Kempa, J., Wdowczyk, J., and Wolfendale, A.W., 1974, J. Phys. A. Math., Nucl. Gen., 7, 1213.

Khrenov, B.A., 1962, Izvest. Akad. Sci. U.S.S.R., 26, 5.

Khristiansen, G.B., Atrashkevitch, V.B., Kalmykov, N.N., and Fomin, Yu. A., 1965, P.I.C.C.R. London, 2, 774.

Kolhörster, W., 1913, 1914, See 'Introduction to Modern Physics', Richtmyer, F.K., Kennard, E.H., and Lauritsen, T., 5th Ed., McGraw-Hill, 1955).

La Pointe, M., et al., 1968, Can. J. Phys., 46,S68.

Lattes, C.M.G., Occhialini, G.P.S., and Powell, C.F., 1947, Nature, London, 159, 453.

Linsley, J., et al., 1962, J. Phys. Soc. Japan, 17, Supple. A III, 91.

Mardson, D.J., 1971, Ph.D. Thesis, University of Leeds.

Millikan, R.H., and Cameron, G.H., 1926, Phys. Rev., 28, 851.

Miyake, S., et al., 1970, Acta Phys. Hung., 29, 463.

Ng, L.K., Wdowczyk, J., and Wolfendale, A.W., 1973, P.I.C.C.R., Denver, 3, 1781.

Nishimura, J., and Kamata, K., 1952, Progr. Theor. Phys., 1, 185.

Nishimura, J., and Kamata, K., 1958, see Kamata, K., and Nishimura, J., 1958.

Ostriker, J.P., and Gunn, J.E., 1969, Astrophysics. J., 157, 1395.

Rada, W.S., Shaat, E.A.M., Smith, A.C., Stewart, T.R., Thompson, M.G., and Treasure, M.W., 1977, Nucl. Inst. and Meth., 145, 283.

Regener, V.H., 1951, Phys. Rev., 81, 161.

Rochester, G.D., and Butler, C.C., 1947 Nature, London, 160, 855.

Roll, P.G., and Wilkinson, D.T., 1966, Phys. Rev. Lett., 16, 405.

Samorski, M., et al., 1971, P.I.C.C.R., Hobart, 3, 959.

Shibata, S., Nagano, M., Matano, T., Suga, K., and Hasegawa, H., 1965, P.I.C.C.R., London, 2, 672.

Smith, A.C., 1976, Ph.D. Thesis, University of Durham.

Smith, A.C., 1978, Nucl. Inst. and Meth., 154, 573.

Thompson, M.G., and Wells, S.C., 1972, Nucl. Inst. and Meth., 102, 35.

Turver, K.E., 1973, Cosmic Rays at Ground Level, (Ed. Wolfendale, A.W., The Institute of Physics, London).

Van staa, R., Aschenbach, B., and Böhm, E., 1973, P.I.C.C.R., Denver, 4, 2676.

Vernov, S.N., et al., 1961, Sov. Phys., J.E.T.P., 41, 340.

Vernov, S.N., et al., 1964, Izvest. Akad. Sci., U.S.S.R., 28, 1886.

Vernov, S.N., et al., 1968b, Izvest. Akad. Sci., U.S.S.R., 32, 458.

Vernov, S.N., et al., 1970, Acta Phys. Hung., 3, 429.

Wdowczyk, J., 1973, Cosmic Rays at Ground Level, (Ed. Wolfendale, A.W., The Institute of Physics, London).

Wells, S.C., 1972, Ph. D. Thesis, University of Durham.

Wilson, C.T.R., 1900, Proc. Cambs. Phil. Soc., 11, 32.